DAHLGREN DIVISION
NAVAL SURFACE WARFARE CENTER
Dahlgren, Virginia 22448-5100

NSWCDD/TR-99/116

REFINEMENTS IN THE AEROPREDICTION CODE BASED ON RECENT WIND TUNNEL DATA

BY FRANK G. MOORE ROY M. MCINVILLE

WEAPONS SYSTEMS DEPARTMENT

DECEMBER 1999

REPORT DOCUMENTATION PAGE

Form Approved
OMB No. 0704-0188

1. AGENCY USE ONLY (Leave blank)	2. REPORT DATE	3. REPORT TYPE AND DATES COVERED
	December 1999	Final

4. TITLE AND SUBTITLE

Refinements in the Aeroprediction Code Based on Recent Wind Tunnel Data

5. FUNDING NUMBERS

6. AUTHOR(s)

Frank G. Moore, Roy M. McInville

7. PERFORMING ORGANIZATION NAME(S) AND ADDRESS(ES)

Commander
Naval Surface Warfare Center
Dahlgren Division (Code G04)
17320 Dahlgren Road
Dahlgren, VA 22448-5100

8. PERFORMING ORGANIZATION REPORT NUMBER

NSWCDD/TR-99/116

9. SPONSORING/MONITORING AGENCY NAME(S) AND ADDRESS(ES)

10. SPONSORING/MONITORING AGENCY REPORT NUMBER

11. SUPPLEMENTARY NOTES

12a. DISTRIBUTION/AVAILABILITY STATEMENT

Approved for public release; distribution is unlimited.

12b. DISTRIBUTION CODE

13. ABSTRACT (Maximum 200 words)

The 1998 (AP98) and prior versions of the aeroprediction code are based primarily on slender body and perturbation theories at low angle of attack and empirical constants that represent the nonlinear aerodynamics as a function of angle of attack, Mach number, aspect and taper ratio, and other missile geometric parameters. The primary data base upon which these empirical nonlinear constants were derived was based on the NASA/Tri-Service component data base taken in the 1970s. This data base was limited in body radius to wing semispan plus body radius ratios (r/s) of 0.5. A more recent data base taken by NASA and the former McDonnell Douglas Corporation, investigated other values of the parameter r/s of 0.25, 0.33 and 0.5. As a result of this new data base, the empirical constants in the AP98 were fine-tuned. This fine-tuning has shown the average normal force coefficient errors to be reduced by anywhere from 10 percent to over 40 percent on various missile configurations. The largest reductions in error were for configurations where the AP98 average accuracy was the worst. These new improved empirical constants will be a part of the next planned release of the aeroprediction code in 2002 (AP02). The AP98 average error on normal force coefficient of ±10 percent will therefore be somewhat better for the AP02.

14. SUBJECT TERMS

aerodynamics, Aeroprediction Code

15. NUMBER OF PAGES

132

16. PRICE CODE

17. SECURITY CLASSIFICATION OF REPORTS	18. SECURITY CLASSIFICATION OF THIS PAGE	19. SECURITY CLASSIFICATION OF ABSTRACT	20. LIMITATION OF ABSTRACT
UNCLASSIFIED	UNCLASSIFIED	UNCLASSIFIED	UL

FOREWORD

The 1998 version of the aeroprediction code (AP98) was based on the use of slender body and linearized theories to predict aerodynamics at low angles of attack. A missile component wind tunnel data base taken in the 1970s at NASA Langley Research Center was used to predict aerodynamic nonlinearities as a function of Mach number, angle of attack, and various missile geometric parameters. A more recent data base also conducted at NASA was made available. This data base was therefore used to refine the empirical constants used in the aeroprediction code to predict the aerodynamic nonlinearities. This report documents the new empirical constants derived and the improvements in accuracy of normal force coefficient afforded by this new set of constants.

The work described in this report was supported through the Office of Naval Research through the Surface Weapons Systems Technology Program managed at the Naval Surface Warfare Center, Dahlgren Division (NSWCDD) by Mr. Robin Staton. Tasking from this program was provided by Mr. Roger Horman and Mr. John Fraysse. Also, some support was provided by the Marine Corps Weaponry Technology Program managed at NSWCDD by Mr. Craig Melton. The authors express appreciation for support received in this work.

Appreciation is also expressed to Mr. Tom Hymer (G23) who assisted the lead author in the last week of the writing of this report to fine-tune some of the empirical constants.

Approved by:

JOHNNY WALTERS, Deputy Head
Weapons Systems Department

CONTENTS

ILLUSTRATIONS

ILLUSTRATIONS (Continued)

ILLUSTRATIONS (Continued)

TABLES

TABLES (Continued)

1.0 INTRODUCTION

The 1998 version of the NSWCDD Aeroprediction Code (AP98)[1] is the most complete and comprehensive semiempirical code produced to date. It includes the capability to predict planar aerodynamics in the roll positions of $\Phi = 0$ deg (fins in "+" or plus orientation as viewed from the rear of the missile) and $\Phi = 45$ deg (fins in "×" or cross roll orientation as viewed from the rear of the missile) over a broad range of flight conditions and configuration geometries with good average accuracy, computational times and ease of use. Flight conditions include angles of attack (AOA) up to 90 deg, control deflections of up to ±30 deg, and Mach numbers up to 20. Configuration geometries include axisymmetric and nonaxisymmetric body shapes with sharp, blunt, or truncated nose tips, with or without a boattail or flare. Up to two sets of planar or cruciform fins are allowed. New technology has recently been developed[2] to allow both six- and eight-fin options in the fin considerations as well. Average accuracies are ±10 percent for normal and axial force and ±4 percent of body length for center of pressure. By average accuracy is meant that enough AOAs or Mach numbers are considered to get a good statistical sample. On occasion a single data point can exceed these average accuracy values. Ease of use has been significantly enhanced over older versions of the Aeroprediction Code (APC) through a personal-computer-based pre- and post-processor package.[3] This package has allowed inputs for configuration geometries to be simplified significantly by many automated nose shape options.

While the AP98 is a very powerful tool, several limitations and areas of improvement still remain. Most of these needs are driven by the desire of future weapon designers to perform trade studies on new and innovative concepts that may fall outside of the current capability of the AP98. An example of this type of requirement is the multi-fin requirement that has just been completed.[2] Another example of this type of requirement is to include the capability to deflect the rear segment of a fin (sometimes referred to as flaperon or aileron) for control, as opposed to the entire fin.

In addition to configuration design flexibility, there are several areas where improvement in the aerodynamics computational process is needed. The semiempirical model for the wing and wing-body interference aerodynamics was based primarily on missile component data bases[4-6] where the parameter r/s was a constant value of 0.5 (see Figure 1 for nomenclature). More recently, a new missile component data base has been made available[7] where data was measured for wing-alone and wing-body configurations with r/s = 0.25, 0.33, and 0.5. This new data base should therefore allow refinements in the AP98 methodology for the wing alone as well as for the effects due to r/s. Other refinements not explicitly considered in the AP98 include an approximate way to account for internal shock interactions and improvements to the wing-tail interference model. The wing-tail interference model was also based on a limited data set.[8] Issues such as internal shock interactions and wing-tail interference should be amenable to treatment by computational fluid dynamics (CFD) codes.[9-11]

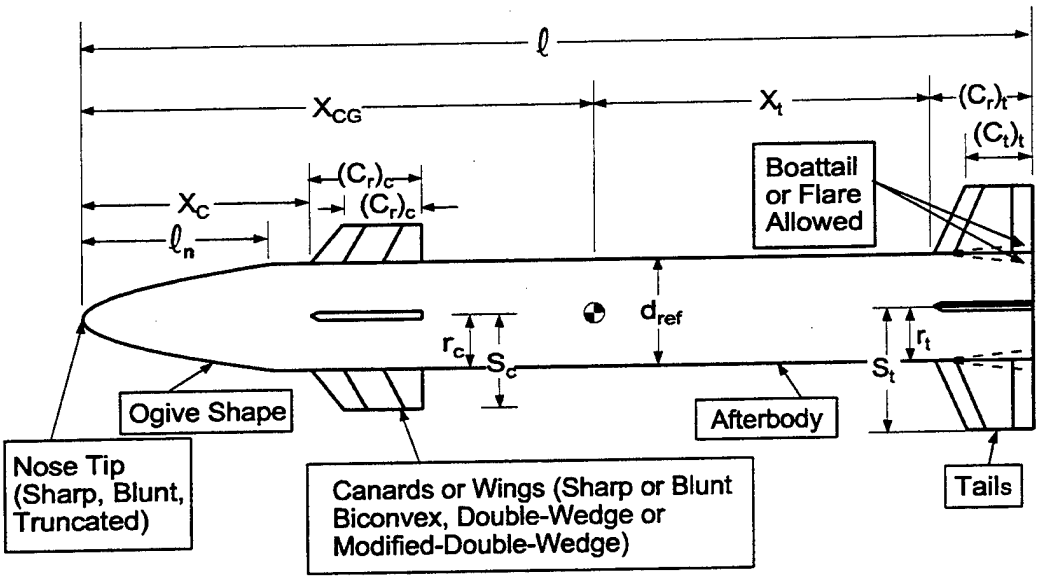

FIGURE 1. TYPICAL AXISYMMETRIC WEAPON CONFIGURATION GEOMETRY OPTIONS AND NOMENCLATURE

The purpose of this report is to examine the recent data base in Reference 7 and make appropriate improvements in the AP98 methodology. Once these improvements have been made, they will be validated against a broad range of configurations other than those upon which the data was measured. Assuming the improvements improve the accuracy of the predictions for the validation cases, the methodology will be integrated into the AP98 and will be transitioned as the AP02 in fiscal year 2002.

2.0 MODIFICATIONS TO THE AP98 BASED ON RECENT WIND TUNNEL DATA

The AP98 uses the so-called direct approach to estimating the nonlinear terms of each of the normal force and center of pressure components. By direct approach is meant that each of the terms in Equation (1) below is broken down into a linear and a nonlinear component. In Equation (1),[12]

$$C_N = C_{N_B} + C_{N_{W(B)}} + C_{N_{B(W)}} + C_{N_{T(B)}} + C_{N_{B(T)}} + C_{N_{T(V)}} \qquad (1)$$

it is understood that the $C_{N_{B(V)}}$ term (not shown) is included in the $C_{N_{B(T)}}$ term. As an example of the direct approach, consider the $C_{N_{W(B)}}$ component of Equation (1), which can be expanded to

$$C_{N_{W(B)}} = \left[\left(C_{N_\alpha}\right)_L + \left(C_{N_\alpha}\right)_{NL}\right]_W \left\{\left[\left(K_{W(B)}\right)_{SBT} + \left(\Delta K_{W(B)}\right)_{NL}\right]\alpha + \left(C_1\left[k_{W(B)}\right]_{SBT} + C_2\right)\delta_W\right\}\left(\frac{A_W}{A_{REF}}\right) \quad (2)$$

The linear or small angle of attack terms of Equation (2) are estimated by linear theory (LT) or slender body theory (SBT). This gives the APC a good fundamental basis for its aerodynamic estimates. The nonlinear corrections due to higher AOA or control deflection are each estimated directly from component wind tunnel data bases. Each of the other terms in Equation (1) is treated in a similar fashion to Equation (2) in the actual implementation into the APC.

The primary data bases used to define the nonlinear terms of Equations (1) and (2) were those of References 4–6 (see Figure 2). In those references, measurements of static aerodynamics for wing alone, body alone, and wing in close proximity to the body were made as a function of roll angle, AOA, Mach number, and control deflection. When the wing in proximity to the body measurements were made, two sting measurements were simultaneously made to record the load on the wing close to the body and the load on the body close to the wing. This allows direct measurement of $C_{N_{W(B)}}$, $C_{N_{B(W)}}$, and C_N of Equation (1). Knowing C_{N_B} and C_{N_W} from previous wind tunnel measurements, values of the interference terms

$$K_{W(B)} = \frac{C_{N_{W(B)}}}{C_{N_w}} \quad (3A)$$

and

$$K_{B(W)} = \frac{\Delta C_{N_{B(W)}}}{C_{N_w}} \quad (3B)$$

can be obtained. $\Delta C_{N_{B(W)}}$ of Equation (3B) is obtained from

$$\Delta C_{N_{B(W)}} = C_N - C_{N_B} - C_{N_{W(B)}} \quad (3C)$$

Reference 13 performed a qualitative error analysis of obtaining $K_{W(B)}$ and $K_{B(W)}$ from Equations (3) and References 4–6. The conclusions of that study were:

a) $K_{W(B)}$ estimates are reasonable for AR ≤ 1.0 at all M and α. More scatter occurs for AR > 1.0.
b) $K_{B(W)}$ estimates are usable for lower AR and M. Best-guess judgement is needed for other conditions.

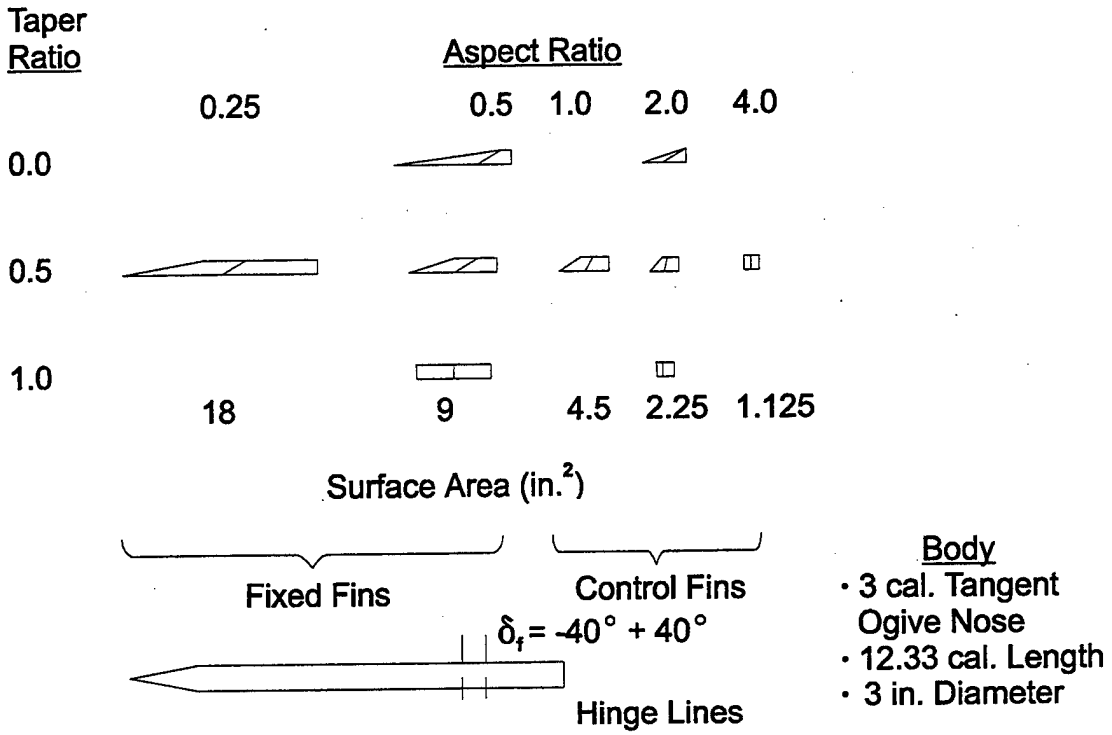

FIGURE 2A. MODELS USED IN LANGLEY[4] WING-BODY TESTS

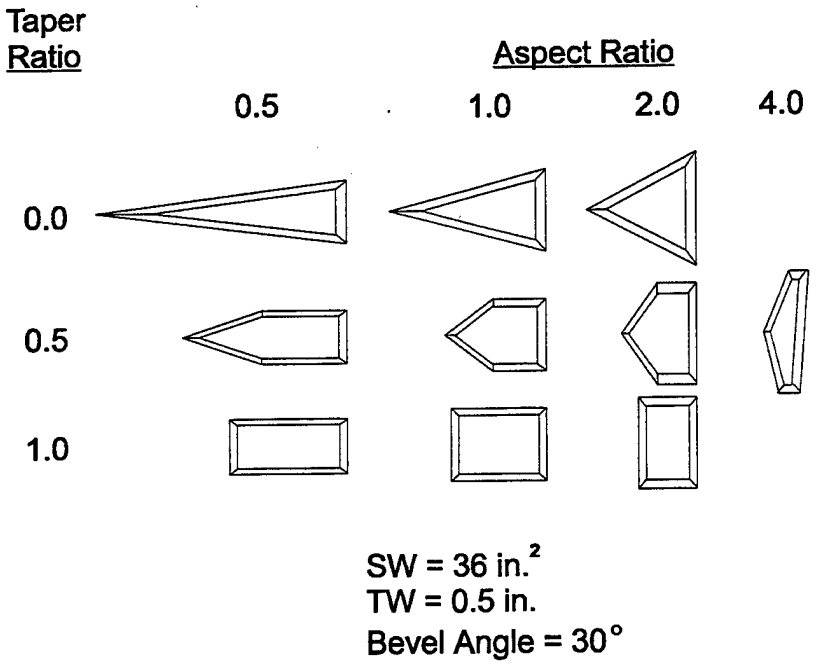

FIGURE 2B. MODELS USED IN STALLINGS AND LAMB[5] WING-ALONE TESTS

These conclusions were primarily driven by the small fins of the Reference 4 data base, which were required in order to keep r/s of Figure 1 constant at a value of 0.5. As a result, Reference 13 recommended that any future component test data for engineering codes should have reasonably sized fins in relation to the body planform area and mounted in the mid-body region to capture most of the afterbody carryover aerodynamics.

The recent wind tunnel test,[7] carried out jointly by then McDonnell Douglas Aerospace and NASA/LRC, followed the recommendation of Reference 13 for larger wings, as most of the wing planforms were equal to or larger than those of Reference 4. Figure 3 shows the configuration geometry and dimensions of the body and wing planforms tested,[7] and Figure 4 shows a scaled pictorial view of the Reference 7 and Reference 4 configurations tested. These can be compared directly to the test of Reference 4 and Figure 2. Several points are worthy of note. First, the wind tunnels used in Reference 4 were the supersonic tunnel at NASA/LRC and the subsonic facility at NASA/AMES, whereas the tunnels used in Reference 7 were both at NASA/LRC. The supersonic tunnel was the same as that of Reference 4, but the transonic and subsonic data were from the NASA/LRC, 8-ft transonic facility. Second, the Mach number range of Reference 4 was from 0.6 to 4.6, whereas that of Reference 7 was from 0.6 to 3.95. Third, the AOA range of Reference 4 was from 0 to 40, whereas the range of Reference 7 was from 0 to 25 to 30 deg, depending on the Mach number. The nose shape of both bodies were identical, but the Reference 7 tests had an afterbody length 1 in. shorter than that of Reference 4. Hence, Reference 4 data is for a 12.33-caliber body and Reference 7 data is for a 12.0-caliber body. The single wing planform areas of the Reference 4 data base that were tested in conjunction with the body varied in area from 1.125 sq. in. to 18 sq. in., whereas those of Reference 7 varied in area from 2.25 sq. in. to 20.25 sq. in. However, the largest fin of Reference 4 was for aspect ratio of 0.25 and the data base was not complete. Hence, effectively the wing area of the Reference 4 data varied from 1.125 to 9 sq. in.; so, in effect, the wing sizes of the Reference 7 data were about twice the size of those tested in Reference 4. Another major difference was the fact that the wing-alone data used in the AP98 was based primarily on Reference 5 and Reference 14. The Reference 5 data was taken using a sting mount in the tunnel and integrated pressure data. While it is believed the wing alone data base of Reference 5 could be slightly low in some cases because of thickness effects, the author believes this is the best wing-alone data base available. The Reference 7 data for wing-alone aerodynamics was taken based on the same wings of Figure 3 that were tested on the body alone, in contrast to the References 4 and 5 data, where different size wings were tested for wing alone and wing in conjunction with the body data (because of requirements for many pressure taps in the wing-alone measurements). The wing-alone data of Reference 7 was obtained on a splitter plate, versus a sting in the Reference 5 data, and as will be shown later, this mount arrangement apparently caused measurement errors at some conditions. Finally, only two fins were mounted on the body in the $\Phi = 0$ roll orientation in the Reference 7 tests, whereas four fins were mounted on the body in the Reference 4 data base and roll angle was varied as well.

Both data sets (References 4 and 5 and Reference 7) measured aerodynamics for body alone, wing alone, and wing in conjunction with the body. As a result, the approach taken here will be to apply the AP98 methodology directly to the Reference 7 normal force coefficients for body alone, wing alone, and wing in conjunction with the body. Based on comparison of the AP98 to the data, areas where improvements are needed will be identified. Modifications to the

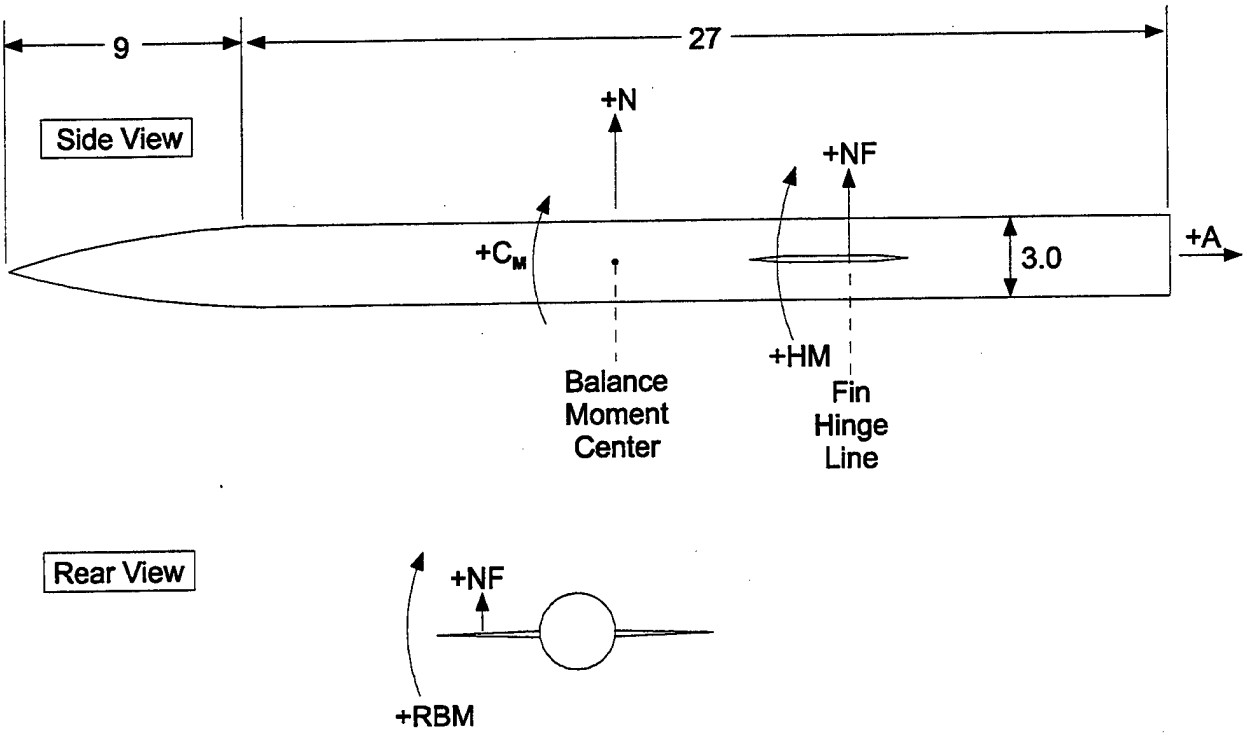

FIGURE 3A. FORCE AND MOMENT SIGN CONVENTIONS OF NASA/MDAC DATA BASE[7]

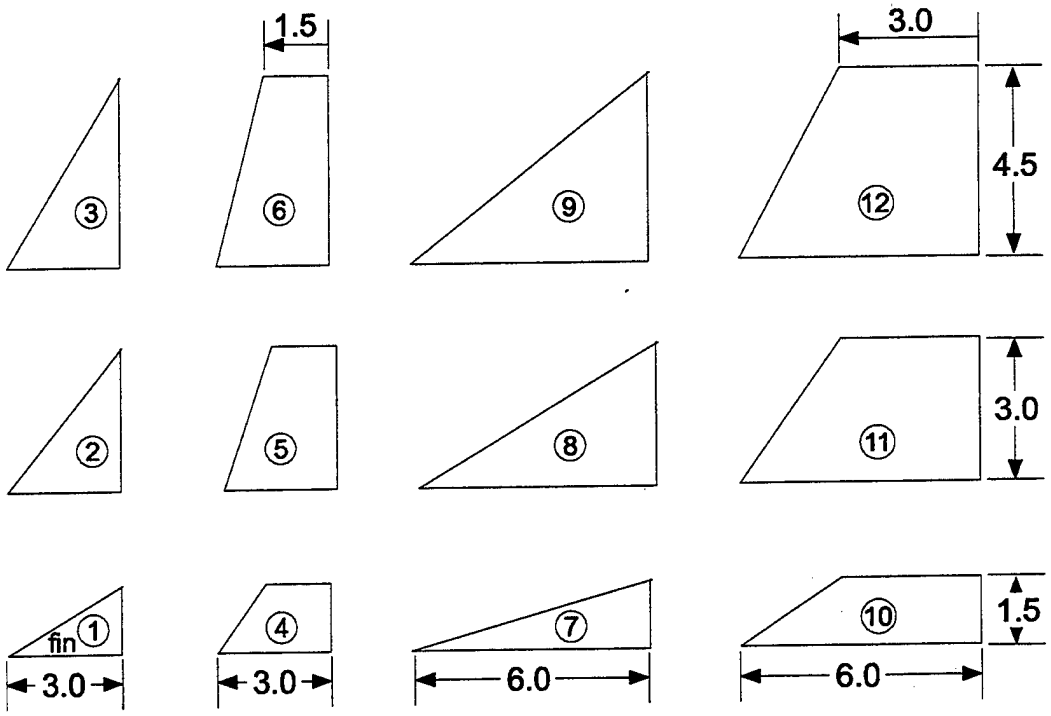

FIGURE 3B. WING PLANFORMS TESTED IN NASA/MDAC DATA BASE[7]
(ALL DIMENSIONS IN INCHES)

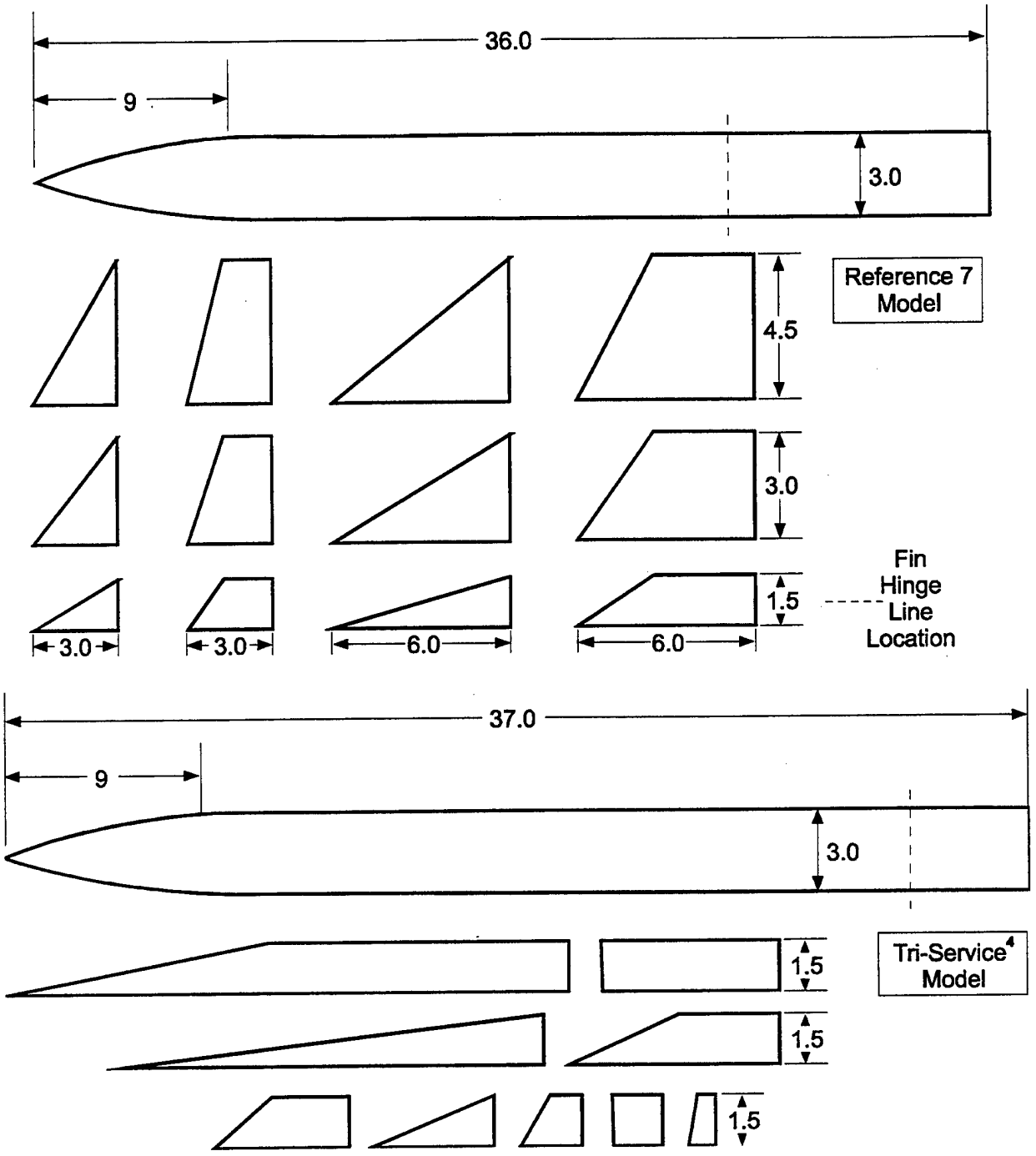

FIGURE 4. SCALED GEOMETRY COMPARISON WITH TRI-SERVICE MODEL[4] AND REFERENCE 7 MODEL

AP98 methodology will then be made. These modifications will then be checked out on the Reference 4 and 7 data bases and then on several missile configurations outside the Reference 4 and 7 data bases. Any fine-tuning necessary in the methodology improvements will be conducted as part of the methodology development process. If the improvements prove to be

effective in an overall sense, the new methodology will be made a part of the next version of the APC, which is scheduled to be released as the AP02.

2.1 BODY-ALONE MODIFICATIONS

The present body-alone static aerodynamics are computed using linearized theories at low AOA and a modified version of the Allen Perkins viscous crossflow for the nonlinear AOA aerodynamic terms. One of the keys in obtaining accurate aerodynamics is in obtaining accurate values of the critical crossflow Reynolds number and Mach number. These parameters are of primary importance at low Mach number. For Mach number 2.0 and greater, they have little influence on the aerodynamic terms. The AP98 currently uses a value of R_{N_c} = 180,000 and M_{N_c} = 0.1 as standard values. However, the user is allowed to change R_{N_c} and M_{N_c} to specified values.

In comparing the AP98 to the body-alone wind tunnel data of Reference 7, good agreement in center of pressure and normal force were obtained. Average errors of normal force were less than 6 percent and center of pressure less than ¼ caliber or 2 percent of the body length. These average errors were calculated using optimum values of the critical crossflow Mach number and Reynolds number, which is quite important for $M_\infty \leq 1.2$ comparisons. R_{N_c} was a constant 330,000, and M_{N_c} varied from 0 at $M_\infty = 0.6$ to 0.06 at $M_\infty = 0.9$. Also, error values were calculated at each 5-deg AOA at all Mach numbers where data was available. This gave a total of 40 data points, sufficiently large to get a good statistical average error.

In viewing the individual comparisons, it was clear that a couple of minor problems existed, which if corrected, could improve these average errors somewhat. The first one has to do with the fact that the current body-alone methodology for implementing compressibility effects into the nonlinear normal force term could be improved upon. The present methodology for the body-alone aerodynamics in the normal plane is:

$$C_{N_B} = C_{N_L} + \eta C_{d_c} \sin^2\alpha \frac{A_P}{A_{ref}} \tag{4A}$$

$$X_{CP} = \frac{(X_{CP})_L C_{N_L} + (X_{CP})_{NL} C_{N_{NL}}}{C_{N_B}} \tag{4B}$$

$$C_{M_B} = -C_{N_B}(X_{CP} - X_O) \tag{4C}$$

In addition, an empirical table of center of pressure shifts was used for the body-alone to partially account for physics not adequately accounted for in the determination of center of pressure. These physics include the following: transonic flow where shock waves can stand on the body, the fact that the linear theory center of pressure does not stay constant as is presently assumed, and the fact that the center of pressure moves in a parabolic fashion (versus a weighted

average as represented by Equation (4)) from its value at $\alpha = 0$ to the centroid of the planform area at a high AOA, say 45 deg.

Three slight changes in the Reference 1 methodology are being implemented as a result of comparisons to the Reference 7 data base. The first has to do with the value of η. η is the normal force of a circular cylinder of given length-to-diameter ratio to that of a circular cylinder of given length. η_0 is the value of η at $M_N = 0$. At present,

$$\begin{aligned} \eta &= \left(\frac{1-\eta_0}{1.8}\right) M_N + \eta_0 \quad \text{for } M_N < 1.8 \\ &= 1 \qquad\qquad\qquad\quad \text{for } M_N \geq 1.8 \end{aligned} \tag{5}$$

Also, η is automatically set to one if $M_\infty \geq 2.75$. This last condition, where η is automatically set to one, appears not to be necessary. In other words, Equation (5) is allowed to be the sole determination of the value of η. This change mainly affects normal force results for conditions just above the cutoff Mach number of 2.75. Figures 5 and 6 compare the revised methodology of removing the $\eta = 1$ for $M_\infty > 2.75$ condition and using only Equation (5) for normal force, versus the current AP98 approach. Figure 5 is the Reference 7 data base and Figure 6 is the Reference 4 data base. Results are shown only for Mach numbers above 2.75. Both normal force coefficient and center of pressure are given. Note that the revised method, which will be incorporated as a part of the AP02, shows improvement in comparison to both the Reference 7 and Reference 4 data base. The average 6 percent error of the AP98 compared to the Reference 7 data base is reduced to an average error of about 4 percent. Also, some improvement in the average error comparisons of the Reference 4 data base is obtained, although this error was not calculated.

The second change implemented as a result of the Reference 7 data base has to do with the empirical table for center of pressure shifts. Some shift changes were implemented, which mainly affect results in the transonic region for lower AOAs. The Reference 7 data base had Mach 0.9 data available, which allowed the results of Reference 1 to be improved upon somewhat. These modified results are shown in Table 1. They result in some slight improvement in the average center of pressure error for the Reference 1 data base from about 0.25 caliber to 0.2 caliber. The 0.2 caliber error is an average error of about 1.6 percent of the body length.

The third body-alone change has to do with the way the linear and nonlinear terms of Equation (3) are treated as α increases above 30 deg. The AP98 methodology assumes

$$\begin{aligned} C_{N_L} &= \left(C_{N_\alpha}\right)\alpha; \alpha \leq 30 \\ C_{N_L} &= \left(C_{N_L}\right)_{\alpha=30}\left(1-\frac{\alpha-30}{60}\right); 30 < \alpha \leq 90 \end{aligned} \tag{6}$$

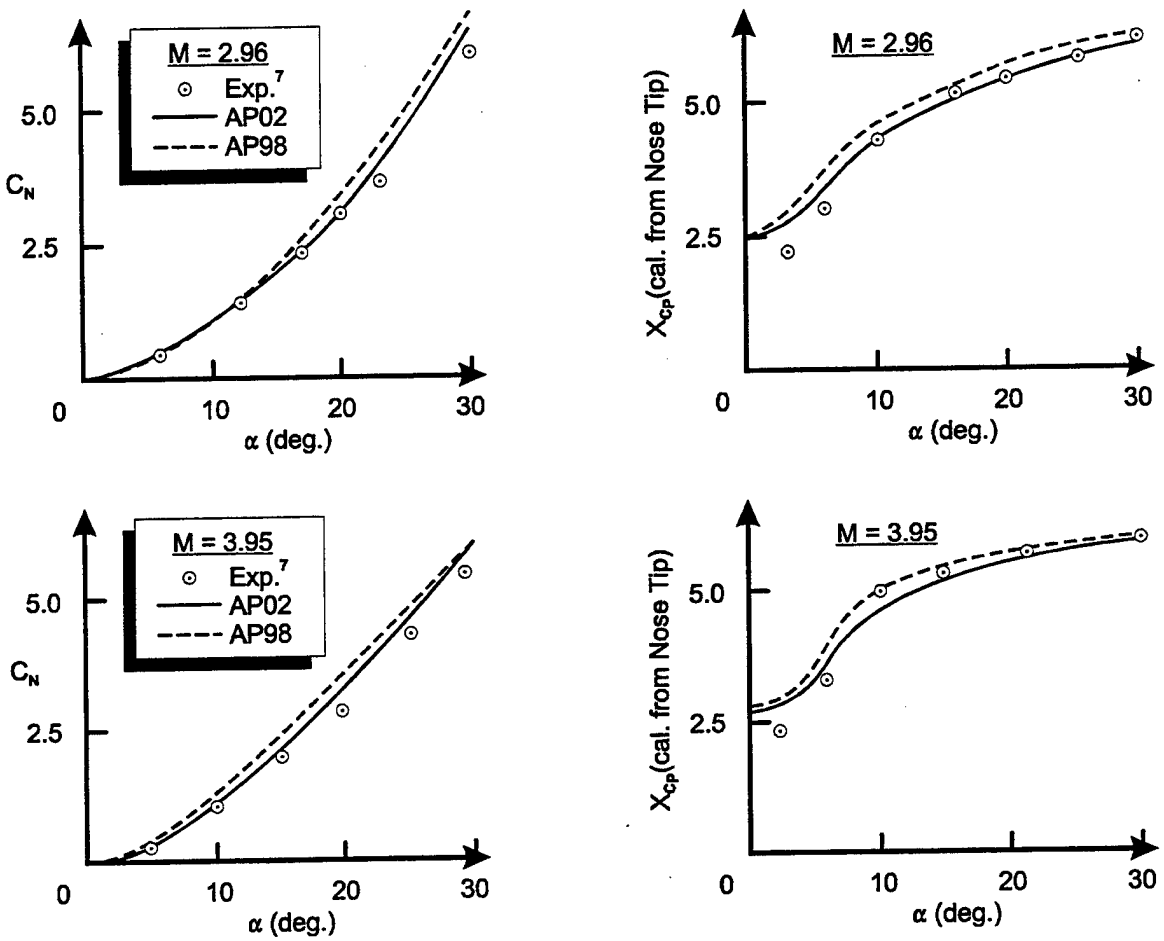

FIGURE 5. COMPARISON OF MODIFIED BODY-ALONE AERODYNAMICS METHOD TO EXPERIMENT FOR FIGURE 3A CASE

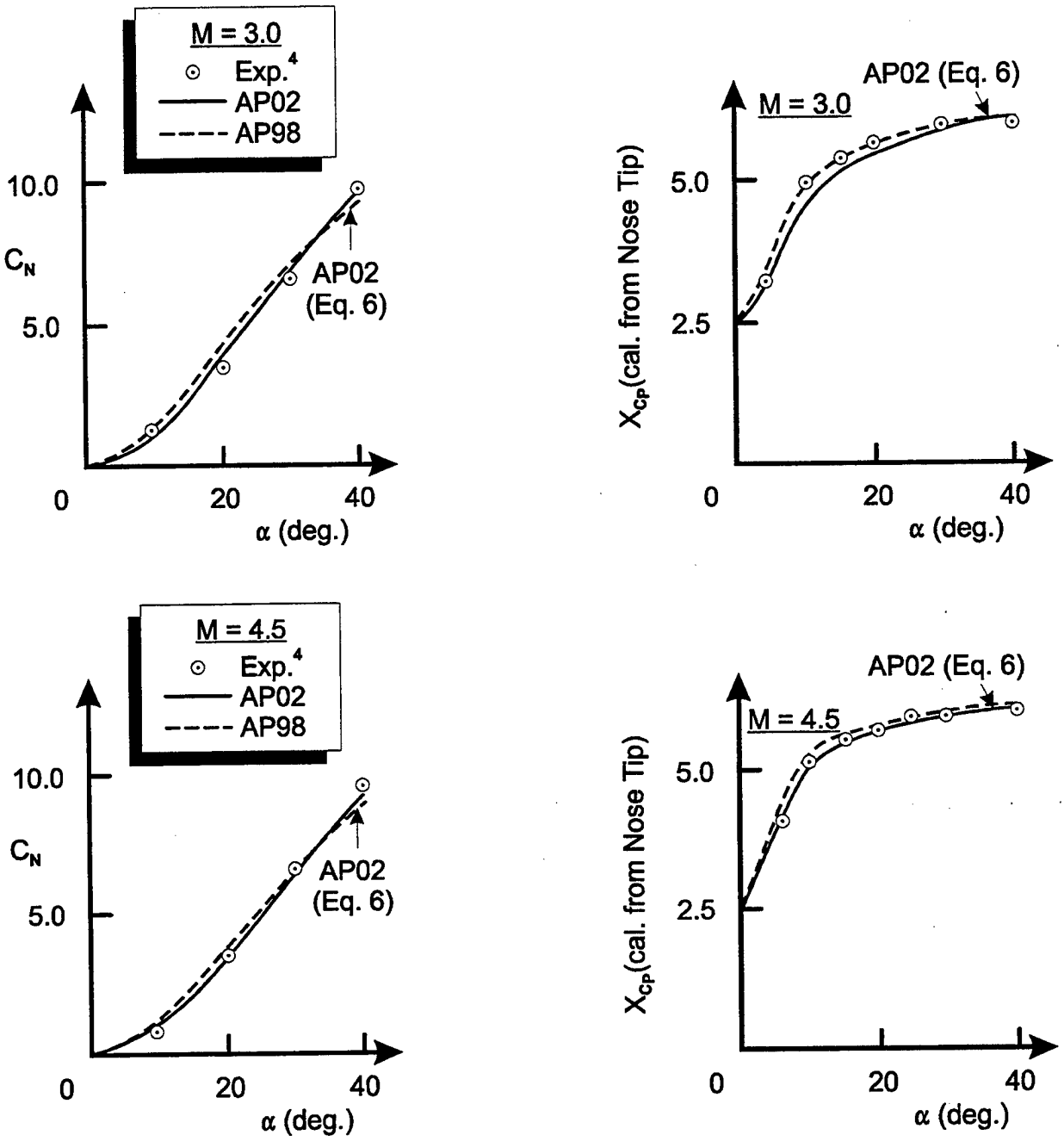

FIGURE 6. COMPARISON OF MODIFIED BODY-ALONE AERODYNAMICS METHOD TO EXPERIMENT FOR FIGURE 2A CASE

TABLE 1. SHIFT IN BODY-ALONE CENTER OF PRESSURE AS A FUNCTION OF MACH NUMBER AND AOA (AS A FRACTION OF BODY LENGTH)

M \ α	0	10	20	30	40	50	60	70	80	90
0.00	0.00	0.025	0.02	0.000	-0.025	-0.040	-0.040	-0.030	-0.010	0.00
0.20	0.00	0.025	0.02	0.005	-0.025	-0.040	-0.045	-0.030	-0.010	0.00
0.40	0.00	0.03	0.025	0.005	-0.025	-0.040	-0.050	-0.030	-0.015	0.00
0.60	0.00	0.03	0.025	0.00	-0.035	-0.055	-0.070	-0.050	-0.030	0.00
0.80	0.00	0.030	0.020	-0.025	-0.050	-0.070	-0.070	-0.050	-0.015	0.00
0.90	0.00	0.030	0.020	-0.02	-0.050	-0.070	-0.070	-0.040	-0.015	0.00
1.00	0.00	0.02	-0.01	-0.02	-0.040	-0.040	-0.040	-0.030	-0.005	0.00
1.15	0.00	0.02	-0.01	-0.02	-0.020	-0.025	-0.030	-0.025	-0.005	0.00
1.30	0.00	0.02	-0.01	-0.01	-0.010	-0.010	-0.010	-0.005	0.000	0.00
1.50	0.00	0.02	-0.01	0.000	0.000	0.000	-0.010	-0.005	0.000	0.00
2.00	0.00	0.02	0.02	0.020	0.015	0.010	0.005	0.000	0.000	0.00
2.50	0.00	0.02	0.02	0.02	0.015	0.010	0.005	0.000	0.000	0.00
5.99	0.00	0.02	0.02	0.02	0.015	0.010	0.005	0.000	0.000	0.00
≥6.00	0.00	0.02	0.02	0.02	0.015	0.01	0.005	0.000	0.000	0.00

As seen in Figure 5, which shows comparisons up to 40 deg AOA, Equation (6) yields results that are slightly low compared to data for $\alpha > 30$ deg. In reality, the linear term does not decay in the fashion of Equation (6), but is probably more parabolic in nature. A better representation of the physics is therefore assumed to be

$$
\begin{aligned}
C_{N_L} &= \left(C_{N_\alpha}\right)\alpha;\ \alpha \le 30^\circ \\
C_{N_L} &= \left(C_{N_L}\right)_{\alpha=30}\ 30^\circ < \alpha \le 45^\circ \\
C_{N_L} &= \left(C_{N_L}\right)_{\alpha=30}\left(1-\frac{\alpha-45}{45}\right);\ 45 < \alpha \le 90^\circ
\end{aligned}
\qquad (7)
$$

Equation (7) provides some additional slight improvements in body-alone normal force and center of pressure for $\alpha > 30$ deg. These slight improvements are shown on Figure 6 as "AP02." The results using Equation (6) are noted as "AP02 (Eq. 6)." It is somewhat hard to distinguish the values of the AP02 from the "AP02 (Eq. 6)" in Figure 6 because of the scale. As an example, for $M_\infty = 3.0$, $\alpha = 40$ using Equation (7) (which is denoted as "AP02"), $C_N = 9.38$, whereas when Equation (6) is used, "AP02 (Eq. 6)," $C_N = 9.1$. These values compare to the experimental data value of 9.4. The center of pressure is 6.2 calibers from the nose tip with Equation (7) and 6.3 calibers with Equation (6). The experimental data is 6.2 calibers. Similar improvements of using Equation (7) versus Equation (6) are found at $M_\infty = 4.5$ of Figure 6.

2.2 WING-ALONE MODIFICATIONS

The wing-alone methodology of Reference 1 assumed the wing-alone normal force could be predicted from a fourth-order equation in AOA. That is, assuming no wing camber,

$$C_{N_w} = a_1\alpha_w + a_2\alpha_w^2 + a_3\alpha_w^3 + a_4\alpha_w^4 \tag{8A}$$

$$a_2 = 34.044\,(C_N)_{\alpha=15^\circ} - 4.824\,(C_N)_{\alpha=35^\circ} + 0.426\,(C_N)_{\alpha=60^\circ} - 6.412a_1 \tag{8B}$$

$$a_3 = -88.240\,(C_N)_{\alpha=15^\circ} + 23.032\,(C_N)_{\alpha=35^\circ} - 2.322\,(C_N)_{\alpha=60^\circ} + 11.464a_1 \tag{8C}$$

$$a_4 = 53.219\,(C_N)_{\alpha=15^\circ} - 17.595\,(C_N)_{\alpha=35^\circ} + 2.661\,(C_N)_{\alpha=60^\circ} - 5.971a_1 \tag{8D}$$

The term a_1 of Equation (8) is the value of wing-alone lift curve slope at $\alpha = 0$ given by linear theory. The terms $(C_N)_{\alpha=15^\circ}$, $(C_N)_{\alpha=35^\circ}$, and $(C_N)_{\alpha=60^\circ}$ are values of the wing-alone normal force coefficients at $\alpha = 15$, 35, and 60 deg, respectively, defined by the data bases of References 5, 6, and 14. Above α_w of 60 deg, extrapolation of the aerodynamics at α_w of 60 deg is used. For more details of the method, the reader is referred to Reference 15.

The center of pressure of the wing-alone and wing-body normal force is assumed to vary in a quadratic fashion between its linear theory value near $\alpha = 0$ and the centroid of the planform area at $\alpha = 60$ deg. If A and B are the centers of pressure of the linear and nonlinear normal force terms (in percent of mean geometric chord), and $\alpha_W = \alpha + \delta$, then the center of pressure of the wing-body or wing-alone lift is

$$(X_{CP})_{WB} = (X_{CP})_W = A + \frac{1}{36}|\alpha_W|\,(B-A) + \frac{1}{5400}\alpha_W^2\,(A-B) \tag{9}$$

Equation (9) is the methodology used for roll position of 0 deg. For roll position of 45 deg, an equation for a center of pressure shift was derived in Reference 16 to account for the difference in load on the windward and leeward planes. This shift is added to Equation (9) for the roll position of $\Phi = 45$ deg and is

$$(\Delta X_{CP})_{WB} = -\left[r + \left(\frac{b}{c_r + c_t}\right)\left(\frac{c_r}{2} - \frac{c_t}{3}\right)\right]\cos(\Phi)^2\,\sin(2\alpha)\left(\frac{0.8\alpha}{65}\right);\ \alpha \le 65 \tag{10A}$$

$$= -0.8\left[r + \left(\frac{b}{c_r + c_t}\right)\left(\frac{c_r}{2} - \frac{c_t}{3}\right)\right]\cos\Phi^2\,\sin(2\alpha);\ \alpha > 65^\circ \tag{10B}$$

Equations (10A) and (10B) contain a correction to the original center of pressure shift derived in Reference 16. This change is the square of the cos (Φ) term in Equation (10), whereas in Reference 16, the cos (Φ) term was to the first power. The reason for the square is the fact that the cos (Φ) term does two things. First, it rotates the normal force to a plane normal to the

body axis as opposed to being normal to the wing. Second, the cos (Φ) term rotates the radius vector to the lateral center of pressure of the wing from the Φ roll position to the horizontal plane. Reference 16 omitted this last rotation, causing a slightly more forward center of pressure shift at roll than was warranted. As already mentioned, one of the keys to the Reference 1 method was the development of the wing-alone normal force coefficient tables for values of α_W of 15, 35, and 60 deg.

The NASA/MDAC[7] wing-alone data base had, in principle, a couple of advantages over the data bases used to develop the wing-alone tables at α = 15, 35, and 60 deg used in the wing-alone prediction methodology of the AP98.[1] First of all, the Reference 7 data base measured wing-alone data for α = 0 to 90 deg and from M_∞ = 0.6 to 4.0. The data bases comprising the tables in Reference 1 consisted of several different sets of data (see References 5, 6, and 14) to cover the Mach number range of interest. In some cases, data from References 5, 6, and 14 was available only to 60 deg AOA, and in some data bases, the data tended to give a stall effect at higher AOA and so was not useable. On the other hand, data from Reference 7 was more limited in wing planforms considered than in some of the other data bases (References 5, 6, and 14).

As a result of the new data base from Reference 7, it was decided to compare the Reference 7 data base to the AP98 tables as well as the Stallings data,[5] which the author still believes is the best wing-alone data base available. Comparisons were made as a function of AOA, aspect ratio, Mach number, and taper ratio. Figures 7 and 8 compare the results of the Stallings data base[5] and the recent NASA/MDAC[7] data base at Mach numbers of 1.6 and 4.0, respectively, for fins 7 and 8 of Reference 7. Fin 7 is of aspect ratio 1.0 with taper ratio 0, and has a semispan of 1.5 in., whereas fin 8 is of aspect ratio 2, taper ratio 0, and semispan 3.0 in. Also shown on the figures are the results from the AP98 method and revisions to the wing-alone tables to be incorporated in the AP02. Several points are worthy of note. First of all, at both M = 1.6 and M = 4.0, the Reference 7 and 5 data are in excellent agreement for fin 8 up to AOA of 40 to 45 deg. Above α = 45 deg, the Reference 7 data stalls. Also, the Reference 7 data is consistently about 10 percent lower than the Reference 5 data for fin 7 at M = 1.6 and 4.0. It is theorized that since the Reference 7 data was taken with a splitter plate and Reference 5 with a sting, the differences in the data are due to the measurement. It is suspected that for the lower semispan, boundary layer buildup ahead of the fin on the splitter plate is the source of the 10 percent lower value of C_{N_w} of Reference 7 data compared to Reference 5. In other words, for small span wings, the lower dynamic pressure due to the boundary layer near the root chord has more of an effect than for the larger span wings. This effect is magnified for small taper ratios since the wing cross-sectional area is the largest at the root chord. It is not known why the flow stalls above about 45 deg for the splitter plate results. However, this was the case for most of the Reference 7 results. As a result of these two phenomena, it was decided to use considerable judgement before using any of the Reference 7 results for the 1.5 in. semispan or for any span above α = 45 deg. The final point to be made in viewing Figures 7 and 8 is that the revised values of C_{N_w}, which will be incorporated into the AP02, are closer to the Stallings[5] data than the AP98. The AP98 had intentionally increased the values of C_{N_w} somewhat to account for the fact that the Stallings data was taken on fairly thick wings in order to accommodate many pressure taps. It was theorized that these thick wings would lower C_{N_w} unrealistically. The revised data decreases this thickness penalty and is therefore much closer to the Stallings data.

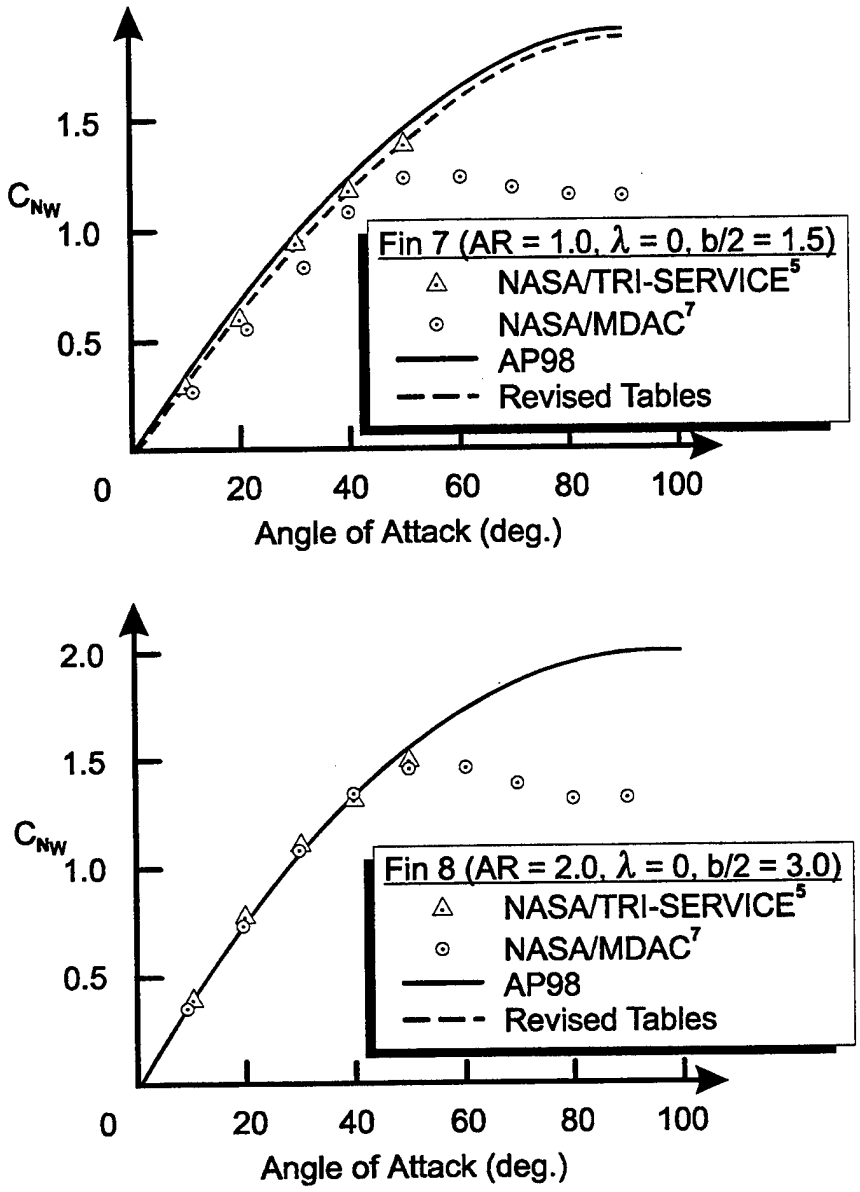

FIGURE 7. COMPARISON OF NASA/MDAC[7] WING-ALONE DATA BASE TO THAT OF STALLINGS[5] (M = 1.6)

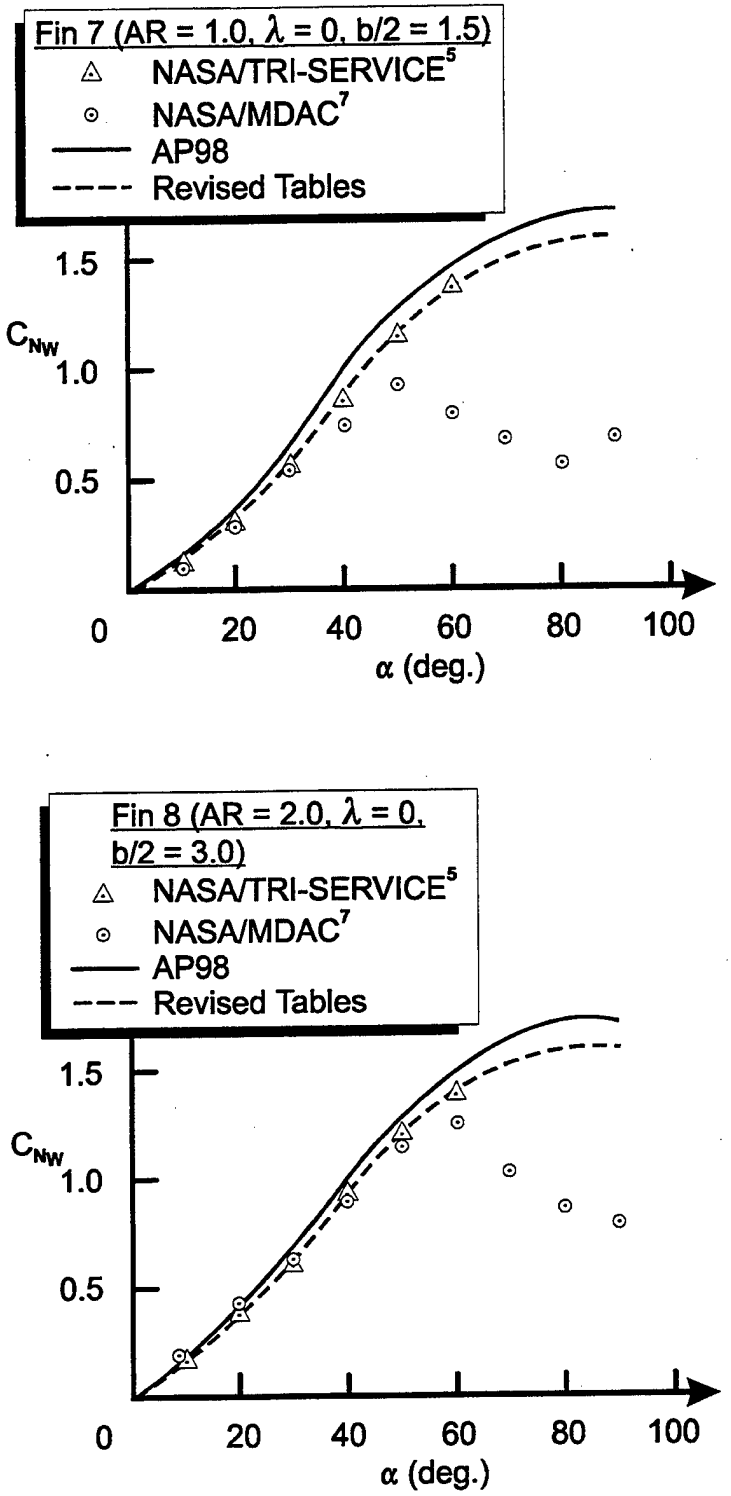

FIGURE 8. COMPARISON OF NASA/MDAC[7] WING-ALONE DATA BASE TO THAT OF STALLINGS[5] (M = 4.0)

After analyzing the data bases of References 5, 7, and 14 through plots of C_{N_w} versus Mach number, C_{N_w} versus AOA, and C_{N_w} versus aspect ratio, general ground rules were reached on how to revise the AP98 wing-alone tables based on the new Reference 7 data base. These ground rules are listed in Table 2. As a result of the logic in Table 2, only slight changes were made in the AP98 wing-alone tables.

TABLE 2. GROUND RULES FOR USING NASA/MDAC[7] WING-ALONE DATA TO REVISE AP98[1] TABLES

1. Use data above $\alpha = 45$ deg with caution, because of inconsistency with Stallings data at $M \geq 1.6$ (caused by stall effect in Reference 7 data).
2. Ignore data on two smallest fins; boundary layer effects apparently decreased C_{N_w} compared to Stallings data.
3. If Stallings and NASA/MDAC data are both available, put more weight on Stallings data base.
4. At $M = 1.6$, Stallings data was extrapolated from $\alpha = 50$ deg to $\alpha = 60$ deg. Hence, we modified data slightly lower in most cases. However, for $M > 1.6$, data was available to $\alpha = 60$ deg.
5. Revise $\lambda = 1.0$ in analogy to $\lambda = 0$ and 0.5 for MDAC data and previous tables since $\lambda = 1.0$ data was not available from NASA/MDAC wind tunnel test.

The data of Reference 7 was for aspect ratios of 0.67, 1.33, 2.0, 3.0, 4.0, and 6.0, whereas that of Reference 5 was for aspect ratios of 0.5, 1.0, 2.0, and 4.0.

The final revised set of wing-alone tables is given as Tables 3 through 5. These tables will be a part of the AP02 and will replace those currently used in the AP98. These tables are shown plotted in Figures 9 through 11 for taper ratios of 0, 0.5, and 1.0 as a function of aspect ratio and Mach number. As already mentioned, values shown here are close, but slightly different than those used for the AP98.

2.3 REFINEMENTS FOR WING-BODY AND BODY-WING INTERFERENCE FACTOR NONLINEARITIES

This section of the report will consider refinements in the empirical factors used to model the nonlinearities in the wing-body and body-wing interference factors due to AOA. No changes will be made in the nonlinear empirical constants associated with the interference factors due to control deflection, since the Reference 7 data base did not consider control deflection as a parameter. Also, the focus here will be on the roll orientation of $\Phi = 0$ deg (fins in plus "+" roll orientation). However, when changes are made in the empirical constants for $\Phi = 0$ deg, the constants for $\Phi = 45$ deg will be considered for change in a complementary way to the $\Phi = 0$ deg results.

TABLE 3. VALUES OF $(C_{N_W})_{\alpha=15°}$

ASPECT RATIO	TAPER RATIO	MACH NUMBER									
		0	0.6	0.8	1.0	1.2	1.6	2.0	3.0	4.5	≥6.0
≤0.1	0.0	.18	.18	.18	.225	.24	.24	.21	.17	.14	.11
	0.5	.19	.19	.19	.225	.24	.24	.21	.17	.14	.11
	1.0	.19	.19	.19	.225	.24	.24	.21	.17	.14	.11
0.5	0.0	.28	.29	.30	.32	.32	.32	.30	.24	.18	.16
	0.5	.39	.41	.415	.43	.43	.45	.38	.30	.22	.19
	1.0	.34	.34	.36	.42	.42	.43	.37	.30	.22	.19
1.0	0.0	.43	.44	.46	.50	.54	.46	.42	.32	.22	.18
	0.5	.47	.50	.55	.65	.66	.58	.45	.34	.24	.21
	1.0	.46	.48	.52	.58	.60	.54	.45	.35	.26	.22
2.0	0.0	.55	.59	.65	.72	.70	.62	.50	.34	.27	.23
	0.5	.56	.59	.66	.76	.80	.68	.54	.40	.30	.27
	1.0	.65	.66	.71	.75	.80	.67	.54	.40	.29	.27
≥4.0	0.0	.65	.66	.71	.79	.83	.70	.59	.39	.31	.26
	0.5	.69	.71	.75	.88	.91	.75	.69	.45	.32	.29
	1.0	.69	.71	.75	.88	.91	.75	.67	.45	.31	.29

TABLE 4. VALUES OF $(C_{N_W})_{\alpha=35°}$

ASPECT RATIO	TAPER RATIO	MACH NUMBER									
		0	0.6	0.8	1.0	1.2	1.6	2.0	3.0	4.5	≥6.0
≤0.1	0.0	1.13	1.13	1.13	1.03	.92	.76	.65	.59	.53	.50
	0.5	.97	1.0	1.0	1.0	.95	.86	.75	.69	.60	.56
	1.0	.97	1.0	1.0	1.0	.97	.91	.8	.74	.65	.62
0.5	0.0	1.10	1.1	1.1	1.03	1.01	.95	.85	.72	.66	.62
	0.5	1.10	1.13	1.16	1.28	1.25	1.12	.95	.80	.72	.70
	1.0	1.06	1.08	1.13	1.19	1.22	1.15	1.0	.82	.70	.68
1.0	0.0	1.23	1.23	1.24	1.25	1.19	1.10	.99	.82	.72	.70
	0.5	1.26	1.28	1.30	1.33	1.40	1.20	1.0	.85	.78	.75
	1.0	1.22	1.24	1.26	1.29	1.36	1.20	1.08	.90	.78	.74
2.0	0.0	.99	1.01	1.13	1.20	1.28	1.18	1.05	.90	.76	.72
	0.5	1.00	1.07	1.18	1.31	1.41	1.28	1.18	.98	.84	.80
	1.0	.98	1.05	1.17	1.23	1.34	1.26	1.13	.97	.85	.80
≥4.0	0.0	.97	1.05	1.17	1.20	1.33	1.20	1.10	.95	.82	.78
	0.5	1.03	1.08	1.22	1.30	1.40	1.30	1.22	1.02	.89	.85
	1.0	1.03	1.09	1.21	1.3	1.4	1.3	1.22	1.02	.89	.85

TABLE 5. VALUES OF $(C_{N_W})_{\alpha=60°}$

ASPECT RATIO	TAPER RATIO	MACH NUMBER									
		0	0.6	0.8	1.0	1.2	1.6	2.2	3.0	4.5	≥6.0
≤0.5	0.0	1.10	1.11	1.15	1.26	1.33	1.37	1.45	1.4	1.35	1.3
	0.5	1.34	1.35	1.4	1.45	1.52	1.56	1.48	1.43	1.39	1.36
	1.0	1.29	1.30	1.32	1.37	1.47	1.52	1.48	1.44	1.39	1.36
1.0	0.0	1.44	1.46	1.49	1.53	1.56	1.61	1.57	1.44	1.37	1.34
	0.5	1.40	1.42	1.45	1.53	1.58	1.70	1.59	1.48	1.42	1.38
	1.0	1.33	1.34	1.35	1.44	1.62	1.72	1.58	1.47	1.40	1.37
2.0	0.0	1.32	1.33	1.36	1.48	1.59	1.74	1.68	1.47	1.38	1.35
	0.5	1.30	1.31	1.37	1.48	1.63	1.8	1.76	1.56	1.46	1.43
	1.0	1.30	1.31	1.37	1.48	1.63	1.76	1.73	1.53	1.46	1.43
≥4.0	0.0	1.27	1.28	1.37	1.50	1.64	1.80	1.70	1.49	1.4	1.37
	0.5	1.31	1.32	1.40	1.5	1.64	1.8	1.77	1.56	1.5	1.46
	1.0	1.31	1.32	1.40	1.5	1.64	1.78	1.75	1.55	1.48	1.45

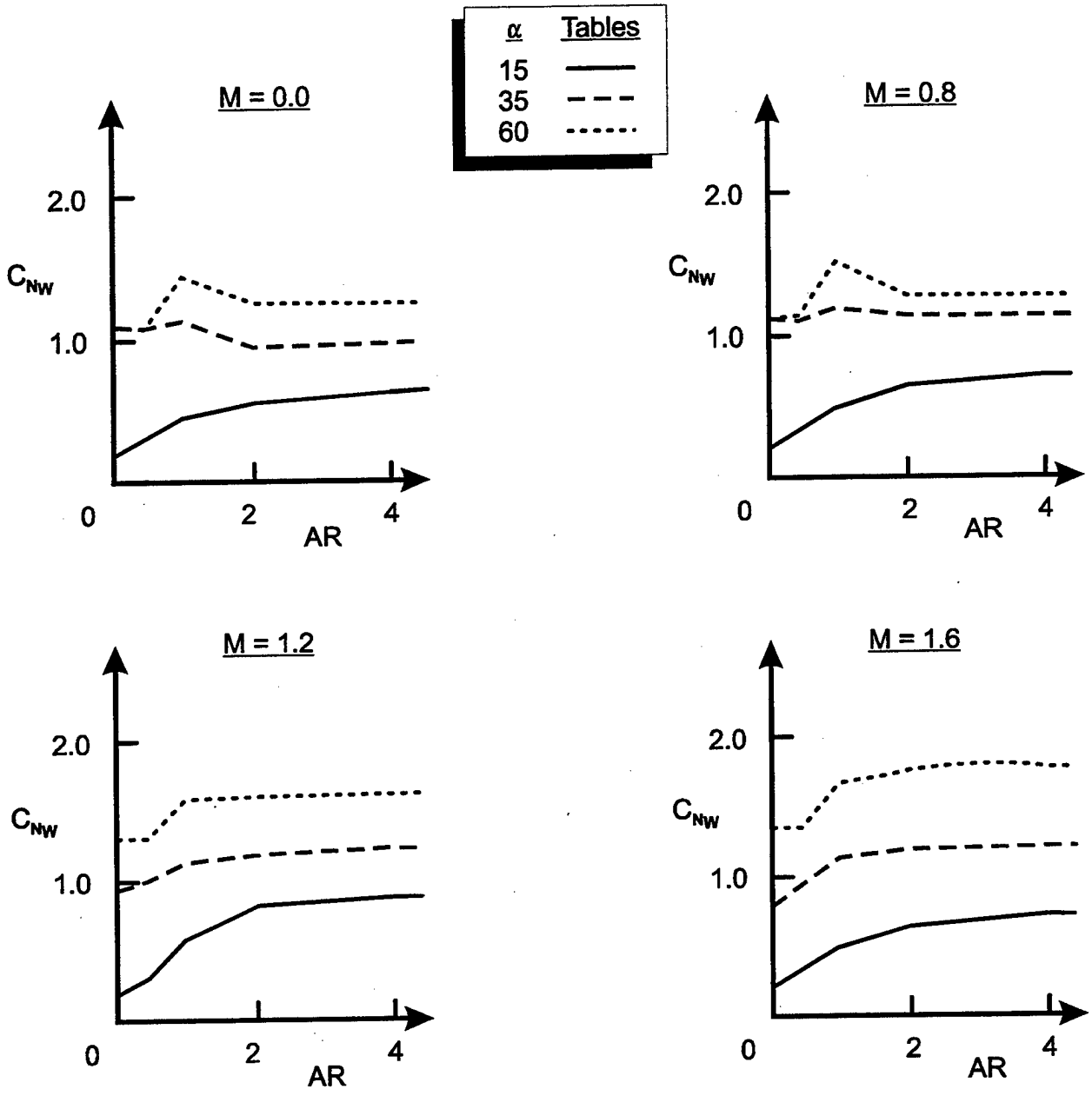

FIGURE 9. REVISED WING-ALONE DATA BASE ($\lambda = 0$)

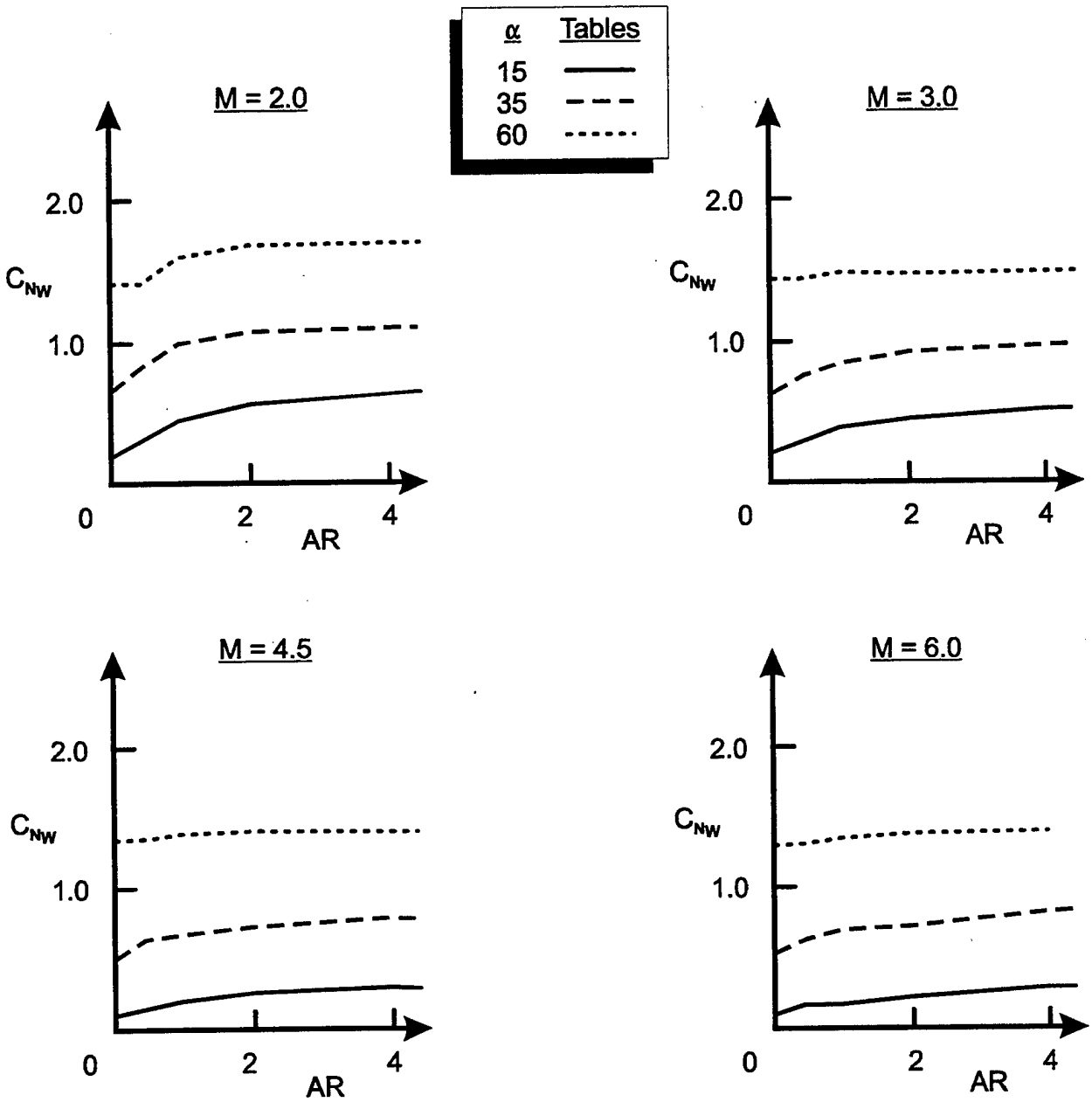

FIGURE 9. REVISED WING-ALONE DATA BASE ($\lambda = 0$) (Continued)

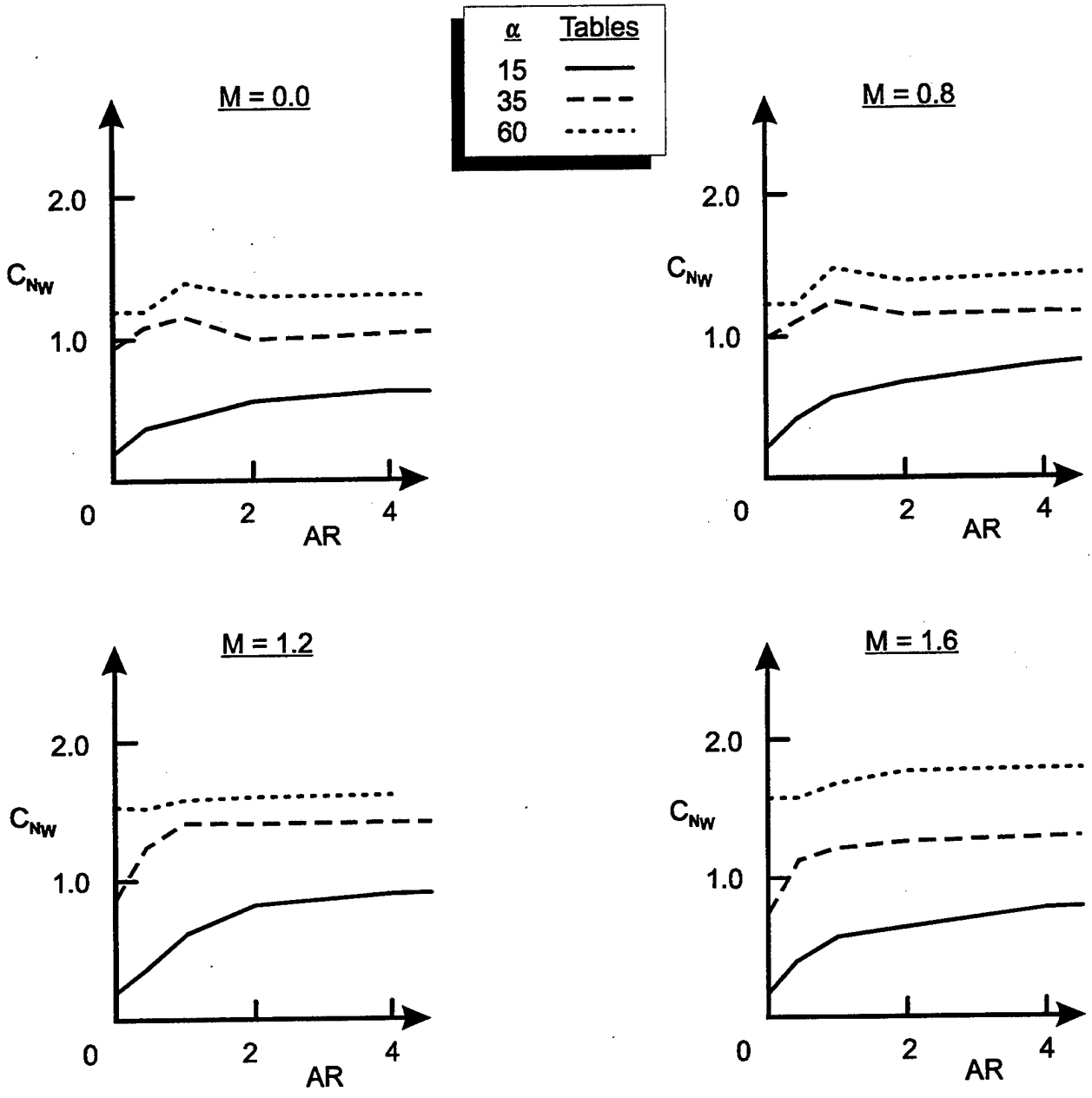

FIGURE 10. REVISED WING-ALONE DATA BASE ($\lambda = 0.5$)

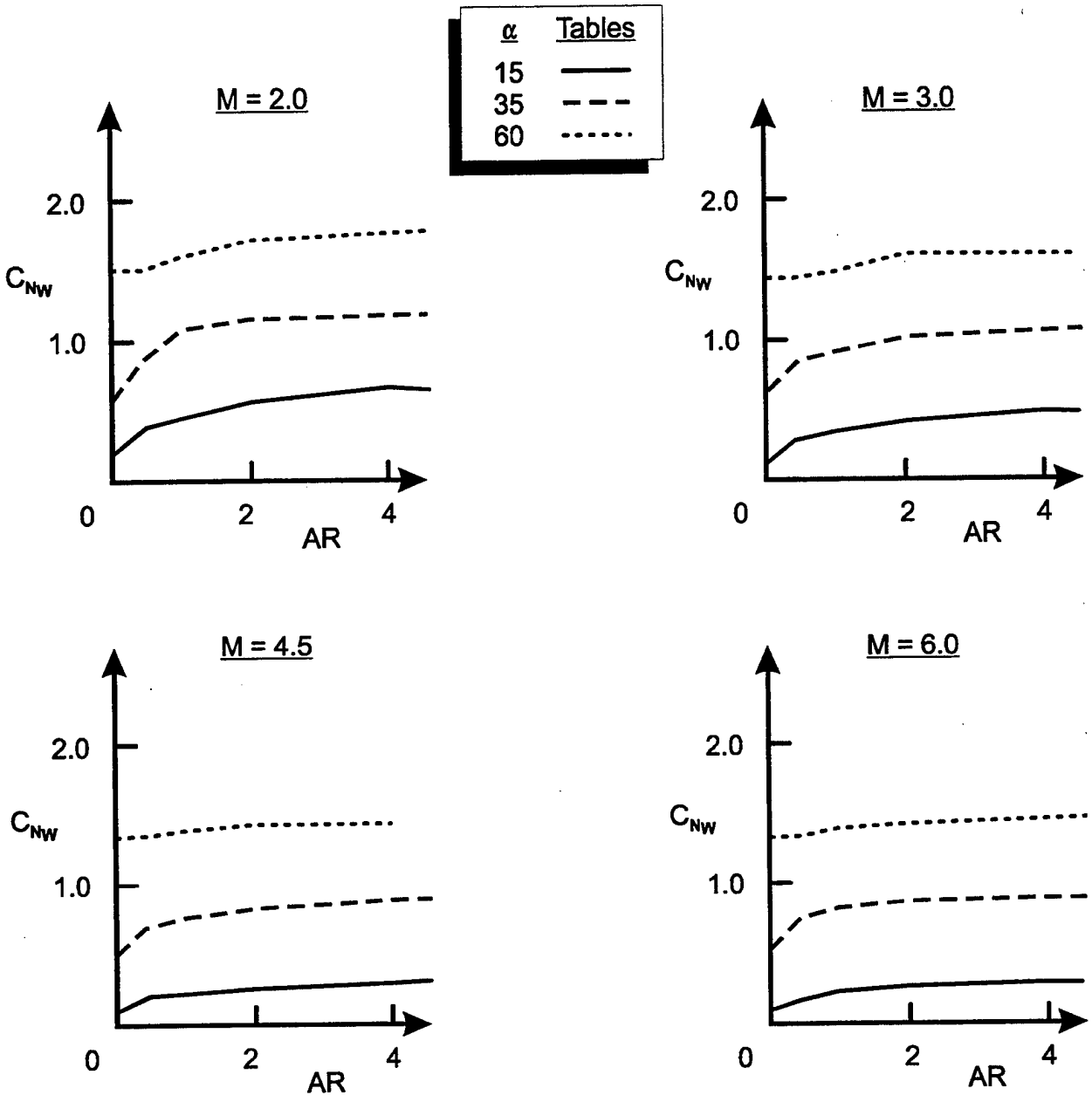

FIGURE 10. REVISED WING-ALONE DATA BASE ($\lambda = 0.5$) (Continued)

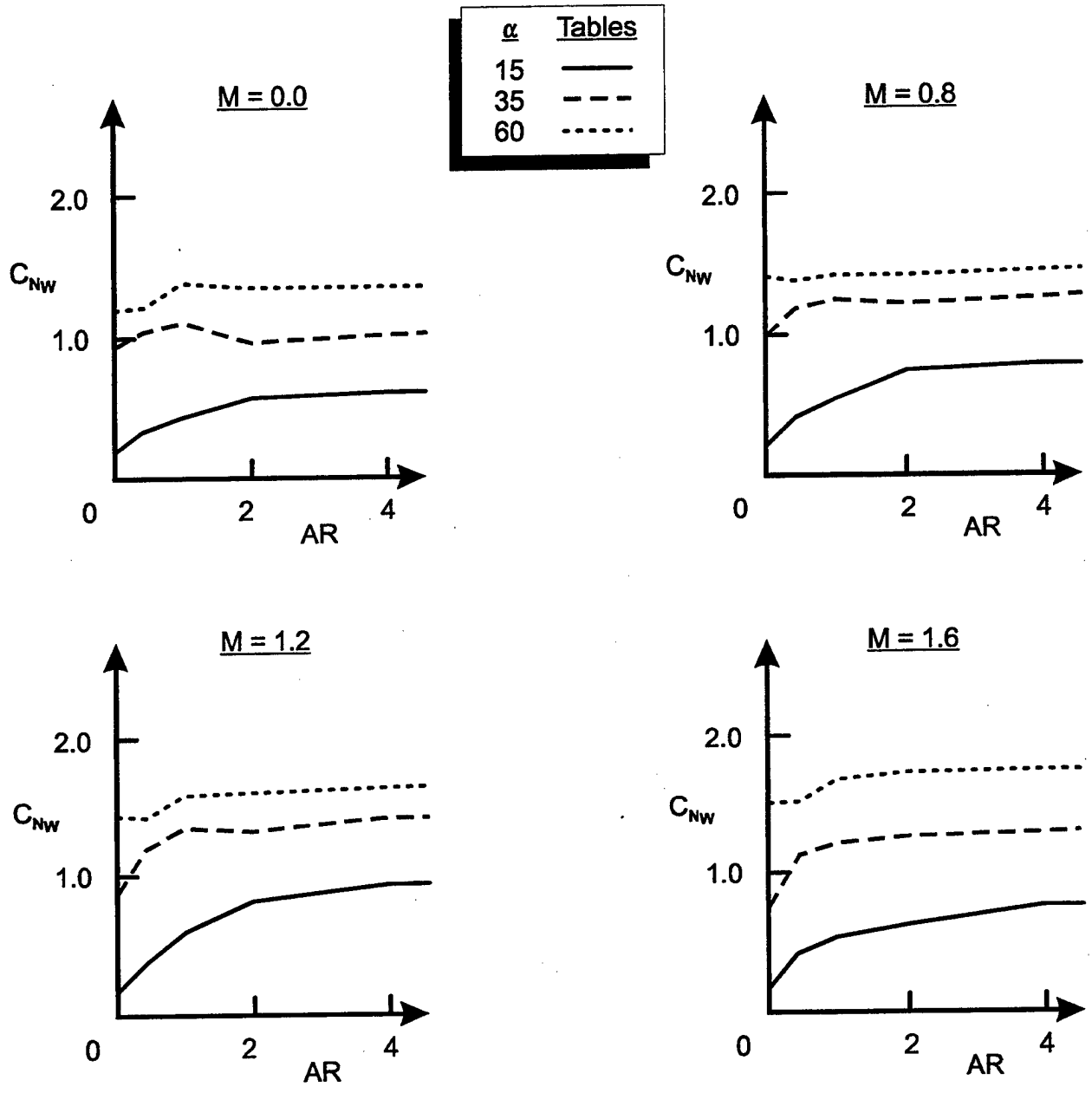

FIGURE 11. REVISED WING-ALONE DATA BASE ($\lambda = 1.0$)

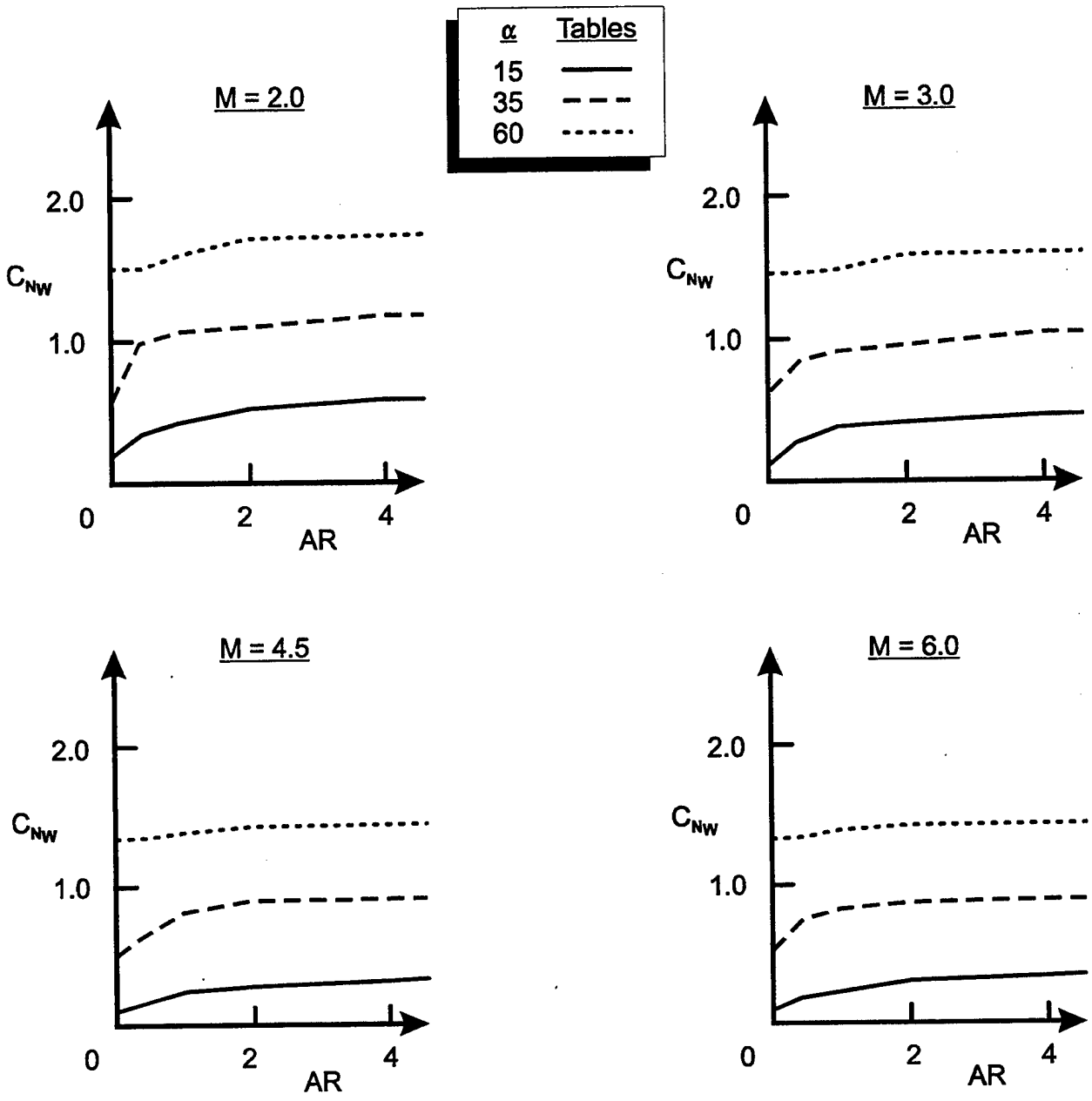

FIGURE 11. REVISED WING-ALONE DATA BASE ($\lambda = 1.0$) (Continued)

To better understand the interference lift components, it is instructive to examine the total normal force of a configuration as defined by Pitts et al.[12] This is given by

$$C_N = C_{N_B} + \left[\left(K_{W(B)} + K_{B(W)}\right)\alpha + \left(k_{W(B)} + k_{B(W)}\right)\delta_W\right]\left(C_{N_\alpha}\right)_W + \left[\left(K_{T(B)} + K_{B(T)}\right)\alpha + \left(k_{T(B)} + k_{B(T)}\right)\delta_T\right]\left(C_{N_\alpha}\right)_T + C_{N_{T(V)}} + C_{N_{B(V)}} \quad (11)$$

The first term in Equation (11) is the normal force of the body alone, including the linear and nonlinear components; the second term is the contribution of the wing (or canard), including interference effects and control deflection; the third term is the contribution of the tail, including interference effects and control deflection; and the last terms are the negative downwash effect on the tail or body due to wing-shed or body-shed vortices. The K's represent the interference of the configuration with respect to AOA, and the k's represent the interference with respect to control deflection. Each of these interference factors is estimated by slender body or linear theory. As such, they are independent of AOA.

The terms that will be considered in this report for refinements are $K_{W(B)}$, $K_{B(W)}$, $K_{T(B)}$ and $K_{B(T)}$. These four interference factors are defined in the general form

$$K = K_{\substack{SBT \\ LT}} + \Delta K(M_\infty, \alpha, AR, \lambda) \tag{12}$$

The first term of Equation (12) is defined by linear theory or slender body theory, whereas the second term is defined by utilizing several large wind tunnel data bases to back out the nonlinearities as a function of Mach number, angle of attack, aspect ratio and taper ratio. The general nonlinear trend of those two interference terms is shown in Figure 12. This general trend is basically the same for both the $\Phi = 0$ and $\Phi = 45$ deg roll orientations. However, the five tables of data that define the empirical constants in the equations of Figure 12 are different for $\Phi = 0$ and $\Phi = 45$ deg for both $K_{W(B)}$ and $K_{B(W)}$. As already discussed, for cruciform missiles, SBT gives no roll independence for low AOA values of $K_{W(B)}$ and $K_{B(W)}$.

As seen in Figure 12, $K_{W(B)}$ in general can deviate slightly from SBT or LT near AOA of 0 deg. It then decreases until it reaches a minimum value and then approaches a value of 1.0 at high AOA. On the other hand, $K_{B(W)}$ can either increase or decrease past AOA of 0 deg. Eventually, it also decreases until it reaches some minimum value at high AOA. The physics of what occurs in this nonlinear behavior and the details of the interference factor nonlinearities are given in References 13 and 16. For ease of reference for the reader, a brief discussion of the physics of the flow that underlies Figure 12 will be given here.

In examining the nonlinear models for $K_{W(B)}$ and $K_{B(W)}$ of Figure 12, it is instructive to try to correlate the mathematical models with the physics of the flow. The wing-body interference factor is somewhat easier to understand than the body-wing interference. The wing-body experimental data show that at low Mach number, SBT slightly underpredicts the experimental data. AS AOA is increased, $K_{W(B)}$ starts decreasing and in some cases decreases below its wing-alone value. As AOA increases, $K_{W(B)}$ approaches its wing-alone value. As Mach number increases, the positive interference lift on the wing, caused by the presence of the body, is lost faster and faster as AOA increases. That is, the wing-alone solution is recovered much faster at high Mach number as AOA increases, than at low Mach number. This is believed to be the result of the Newtonian Impact mechanism where, at high Mach number, the momentum of the air particle is lost almost entirely upon direct impact on a surface, as opposed to wrapping around the surface and carrying some of the momentum with it, as at low Mach numbers.

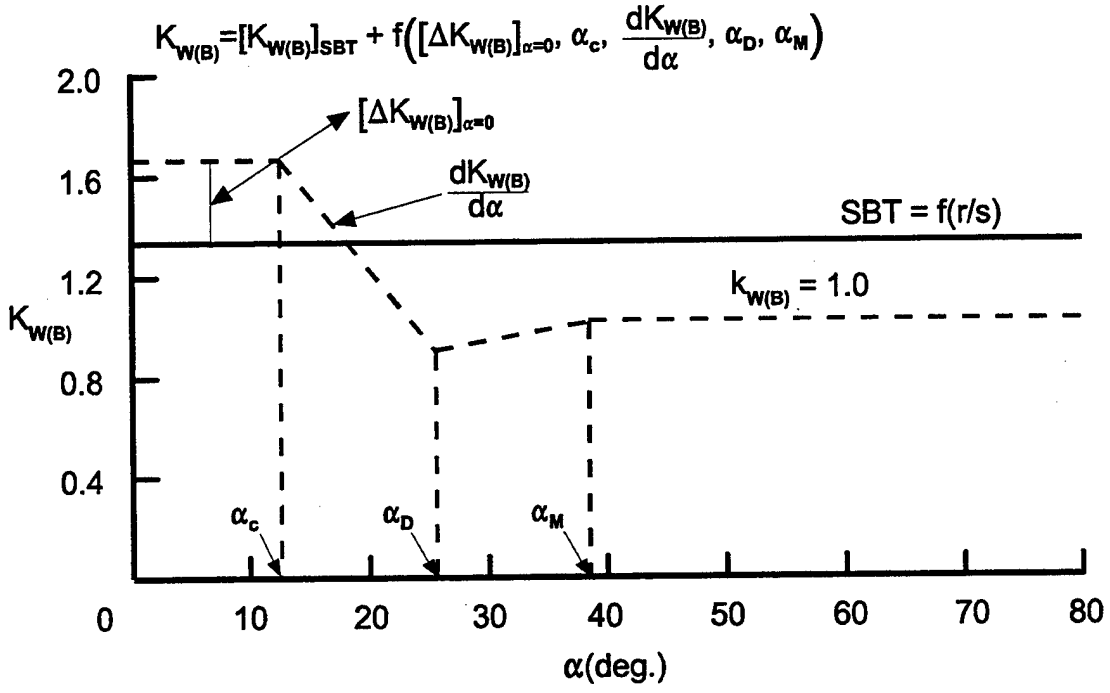

FIGURE 12A. GENERIC REPRESENTATION OF $K_{W(B)}$ WITH AOA

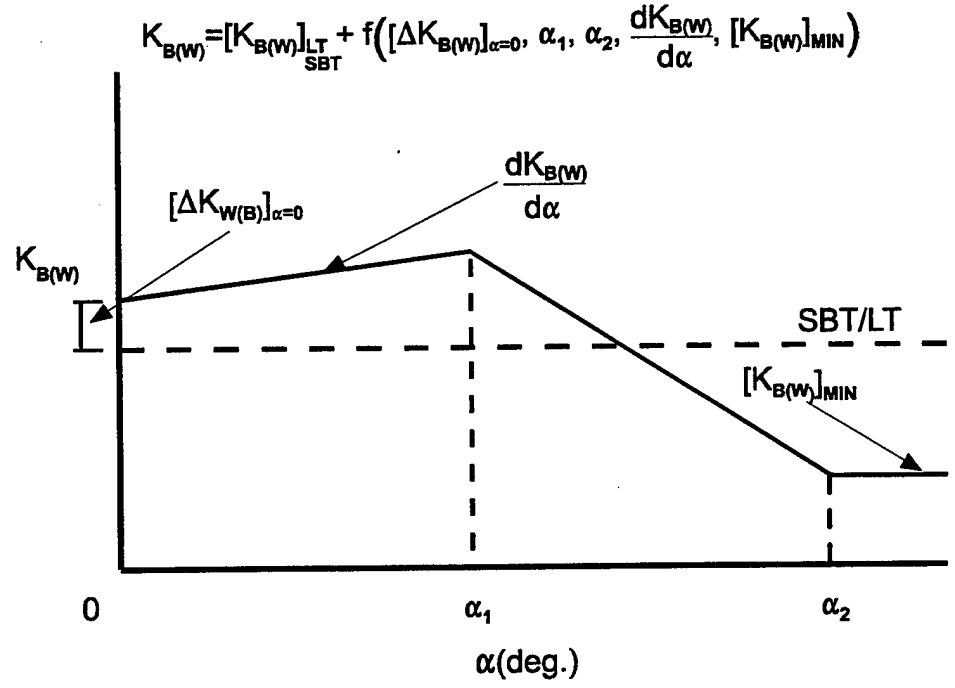

FIGURE 12B. GENERIC REPRESENTATION OF $K_{B(W)}$ WITH AOA

The $K_{B(W)}$ model contains body vortex effects, nose- and wing-to-wing shock effects, as well as the usual added dynamic pressure of the body caused by the presence of the wing. While some of the trends in Figure 12 can be rationalized, others cannot except in light of these combination effects. The alternative to simultaneously modeling several physical phenomena is to try to estimate the effects of the body vortices and nose- and wing-shock interactions and subtract them from the experimental data for the configuration tested and then add them back in analytically for another configuration of interest. This process not only complicates the methodology, but adds additional inherent errors because these effects cannot be easily and accurately estimated. The present approach neglects some of the scale effects caused by the position of the wing on the body. However, this error is probably smaller than the results of approximating analytically the other effects, subtracting them, and then adding them again for a different geometrical configuration.

In general, $K_{B(W)}$ actually increases with AOA at low Mach numbers to a certain point, where it starts decreasing analogous to $K_{W(B)}$. However, a certain amount of lift or force enhancement is gained all the way to $\alpha = 90$ deg for low Mach numbers as shown in Figure 12. This phenomenon is assumed to occur all the way to M = 6.0 based on extrapolated data from the point where experimental data end, which is AOA of 25 to 40 deg depending on Mach number, to $\alpha = 90$ deg shown in Figure 12.

Additional higher AOA data above $\alpha = 40$ deg is needed for both $K_{W(B)}$ and $K_{B(W)}$ to modify the assumed extrapolations of the models for $K_{W(B)}$ and $K_{B(W)}$ at high AOA. However, until additional data are available, the approximate nonlinear models for $K_{W(B)}$ and $K_{B(W)}$ can be used to estimate aerodynamics for engineering use. This statement will be validated for a limited set of flight conditions in a later section.

The way the nonlinearities are treated for the second term of Equation (12) is by using five tables for $\Delta K_{W(B)}$ and five tables for $\Delta K_{B(W)}$. Also, these tables are different for $\Phi = 0$ and 45 deg roll orientation. These tables define the parameters shown in Figure 12. The definition of these 10 parameters is as follows:

$[\Delta K_{W(B)}]_{\alpha=0}$ = difference between SBT and data at $\alpha = 0$

α_C = angle of attack where $K_{W(B)}$ starts decreasing

$\frac{d K_{W(B)}}{d\alpha}$ = rate of decrease of $K_{W(B)}$ between $\alpha = \alpha_C$ and $\alpha = \alpha_D$

α_D = angle of attack where $K_{W(B)}$ reaches an initial minimum

α_M = angle of attack where $K_{W(B)}$ reaches a constant value

$[\Delta K_{B(W)}]_{\alpha=0}$ = difference between SBT/LT and data at $\alpha = 0$

$\frac{dK_{B(W)}}{d\alpha}$ = rate of change of $K_{B(W)}$ between $\alpha = 0$ and $\alpha = \alpha_1$

α_1 = angle of attack where $dK_{B(W)}/d\alpha$ changes sign

α_2 = angle of attack where $K_{B(W)}$ reaches a constant

$[K_{B(W)}]_{MIN}$ = constant value of $K_{B(W)}$ above $\alpha = \alpha_2$ as a percent of linear theory or slender body theory

The mathematical models for $K_{W(B)}$ and $K_{B(W)}$ are once again defined based on SBT/LT and the empirical data for the constants defined previously. The specific equations for $K_{W(B)}$ are

$$K_{W(B)} = \left[K_{W(B)}\right]_{SBT} + \left[\Delta K_{W(B)}\right]_{\alpha=0}; \alpha \le \alpha_C \tag{13A}$$

$$= \left[K_{W(B)}\right]_{SBT} + \left[\Delta K_{W(B)}\right]_{\alpha=0} + \left|\left(|\alpha| - \alpha_C\right)\right| \frac{dK_{W(B)}}{d\alpha}; \alpha_C < \alpha \le \alpha_D \tag{13B}$$

$$= 1 - \left(\frac{\alpha_M - |\alpha|}{\alpha_M - \alpha_D}\right)\left(1 - \left[K_{W(B)}\right]_{\alpha=\alpha_D}\right); \alpha_D < \alpha \le \alpha_M \tag{13C}$$

$$K_{W(B)} = \left[K_{W(B)}\right]_{\alpha=\alpha_M}; \alpha > \alpha_M \tag{13D}$$

The specific mathematical model for $K_{B(W)}$ is given by Equations (14A) through (14C).

For $\alpha \le \alpha_1$,

$$K_{B(W)} = \left[K_{B(W)}\right]_{\substack{LT \\ SBT}} + \left[\Delta K_{B(W)}\right]_{\alpha=0} + |\alpha| \frac{dK_{B(W)}}{d\alpha} \tag{14A}$$

For $\alpha_1 < \alpha \le \alpha_2$,

$$K_{B(W)} = \left[K_{B(W)}\right]_{\alpha=\alpha_1} + \left(\frac{\alpha_1 - \alpha}{\alpha_2 - \alpha_1}\right)\left\{\left[K_{B(W)}\right]_{\alpha=\alpha_1} - \left[K_{B(W)}\right]_{MIN}\right\} \tag{14B}$$

For $\alpha > \alpha_2$,

$$K_{B(W)} = \left[K_{B(W)}\right]_{MIN} \tag{14C}$$

Tables 6 through 15 give the revised set of values for the 10 empirical constants of Figure 12 for the $\Phi = 0$ deg roll orientation and Tables 16 through 26 give values of these same constants for $\Phi = 45$ deg roll.

The revised values of the empirical constants in Tables 6 through 26 were derived primarily based on comparing the AP98 (including the revisions of Sections 2.1 and 2.2 of this report) to the wing-body data base of Reference 7. The empirical constants were then adjusted on a case-by-case basis to improve the overall predictions of theory to data. Some tables were hardly changed from those of Reference 1. Other tables, such as Tables 12 and 23, were changed more significantly.

TABLE 6. DATA FOR $[\Delta K_{W(B)}]_{\alpha=0}$ AT $\Phi = 0$ DEG

		MACH NUMBER										
ASPECT RATIO	TAPER RATIO	≤0.1	0.6	0.8	1.2	1.5	2.0	2.5	3.0	3.5	4.5	≥5.0
≤0.25	0, 0.5, 1.0	0	.25	.25	.15	0	0	0	0	0	0	0
0.5	0.5	.05	.05	.05	.05	0	0	0	0	0	0	0
1.0	0.5	.25	.15	.05	0	0	0	0	0	0	0	0
≥2.0	0.5	.20	.1	0	0	0	0	0	0	0	0	0
0.5	0	.30	.35	.2	.18	0	0	0	0	0	0	0
1.0	0	.35	.29	.16	.06	0	0	0	0	0	0	0
≥2.0	0	.27	.29	.10	.10	0	0	0	0	0	0	0
0.5	1.0	.05	.05	.05	.05	0	0	0	0	0	0	0
1.0	1.0	.25	.15	.05	0	0	0	0	0	0	0	0
≥2.0	1.0	.20	.1	0	.10	0	0	0	0	0	0	0

TABLE 7. DATA FOR α_C (deg) AT $\Phi = 0$ DEG

MACH NUMBER												
ASPECT RATIO	TAPER RATIO	≤0.1	0.6	0.8	1.2	1.5	2.0	2.5	3.0	3.5	4.5	≥5.0
≤0.25	0, 0.5, 1.0	30.0	22.0	22.0	10.0	0	0	0	0	0	0	0
0.5	0.5	30.0	17.3	11.5	10.0	0	0	0	0	0	0	0
1.0	0.5	30.0	20.0	15.0	10.0	0	0	0	0	0	0	0
≥2.0	0.5	20.0	15.0	10.0	15.0	0	0	0	0	0	0	0
0.5	0	20.0	12.0	10.0	10.0	0	0	0	0	0	0	0
1.0	0	40.0	20.0	15.0	10.0	0	0	0	0	0	0	0
≥2.0	0	10.0	20.0	15.0	15.0	0	0	0	0	0	0	0
0.5	1.0	30.0	17.3	10.0	10.0	0	0	0	0	0	0	0
1.0	1.0	30.0	15.0	12.5	10.0	0	0	0	0	0	0	0
≥2.0	1.0	10.0	15.0	15.0	15.0	0	0	0	0	0	0	0

TABLE 8. DATA FOR $\left[K_{W(B)}\right]_{\alpha=\alpha_D}$ AT $\Phi = 0$ DEG

MACH NUMBER												
ASPECT RATIO	TAPER RATIO	≤0.1	0.6	0.8	1.2	1.5	2.0	2.5	3.0	3.5	4.5	≥5.0
≤0.25	0, 0.5, 1.0	1.0	1.0	1.0	1.0	1.0	1.0	1.0	1.0	1.0	1.0	1.0
0.5	0.5	1.0	1.0	1.0	1.0	1.0	1.0	.95	1.0	.97	1.0	1.0
1.0	0.5	1.0	1.0	1.0	1.0	1.0	1.0	1.0	1.0	1.0	1.0	1.0
≥2.0	0.5	1.0	1.0	1.0	1.0	1.0	1.0	1.0	1.0	1.0	1.0	1.0
0.5	0	1.0	1.0	1.0	1.05	.90	.90	.90	.90	.90	.90	1.0
1.0	0	1.0	1.0	1.0	.95	1.0	1.0	1.0	1.0	1.0	1.0	1.0
≥2.0	0	1.0	1.0	.95	1.0	1.0	1.0	1.0	1.0	1.0	1.0	1.0
0.5	1.0	1.0	1.0	1.0	1.0	1.0	1.0	1.05	1.15	1.13	1.15	1.0
1.0	1.0	1.0	1.0	1.0	.95	.95	.95	1.0	1.0	1.0	1.0	1.0
≥2.0	1.0	1.0	1.0	1.0	1.0	1.0	1.0	1.0	.93	.90	.95	1.0

TABLE 9. DATA FOR α_D (deg) AT $\Phi = 0$ DEG

		MACH NUMBER										
ASPECT RATIO	TAPER RATIO	≤0.1	0.6	0.8	1.2	1.5	2.0	2.5	3.0	3.5	4.5	≥5.0
≤0.25	0, 0.5, 1.0	80.0	40.0	38.0	35.0	35.0	35.0	30.0	25.0	20.0	15.0	15.0
0.5	0.5	70.0	33.0	31.4	27.5	30.0	16.8	17.8	17.0	15.0	15.0	14.0
1.0	0.5	60.0	32.5	44.0	22.0	20.0	22.5	17.5	18.0	10.0	17.0	15.0
≥2.0	0.5	45.0	35.0	44.0	40.0	25.0	16.5	17.0	16.0	10.0	12.0	15.0
0.5	0	70.0	30.0	30.0	21.2	25.0	15.0	14.0	15.0	15.0	12.0	11.5
1.0	0	65.0	31.0	39.0	20.0	18.0	21.5	16.0	17.0	11.0	13.0	13.0
≥2.0	0	50.0	35.0	35.0	30.0	25.0	20.0	17.7	17.0	12.0	12.6	11.5
0.5	1.0	70.0	33.0	34.2	26.0	30.0	14.2	17.0	13.4	11.8	12.2	11.5
1.0	1.0	60.0	33.0	40.0	21.0	20.0	22.0	17.0	16.0	9.0	14.0	12.0
≥2.0	1.0	45.0	35.0	35.0	40.0	25.0	18.0	15.0	15.5	12.0	12.6	11.5

TABLE 10. DATA FOR α_M (deg) AT $\Phi = 0$ DEG

		MACH NUMBER										
ASPECT RATIO	TAPER RATIO	≤0.1	0.6	0.8	1.2	1.5	2.0	2.5	3.0	3.5	4.5	≥5.0
≤0.25	0, 0.5, 1.0	80.0	45.0	45.0	40.0	44.0	38.0	50.0	46.0	50.0	50.0	46.0
0.5	0.5	80.0	33.0	31.4	40.0	50.0	17.0	40.0	17.0	40.0	15.0	14.0
1.0	0.5	80.0	33.0	45.0	45.0	50.0	50.0	50.0	36.0	33.0	17.0	17.0
≥2.0	0.5	80.0	43.0	45.0	45.0	50.0	50.0	50.0	36.0	33.0	17.0	17.0
0.5	0	80.0	30.0	30.0	40.0	50.0	48.0	50.0	50.0	50.0	50.0	50.0
1.0	0	80.0	31.0	40.0	50.0	42.0	50.0	50.0	50.0	44.0	40.0	40.0
≥2.0	0	80.0	43.0	45.0	45.0	50.0	50.0	50.0	50.0	50.0	50.0	35.0
0.5	1.0	80.0	33.0	34.2	50.0	31.0	50.0	50.0	50.0	50.0	50.0	50.0
1.0	1.0	80.0	33.0	40.0	50.0	42.0	50.0	50.0	50.0	44.0	40.0	40.0
≥2.0	1.0	80.0	43.0	45.0	45.0	25.0	18.0	15.0	36.0	33.0	37.0	30.0

TABLE 11. DATA FOR $[\Delta K_{B(W)}]_{\alpha=0}$ AT $\Phi = 0$ DEG

MACH NUMBER												
ASPECT RATIO	TAPER RATIO	≤0.1	0.6	0.8	1.2	1.5	2.0	2.5	3.0	3.5	4.5	≥5.0
≤0.25	0, 0.5, 1.0	0.0	0.0	0.0	0.0	0.0	0.0	0.0	0.0	0.0	0.0	0.0
0.5	0.5	0.0	-.28	-.15	.16	.15	.05	0.0	0.0	0.0	0.0	0.0
1.0	0.5	0.0	-.20	-.20	.15	.10	.15	0.0	0.0	0.0	0.0	0.0
≥2.0	0.5	0.0	-.20	-.07	.1	.18	.10	0.0	0.0	0.0	0.0	0.0
0.5	0	0.0	-.33	-.30	.28	.20	.10	.08	0.0	0.0	0.0	0.0
1.0	0	0.0	-.24	-.25	.05	.2	.05	0.0	0.0	0.0	0.0	0.0
≥2.0	0	0.0	-.20	0.0	.17	0.0	0.0	0.0	0.0	0.0	0.0	0.0
0.5	1.0	0.0	-.28	-.15	.13	.15	.10	0.0	0.0	0.0	0.0	0.0
1.0	1.0	0.0	-.20	-.20	.22	.10	.05	0.0	0.0	0.0	0.0	0.0
≥2.0	1.0	0.0	-.20	-.07	.17	.20	.10	.15	0.0	0.0	0.0	0.0

TABLE 12. DATA FOR $dK_{B(W)}/d\alpha$ (per deg) AT $\Phi = 0$ DEG

MACH NUMBER												
ASPECT RATIO	TAPER RATIO	≤0.1	0.6	0.8	1.2	1.5	2.0	2.5	3.0	3.5	4.5	≥5.0
≤0.25	0, 0.5, 1.0	0.0	0.0	0.0	0.0	0.0	0.0	-.006	-.008	-.010	-.020	-.024
0.5	0.5	.003	.023	.023	-.009	-.018	-.020	-.015	-.014	-.015	-.016	-.020
1.0	0.5	.003	.012	.006	-.0075	-.014	-.016	-.013	-.014	-.015	-.020	-.020
≥2.0	0.5	.003	.006	0.0	0.0	0.0	-.008	-.012	-.014	-.015	-.016	-.020
0.5	0	.003	.035	.028	0.0	0.0	0.0	-.004	-.014	-.015	-.016	-.020
1.0	0	.003	.020	.0225	-.0075	-.011	-.012	-.013	-.014	-.015	-.020	-.020
≥2.0	0	.003	.008	.006	0.0	0.0	-.008	-.012	-.014	-.015	-.016	-.020
0.5	1.0	.003	.038	.033	-.003	-.010	-.020	-.015	-.014	-.015	-.016	-.020
1.0	1.0	.003	.007	.005	-.0075	-.014	-.016	-.015	-.016	-.016	-.020	-.020
≥2.0	1.0	.003	.006	0.0	0.0	0.0	-.008	-.012	-.014	-.015	-.016	-.020

TABLE 13. DATA FOR α_1 (deg) AT $\Phi = 0$ DEG

		MACH NUMBER										
ASPECT RATIO	TAPER RATIO	≤0.1	0.6	0.8	1.2	1.5	2.0	2.5	3.0	3.5	4.5	≥5.0
≤0.25	0, 0.5, 1.0	15.0	21.1	16.5	45.0	37.0	30.0	23.3	20.5	18.0	15.0	10.0
0.5	0.5	30.0	22.2	16.7	62.0	43.0	40.0	25.0	25.0	25.0	20.0	20.0
1.0	0.5	30.0	25.0	20.0	70.0	20.0	0.00	10.0	10.0	10.0	10.0	10.0
≥2.0	0.5	30.0	20.0	20.0	40.0	30.0	30.0	30.0	24.0	20.4	26.0	26.0
0.5	0	30.0	15.0	15.0	25.0	25.0	20.0	20.0	10.0	27.0	20.0	20.0
1.0	0	30.0	25.0	20.0	70.0	20.0	0.00	10.0	10.0	10.0	10.0	10.0
≥2.0	0	30.0	25.0	20.0	40.0	30.0	30.0	30.0	32.0	30.0	20.0	20.0
0.5	1.0	30.0	17.0	15.5	48.5	43.0	40.0	25.0	26.5	21.6	20.0	20.0
1.0	1.0	30.0	25.0	20.0	70.0	20.0	0.00	10.0	10.0	10.0	10.0	10.0
≥2.0	1.0	30.0	20.0	40.0	40.0	48.0	47.0	32.0	26.0	20.0	26.0	26.0

TABLE 14. DATA FOR α_2 (deg) AT $\Phi = 0$ DEG

		MACH NUMBER										
ASPECT RATIO	TAPER RATIO	≤0.1	0.6	0.8	1.2	1.5	2.0	2.5	3.0	3.5	4.5	≥5.0
≤0.25	0, 0.5, 1.0	90.0	75.0	65.0	63.4	60.0	55.0	52.5	40.0	47.5	45.0	42.5
0.5	0.5	90.0	75.0	65.0	62.0	43.0	41.0	42.5	25.0	42.0	40.0	40.0
1.0	0.5	90.0	75.0	75.0	80.0	40.0	50.0	40.0	30.0	30.0	30.0	30.0
≥2.0	0.5	90.0	75.0	75.0	80.0	90.0	90.0	42.0	40.0	40.0	40.0	40.0
0.5	0	90.0	75.0	75.0	80.0	49.0	47.8	42.5	43.0	26.5	40.0	40.0
1.0	0	90.0	75.0	75.0	80.0	40.0	50.0	40.0	40.0	30.0	30.0	30.0
≥2.0	0	90.0	75.0	75.0	80.0	90.0	90.0	41.0	40.0	40.0	43.0	43.0
0.5	1.0	90.0	75.0	53.2	48.7	43.0	41.0	42.5	26.5	43.5	40.0	40.0
1.0	1.0	90.0	75.0	74.0	72.0	40.0	50.0	40.0	40.0	30.0	30.0	30.0
≥2.0	1.0	90.0	75.0	75.0	80.0	90.0	90.0	45.0	30.0	40.0	43.0	43.0

TABLE 15. DATA FOR $[K_{B(W)}]_{MIN}$ AS A FRACTION OF SLENDER BODY THEORY AT $\Phi = 0$ DEG

M_∞	$[K_{B(W)}]_{MIN}$
0	0.5
3.8	0.5
4.9	0.25
6.0	0

TABLE 16. DATA FOR $[K_{W(B)}]_{\alpha=0}$ AT $\Phi = 45$ DEG

		MACH NUMBER										
ASPECT RATIO	TAPER RATIO	≤0.1	0.6	0.8	1.2	1.5	2.0	2.5	3.0	3.5	4.5	≥5.0
≤0.25	0, 0.5, 1.0	0.00	0.00	0.00	0.00	0.00	0	0	0	0	0	0
0.5	0.5	0.00	0.00	0.00	-0.13	0.00	0	0	0	0	0	0
1.0	0.5	0.10	0.00	0.00	0.00	-0.10	0	0	0	0	0	0
≥2.0	0.5	0.10	0.00	0.00	0.00	0.00	0	0	0	0	0	0
0.5	0	0.00	0.00	0.00	0.00	0.00	0	0	0	0	0	0
≥2.0	0	0.00	0.00	0.00	0.00	-0.18	0	0	0	0	0	0
0.5	1.0	0.00	0.00	0.00	0.00	0.00	0	0	0	0	0	0
≥2.0	1.0	0.05	0.00	0.00	0.00	0.00	0	0	0	0	0	0
1.0	0	0.35	0.15	0.05	0.00	-0.10	0	0	0	0	0	0
1.0	1.0	0.10	0.00	0.00	0.00	-0.10	0	0	0	0	0	0

TABLE 17. DATA FOR α_C AT $\Phi = 45$ DEG

		MACH NUMBER										
ASPECT RATIO	TAPER RATIO	≤0.1	0.6	0.8	1.2	1.5	2.0	2.5	3.0	3.5	4.5	≥5.0
≤0.25	0, 0.5, 1.0	0.0	22.0	22.0	0.0	0.0	0	0	0	0	0	0
0.5	0.5	15.0	11.5	11.0	10.0	0.0	0	0	0	0	0	0
1.0	0.5	15.0	13.3	0.0	6.5	0.0	0	0	0	0	0	0
≥2.0	0.5	10.0	10.0	0.0	6.5	2.2	0	0	0	0	0	0
0.5	0	30.0	15.0	11.5	10.0	0.0	0	0	0	0	0	0
≥2.0	0	10.0	10.0	0.0	6.5	0.0	0	0	0	0	0	0
0.5	1.0	15.0	11.0	11.0	10.0	0.0	0	0	0	0	0	0
≥2.0	1.0	10.0	10.0	0.0	6.5	1.5	0	0	0	0	0	0
1.0	0	40.0	13.3	0.0	6.5	0.0	0	0	0	0	0	0
1.0	1.0	15.0	13.3	0.0	6.5	0.0	0	0	0	0	0	0

TABLE 18. DATA FOR $\left[K_{W(B)}\right]_{\alpha=\alpha_D}$ AT $\Phi = 45$ DEG

		MACH NUMBER										
ASPECT RATIO	TAPER RATIO	≤0.1	0.6	0.8	1.2	1.5	2.0	2.5	3.0	3.5	4.5	≥6.0
≤0.25	0, 0.5, 1.0	1.0	1.0	1.00	1.00	1.00	1.00	1.00	1.00	1.00	1.00	1.0
0.5	0.5	1.0	1.0	1.00	0.90	0.90	1.00	0.95	1.00	0.97	1.00	1.0
1.0	0.5	1.0	1.0	1.00	0.95	1.00	1.00	1.00	1.00	1.00	1.00	1.0
≥2.0	0.5	1.0	1.0	0.95	0.95	1.00	1.00	1.00	1.00	1.00	1.00	1.0
0.5	0	1.0	1.0	1.00	1.00	0.90	0.90	0.90	0.90	0.90	0.90	1.0
≥2.0	0	1.0	1.0	0.95	1.00	1.00	1.00	1.00	1.00	1.00	1.00	1.0
0.5	1.0	1.0	1.0	1.00	1.00	1.00	1.00	1.00	1.00	1.00	1.00	1.0
≥2.0	1.0	1.0	1.0	1.00	1.00	1.00	1.00	1.00	0.93	0.90	0.95	1.0
1.0	0	1.0	1.0	1.00	0.95	1.00	1.00	1.00	1.00	1.00	1.00	1.0
1.0	1.0	1.0	1.0	1.00	0.95	0.95	0.95	1.00	1.00	1.00	1.00	1.0

TABLE 19. DATA FOR α_D AT $\Phi = 45$ DEG

		MACH NUMBER										
ASPECT RATIO	TAPER RATIO	≤0.1	0.6	0.8	1.2	1.5	2.0	2.5	3.0	3.5	4.5	≥6.0
≤0.25	0, 0.5, 1.0	20.0	40.0	38.0	35.0	30.0	25.0	16.3	15.1	13.9	13.1	10.0
0.5	0.5	59.0	33.0	30.0	25.6	25.0	15.0	15.0	10.0	15.0	15.0	10.0
1.0	0.5	49.0	38.0	32.0	26.0	24.0	17.0	15.0	14.4	10.0	10.0	10.0
≥2.0	0.5	39.0	31.5	30.0	28.0	25.0	16.5	15.0	14.4	10.0	13.0	10.0
0.5	0	59.0	35.5	33.0	39.5	29.5	15.0	25.0	15.0	15.0	10.0	10.0
≥2.0	0	39.0	31.5	30.0	28.0	24.7	17.0	13.5	11.4	10.0	10.0	10.0
0.5	1.0	59.0	35.5	33.0	25.6	29.5	15.0	15.0	15.0	12.0	13.0	10.0
≥2.0	1.0	39.0	31.5	30.0	28.0	23.3	14.0	16.0	15.0	11.8	12.0	10.0
1.0	0	59.0	38.5	32.5	36.0	27.1	17.2	21.0	11.4	10.0	10.0	10.0
1.0	1.0	49.0	38.5	32.5	26.0	26.4	16.0	15.3	15.0	11.8	10.0	10.0

TABLE 20. DATA FOR α_M AT $\Phi = 45$ DEG

		MACH NUMBER										
ASPECT RATIO	TAPER RATIO	≤0.1	0.6	0.8	1.2	1.5	2.0	2.5	3.0	3.5	4.5	≥6.0
≤0.25	0, 0.5, 1.0	35.0	45.0	45.0	40.0	44.0	43.0	38.0	28.0	25.0	29.0	20.0
0.5	0.5	65.0	33.0	30.0	49.0	52.0	40.0	40.0	30.0	25.0	25.0	20.0
1.0	0.5	55.0	38.0	47.0	49.5	66.0	48.5	45.0	41.0	40.0	10.0	20.0
≥2.0	0.5	45.0	31.5	40.0	56.0	57.0	45.0	45.0	41.0	40.0	28.0	20.0
0.5	0	65.0	35.5	33.0	65.0	48.0	50.0	46.0	30.0	30.0	50.0	20.0
≥2.0	0	45.0	31.5	40.0	56.0	55.0	58.5	49.8	44.2	41.5	28.5	20.0
0.5	1.0	65.0	35.5	33.0	49.0	52.0	40.0	28.0	24.0	21.0	13.0	20.0
≥2.0	1.0	45.0	31.5	40.0	56.0	49.5	44.0	40.0	33.0	32.0	28.0	20.0
1.0	0	70.0	38.5	49.0	63.0	60.0	60.5	49.8	44.2	41.5	40.0	20.0
1.0	1.0	55.0	38.5	49.0	49.5	60.0	47.5	40.0	33.0	32.0	20.0	20.0

TABLE 21. DATA FOR $\left[K_{W(B)}\right]_{\alpha=\alpha_M}$ AT Φ = 45 DEG

MACH NUMBER												
ASPECT RATIO	TAPER RATIO	≤0.1	0.6	0.8	1.2	1.5	2.0	2.5	3.0	3.5	4.5	≥6.0
≤0.25	0, 0.5, 1.0	0.80	0.95	1.0	1.0	1.0	1.0	1.0	1.0	1.0	1.0	1.0
0.5	0.5	0.85	0.95	1.0	1.0	1.0	1.0	1.0	1.0	1.0	1.0	1.0
1.0	0.5	0.85	0.90	1.0	1.0	1.0	1.0	1.0	1.0	1.0	1.0	1.0
≥2.0	0.5	0.85	0.90	1.0	1.0	1.0	1.0	1.0	1.0	1.0	1.0	1.0
0.5	0	0.85	0.95	1.0	1.0	1.0	1.0	1.0	1.0	1.0	1.0	1.0
≥2.0	0	0.85	0.95	1.0	1.0	1.0	1.0	1.0	1.0	1.0	1.0	1.0
0.5	1.0	0.85	0.95	1.0	1.0	1.0	1.0	1.0	1.0	1.0	1.0	1.0
≥2.0	1.0	0.85	0.90	1.0	1.0	1.0	1.0	1.0	1.0	1.0	1.0	1.0
1.0	0	0.90	0.95	1.0	1.0	1.0	1.0	1.0	1.0	1.0	1.0	1.0
1.0	1.0	0.85	0.90	1.0	1.0	1.0	1.0	1.0	1.0	1.0	1.0	1.0

TABLE 22. DATA FOR $[\Delta K_{B(W)}]_{\alpha=0}$ AT Φ = 45 DEG

MACH NUMBER												
ASPECT RATIO	TAPER RATIO	≤0.1	0.6	0.8	1.2	1.5	2.0	2.5	3.0	3.5	4.5	≥6.0
≤0.25	0, 0.5, 1.0	0.0	0.0	0.00	0.00	0.0	0	0	0	0	0	0
0.5	0.5	0.0	-0.12	-0.10	0.00	0.0	0	0	0	0	0	0
1.0	0.5	0.0	-0.07	-0.25	0.00	0.0	0	0	0	0	0	0
≥2.0	0.5	0.0	-0.23	-0.18	0.00	0.0	0	0	0	0	0	0
0.5	0	0.0	-0.12	0.00	0.00	0.0	0	0	0	0	0	0
≥2.0	0	0.0	-0.23	-0.18	0.00	0.0	0	0	0	0	0	0
0.5	1.0	0.0	-0.12	0.00	0.00	0.0	0	0	0	0	0	0
≥2.0	1.0	0.0	-0.23	-0.18	0.00	0.0	0	0	0	0	0	0
1.0	0	0.0	-0.05	-0.25	0.00	0.0	0	0	0	0	0	0
1.0	1.0	0.0	-0.07	-0.25	0.00	0.0	0	0	0	0	0	0

TABLE 23. DATA FOR $dK_{B(W)}/d\alpha$ (PER DEG) AT $\Phi = 45$ DEG

MACH NUMBER												
ASPECT RATIO	TAPER RATIO	≤0.1	0.6	0.8	1.2	1.5	2.0	2.5	3.0	3.5	4.5	≥6.0
≤0.25	0, 0.5, 1.0	-0.0050	-0.00557	-0.0200	-0.0215	-0.0250	-0.022	-0.022	-0.025	-0.030	-0.04	-0.04
0.5	0.5	-0.006	-0.006	-0.024	-0.030	-0.032	-0.047	-0.035	-0.0330	-0.0620	-0.060	-0.06
1.0	0.5	-0.0030	0.00000	0.000	-0.024	-0.020	-0.020	-0.02	-0.02	-0.02	-0.02	-0.02
≥2.0	0.5	0.0030	0.00670	0.005	-0.0150	-0.02	-0.0300	-0.045	-0.054	-0.060	-0.062	-0.065
0.5	0	-0.0020	-0.020	-0.027	-0.039	-0.040	-0.053	-0.035	-0.040	-0.050	-0.060	-0.06
≥2.0	0	0.0030	0.00670	0.005	-0.0150	-0.02	-0.0300	-0.045	-0.054	-0.060	-0.062	-0.065
0.5	1.0	0.0015	-0.006	-0.025	-0.030	-0.032	-0.040	-0.0275	-0.0400	-0.060	-0.060	-0.06
≥2.0	1.0	0.0030	0.00670	0.005	-0.0150	-0.02	-0.0300	-0.045	-0.054	-0.060	-0.062	-0.065
1.0	0	0.003	0.0	0.0	-0.024	-0.02	-0.02	-0.02	-0.02	-0.02	-0.02	-0.02
1.0	1.0	-0.003	0.0	0.0	-0.024	-0.02	-0.02	-0.02	-0.02	-0.02	-0.02	-0.02

TABLE 24. DATA FOR α_1 (DEG) AT Φ = 45 DEG

		MACH NUMBER										
ASPECT RATIO	TAPER RATIO	≤0.1	0.6	0.8	1.2	1.5	2.0	2.5	3.0	3.5	4.5	≥6.0
≤0.25	0, 0.5, 1.0	10.0	15.0	15.0	15.0	10.0	10.0	10.0	10.0	10.0	10.0	10.0
0.5	0.5	10.0	57.0	20.0	23.0	23.0	15.0	20.0	15.0	10.0	10.0	10.0
1.0	0.5	10.0	10.0	20.0	25.0	30.0	30.0	15.0	17.5	15.0	15.0	15.0
≥2.0	0.5	10.0	15.0	15.0	15.0	10.0	10.0	10.0	12.0	10.0	10.0	10.0
0.5	0	10.0	24.0	33.0	23.0	19.0	20.0	22.5	15.0	10.0	10.0	10.0
≥2.0	0	10.0	15.0	15.0	15.0	10.0	10.0	10.0	12.0	10.0	10.0	10.0
0.5	1.0	10.0	62.0	24.0	25.0	25.0	16.0	20.0	15.0	10.0	10.0	10.0
≥2.0	1.0	10.0	15.0	15.0	15.0	10.0	10.0	10.0	12.0	10.0	10.0	10.0
1.0	0	10.0	10.0	20.0	25.0	30.0	30.0	15.0	17.5	15.0	15.0	15.0
1.0	1.0	10.0	10.0	20.0	25.0	30.0	30.0	15.0	17.5	15.0	15.0	15.0

TABLE 25. DATA FOR α_2 (DEG) AT Φ = 45 DEG

		MACH NUMBER										
ASPECT RATIO	TAPER RATIO	≤0.1	0.6	0.8	1.2	1.5	2.0	2.5	3.0	3.5	4.5	≥6.0
≤0.25	0, 0.5, 1.0	35.0	55.0	50.0	50.0	45.0	40.0	35.0	32.5	30.0	27.5	25.0
0.5	0.5	75.0	65.0	55.0	43.0	40.0	38.0	44.0	44.0	36.0	30.0	20.0
1.0	0.5	75.0	35.0	30.0	30.0	60.0	60.0	62.0	80.0	80.0	80.0	80.0
≥2.0	0.5	75.0	65.0	30.0	30.0	30.0	60.0	62.0	80.0	42.0	45.0	45.0
0.5	0	75.0	60.0	50.0	52.0	40.0	35.0	44.0	50.0	36.0	30.0	20.0
≥2.0	0	75.0	65.0	30.0	30.0	30.0	60.0	62.0	80.0	42.0	45.0	45.0
0.5	1.0	75.0	65.0	55.0	42.0	40.0	38.0	44.0	40.0	36.0	30.0	20.0
≥2.0	1.0	75.0	65.0	30.0	30.0	30.0	60.0	62.0	80.0	42.0	45.0	45.0
1.0	0	75.0	50.0	30.0	30.0	60.0	60.0	62.0	80.0	80.0	80.0	80.0
1.0	1.0	75.0	35.0	30.0	30.0	60.0	60.0	62.0	80.0	80.0	80.0	80.0

TABLE 26. DATA FOR $[K_{B(W)}]_{MIN}$ (FRACTION OF SBT/LT) AT $\Phi = 45$ DEG

		MACH NUMBER										
ASPECT RATIO	TAPER RATIO	≤0.1	0.6	0.8	1.2	1.5	2.0	2.5	3.0	3.5	4.5	≥6.0
≤0.25	0, 0.5, 1.0	0.25	0.25	0.25	0.12	0.12	0.12	0.12	0.12	0.12	0.12	0
0.5	0.5	0.25	0.25	0.25	0.12	0.12	0.12	0.12	0.12	0.12	0.12	0
1.0	0.5	0.25	0.25	0.25	0.12	0.12	0.12	0.12	0.12	0.12	0.12	0
≥2.0	0.5	0.25	0.25	0.25	0.12	0.12	0.12	0.12	0.12	0.12	0.12	0
0.5	0	0.25	0.25	0.25	0.12	0.12	0.12	0.12	0.12	0.12	0.12	0
≥2.0	0	0.25	0.25	0.25	0.12	0.12	0.12	0.12	0.12	0.12	0.12	0
0.5	1.0	0.25	0.25	0.25	0.12	0.12	0.12	0.12	0.12	0.12	0.12	0
≥2.0	1.0	0.25	0.25	0.25	0.12	0.12	0.12	0.12	0.12	0.12	0.12	0

3.0 COMPARISON OF MODIFIED THEORY TO NASA/MDAC DATA BASE

The first thing one likes to do after making changes to the APC is to compare the new predictions to the data base upon which the changes were based in a comprehensive fashion. The data base of Reference 7 consists of Mach numbers 0.6, 0.9, 1.2, 1.6, 2.0, 2.3, 2.96, and 3.95 for the twelve fin planforms of Figure 3B mounted on the body of Figure 3A. Angles of attack from 0 to 20 deg were considered at the subsonic and transonic Mach numbers, whereas AOAs to 30 deg were considered at the supersonic conditions. Comparisons of the new predictions to the Reference 7 data base and the AP98 are shown in Figures 13 through 24 for each of the twelve body-tail cases shown in Figure 3. In examining Figures 13 through 24, it is seen that the improvements made to the AP98 (listed in the figures as the AP02) improve the normal force coefficient prediction accuracy compared to experiment and the AP98. In a quantitative sense, the errors of the AP02 compared to experiment were measured at $\alpha = 10, 15, 20, 25$, and 30 deg where data was available. The error here is defined by

$$\text{Error}(\%) = \frac{\left| C_{N_{exp}} - C_{N_{THEORY}} \right|}{C_{N_{exp}}} \times 100 \qquad (15)$$

These errors were then averaged by individual Mach number and for all Mach numbers for the 12 fins of Figures 13 through 24. These results are shown in Table 27. As seen in the table, the average errors on normal force coefficient prediction are less than 10 percent for any Mach number and under 5 percent for the entire data base. While not shown, the average total error for the AP98 on normal force is closer to 7 percent. While this is still under the quoted average error of ±10 percent, it is considerably higher than that given by the improvements which will be part of the AP02.

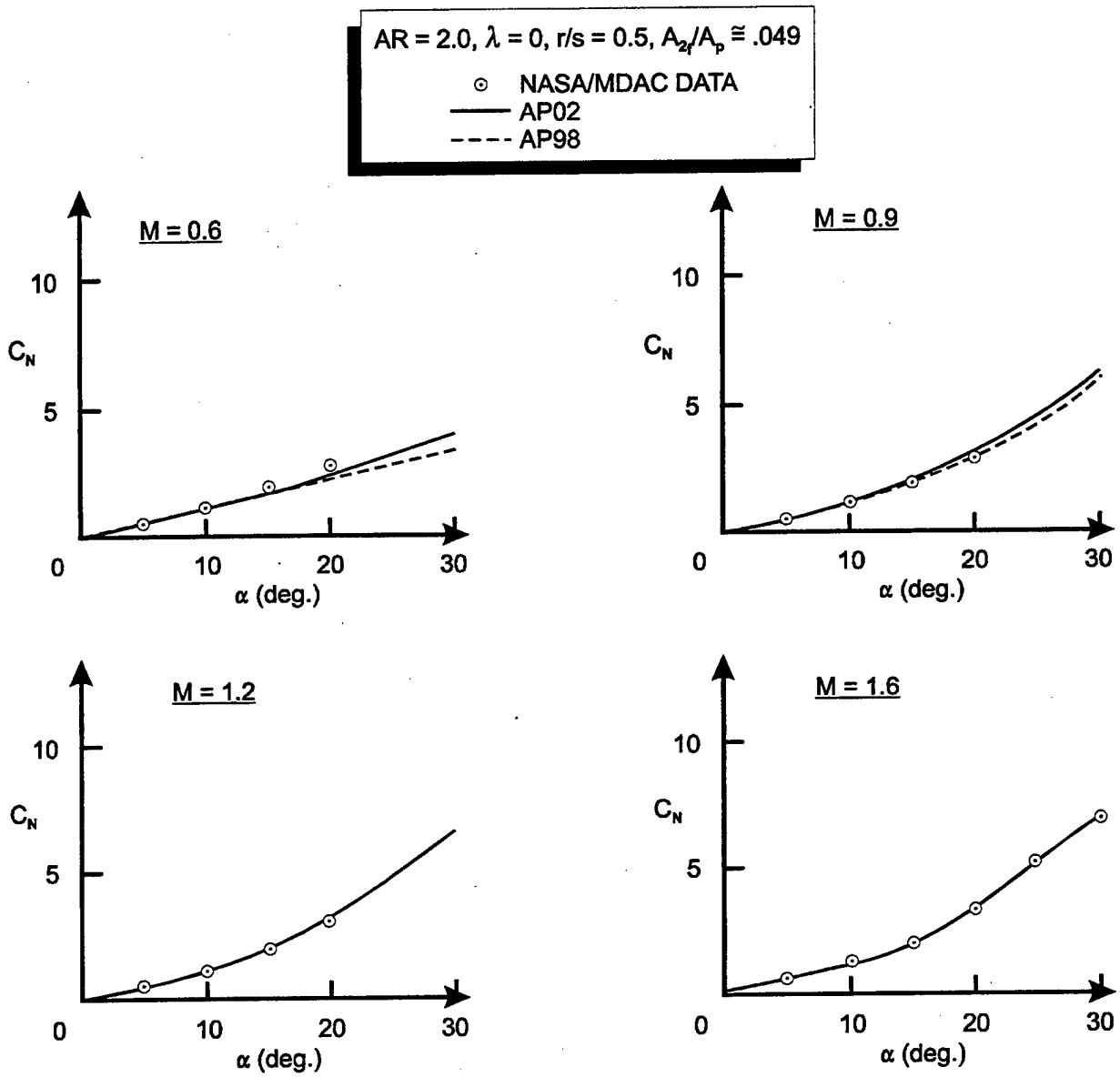

FIGURE 13. COMPARISON OF NASA/MDAC WING-BODY NORMAL FORCE WITH AP98 PREDICTIONS (FIN NO. 1)

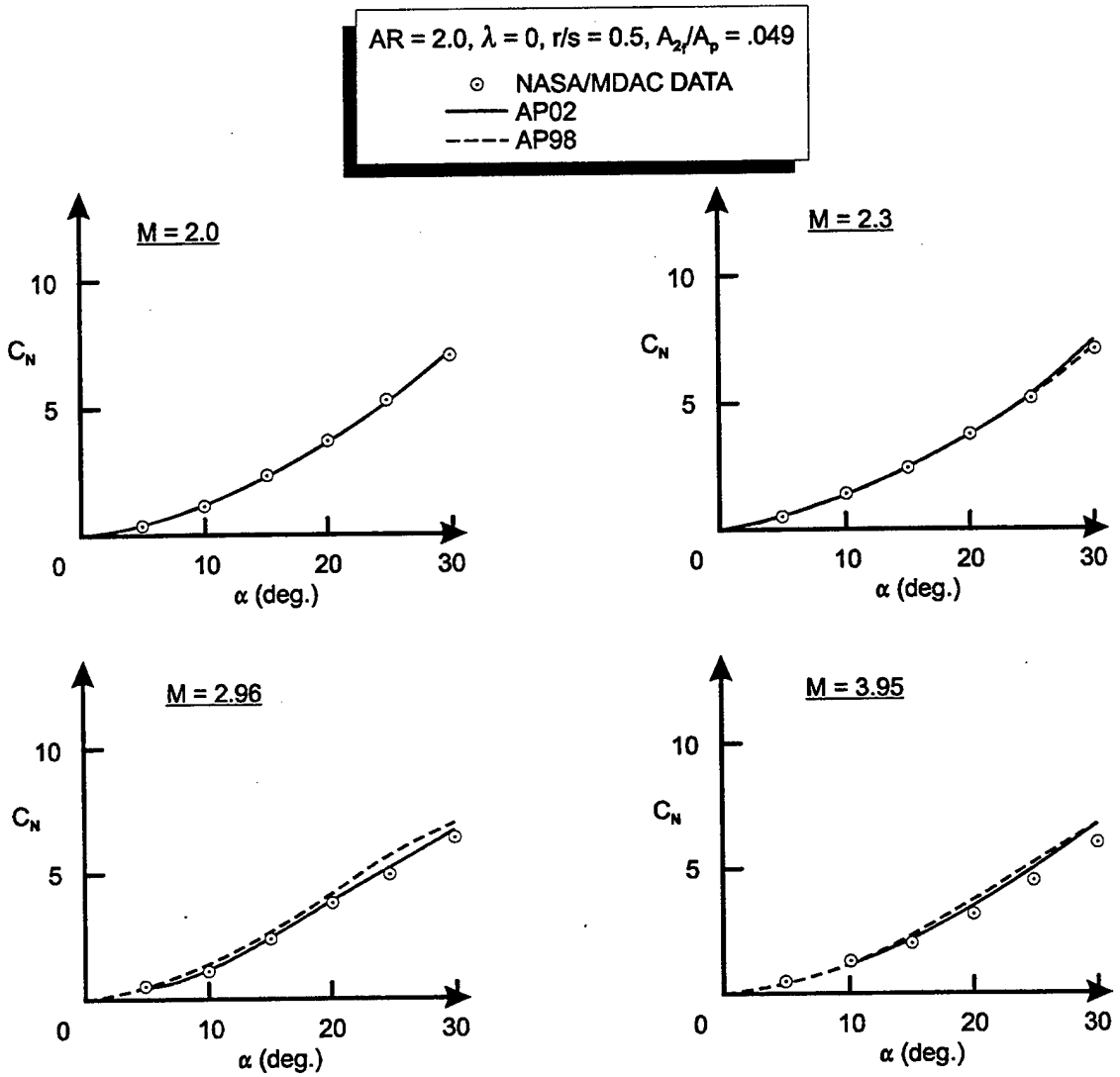

FIGURE 13. COMPARISON OF NASA/MDAC WING-BODY NORMAL FORCE WITH AP98 PREDICTIONS (FIN NO. 1) (Continued)

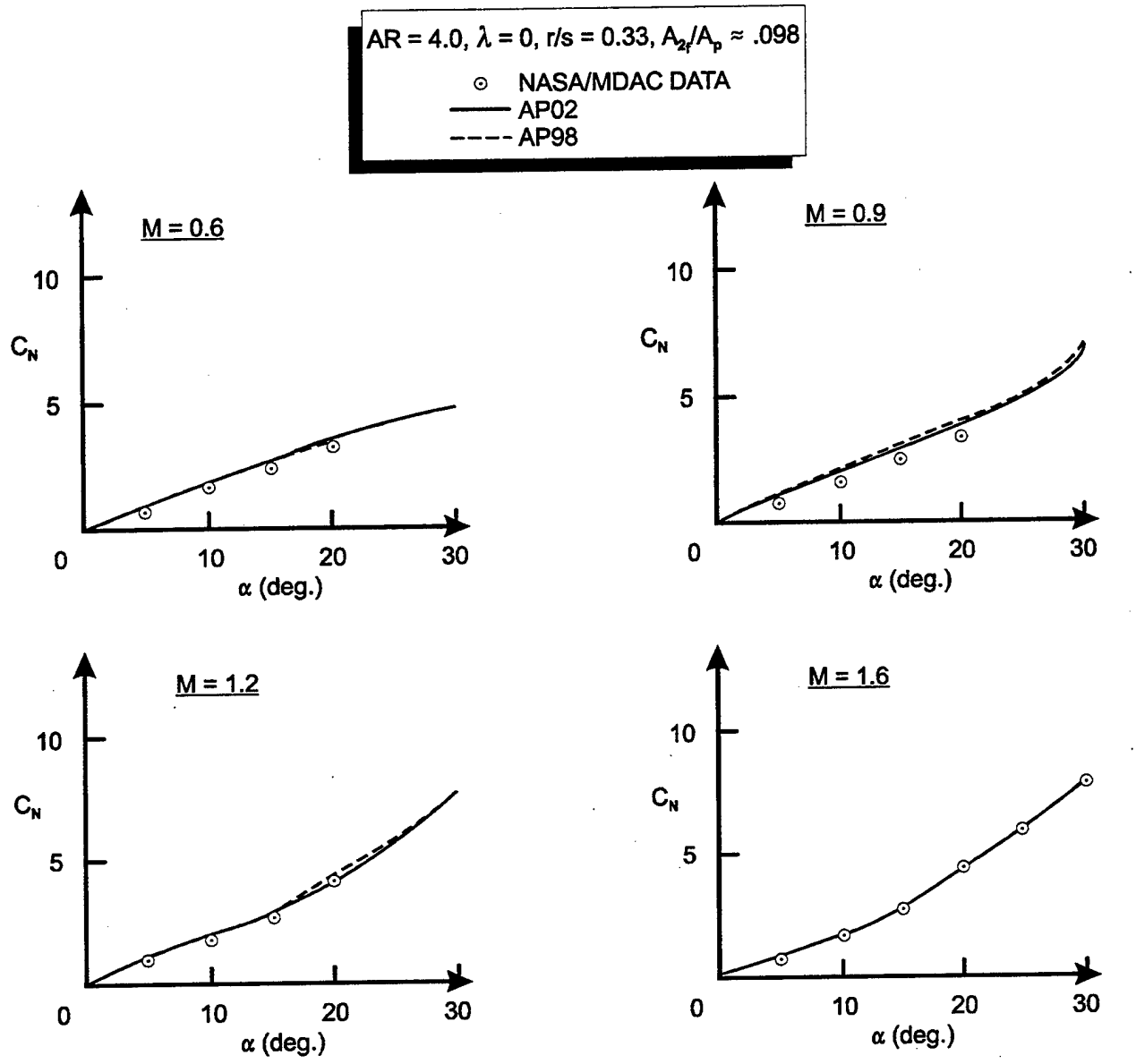

FIGURE 14. COMPARISON OF NASA/MDAC WING-BODY NORMAL FORCE WITH AP98 PREDICTIONS (FIN NO. 2)

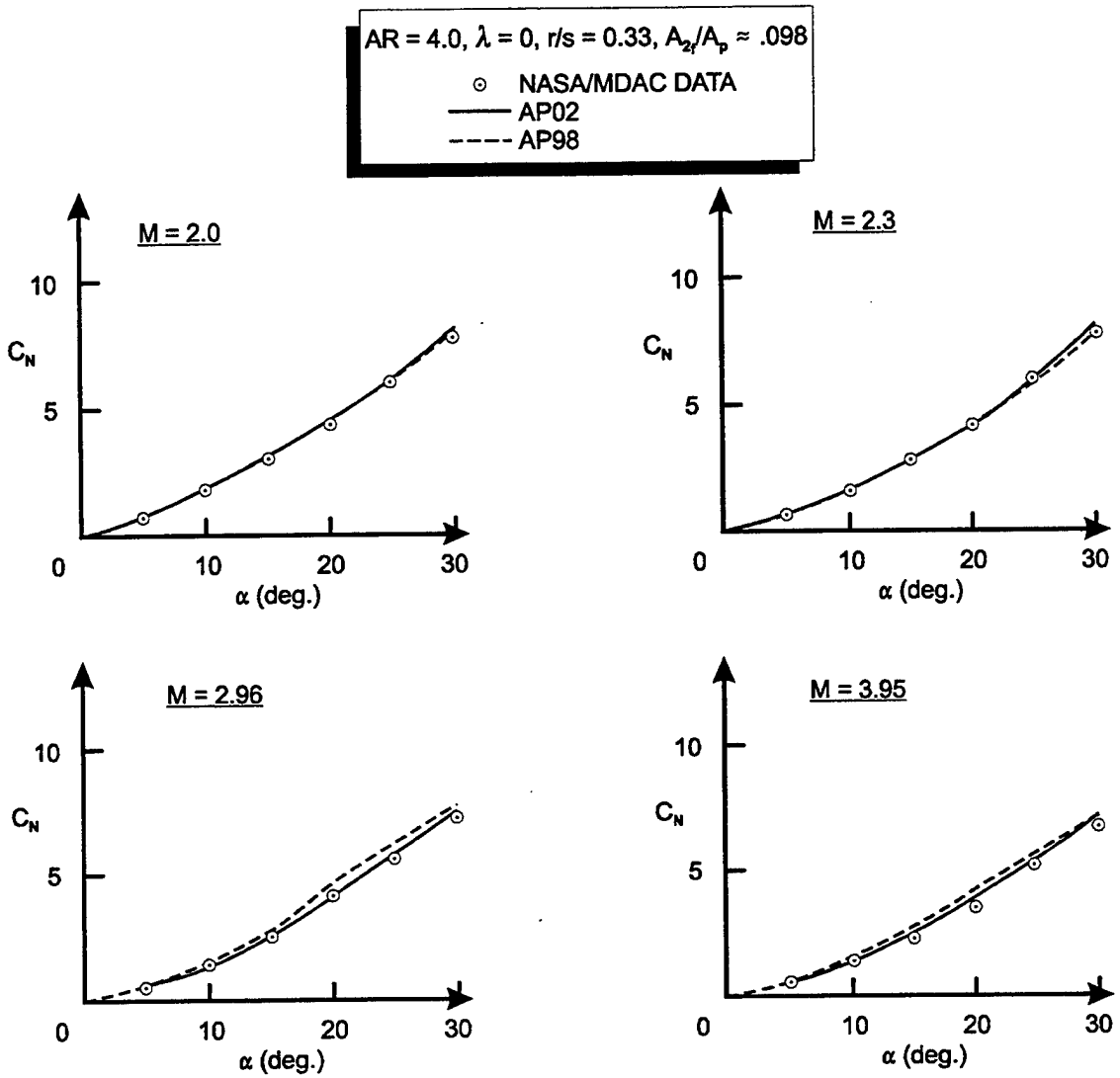

FIGURE 14. COMPARISON OF NASA/MDAC WING-BODY NORMAL FORCE WITH AP98 PREDICTIONS (FIN NO. 2) (Continued)

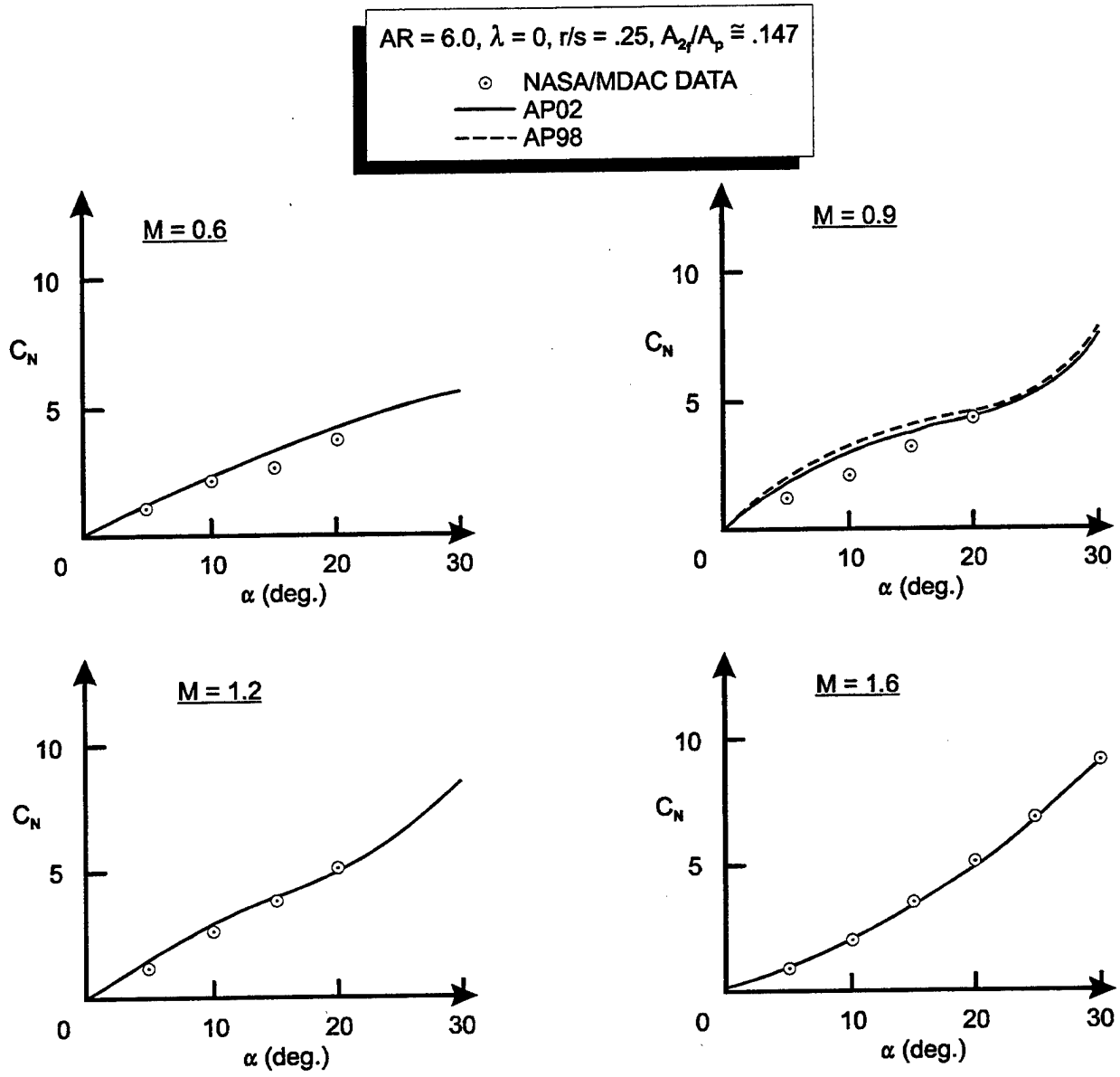

FIGURE 15. COMPARISON OF NASA/MDAC WING-BODY NORMAL FORCE WITH AP98 PREDICTIONS (FIN NO. 3)

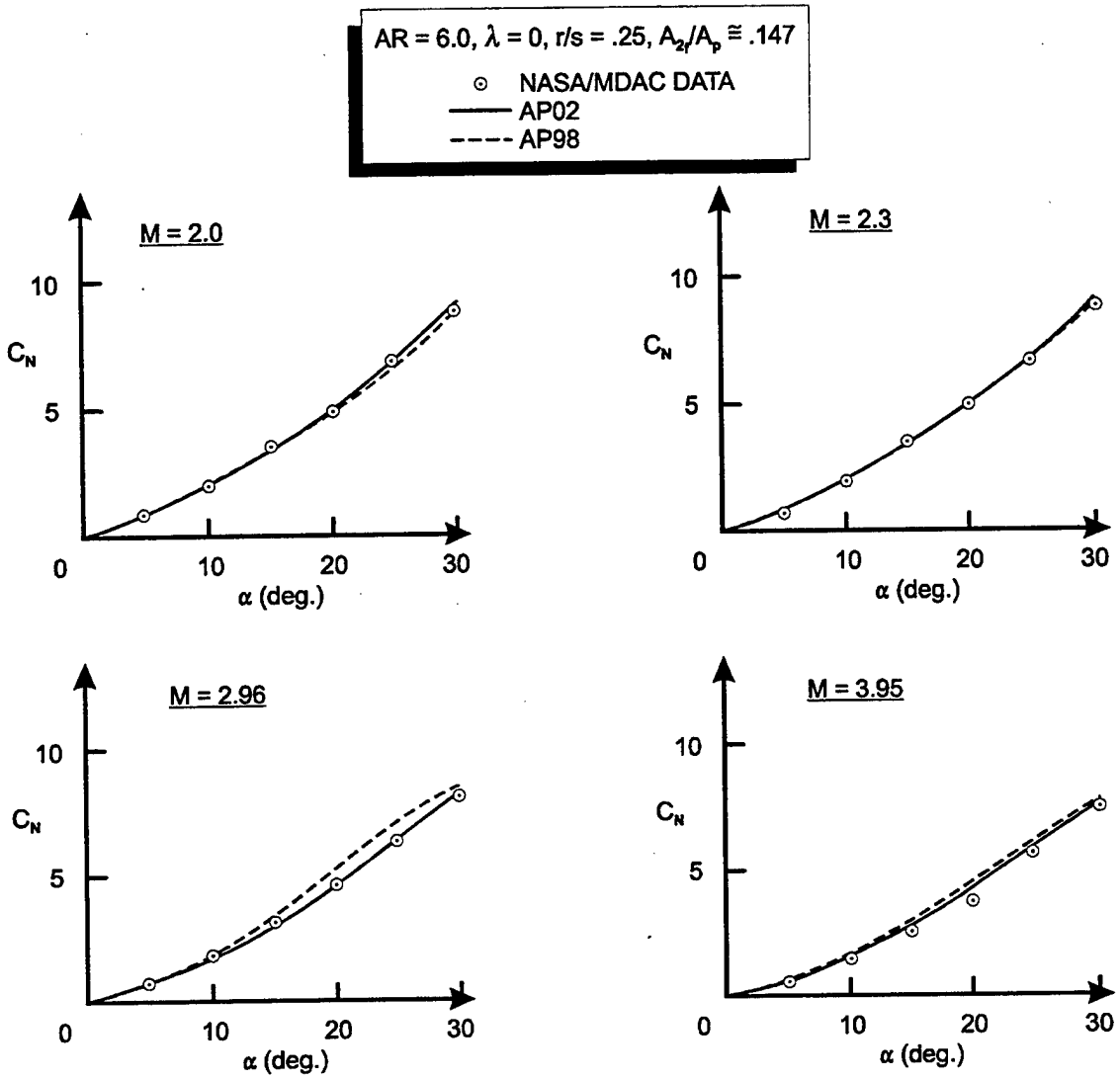

FIGURE 15. COMPARISON OF NASA/MDAC WING-BODY NORMAL FORCE WITH AP98 PREDICTIONS (FIN NO. 3) (Continued)

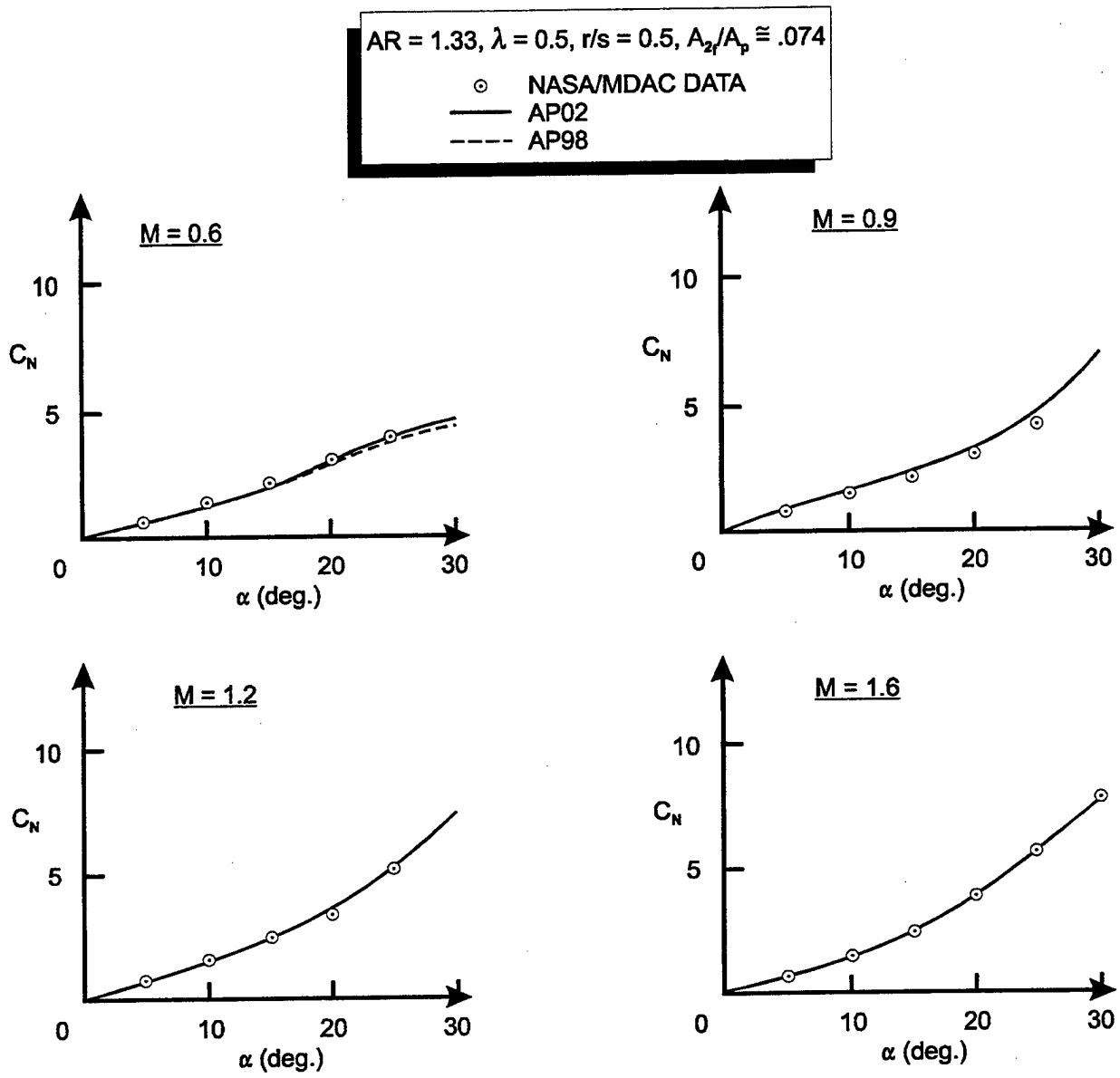

FIGURE 16. COMPARISON OF NASA/MDAC WING-BODY NORMAL FORCE WITH AP98 PREDICTIONS (FIN NO. 4)

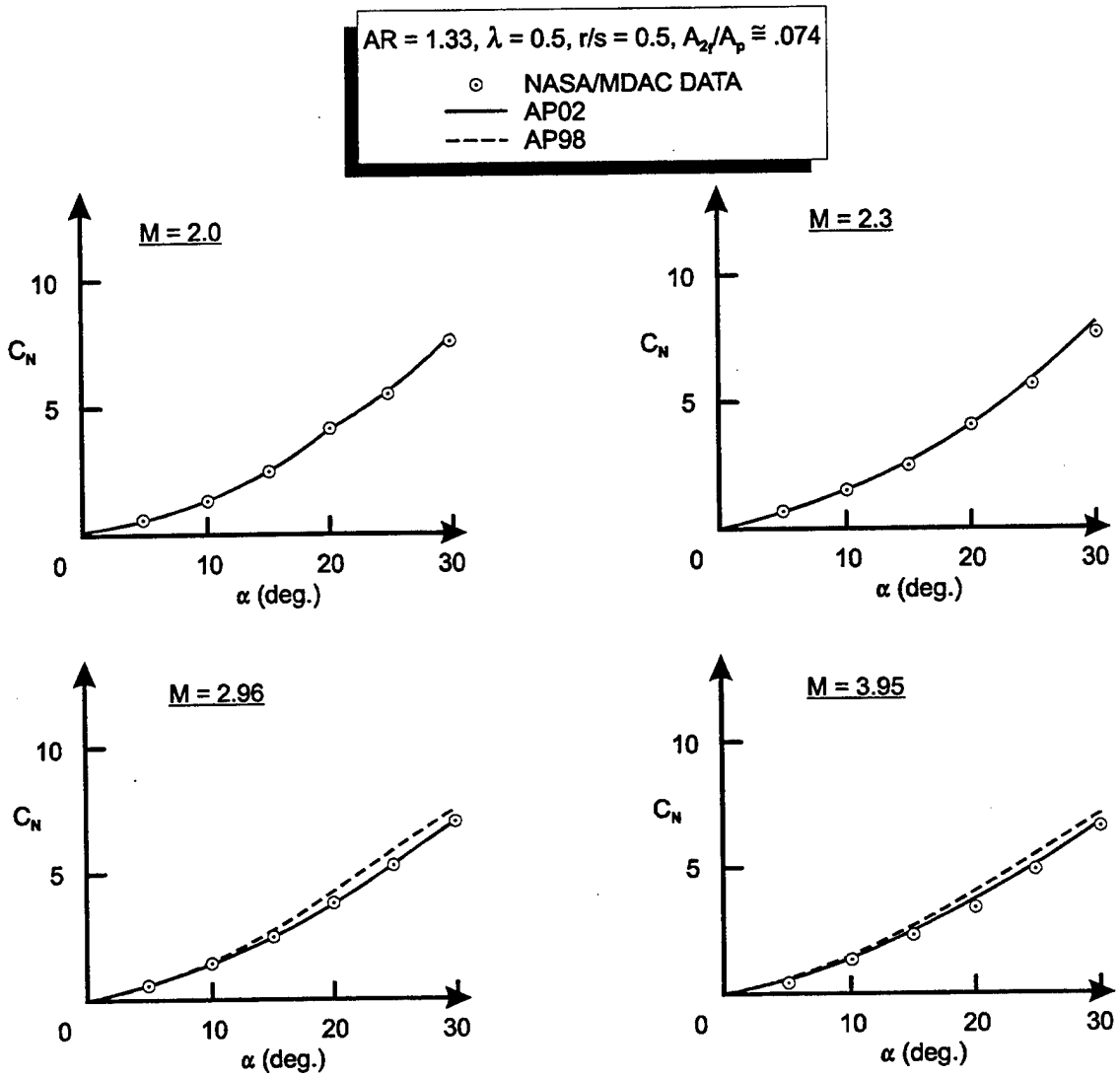

FIGURE 16. COMPARISON OF NASA/MDAC WING-BODY NORMAL FORCE WITH AP98 PREDICTIONS (FIN NO. 4) (Continued)

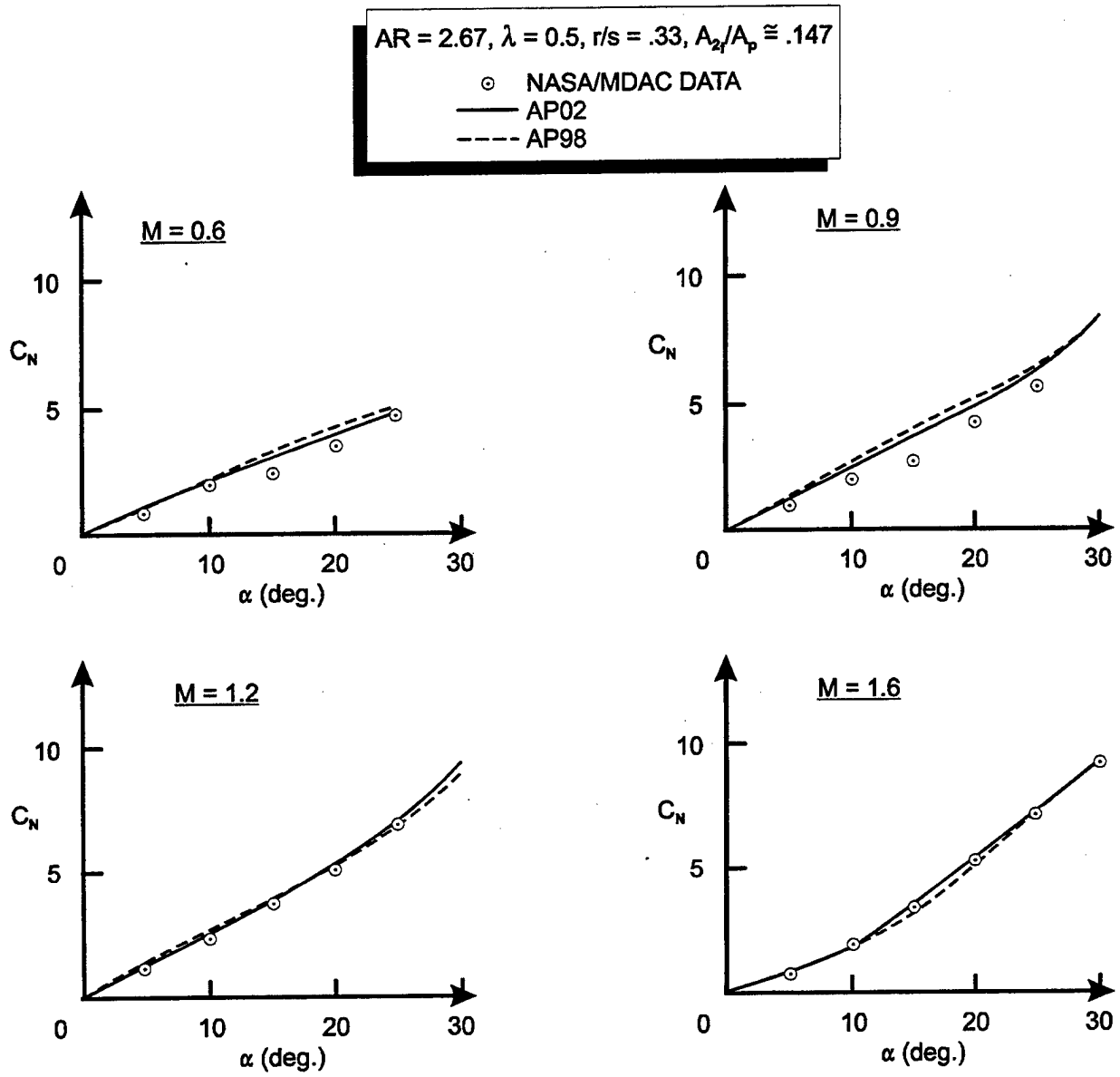

FIGURE 17. COMPARISON OF NASA/MDAC WING-BODY NORMAL FORCE WITH AP98 PREDICTIONS (FIN NO. 5)

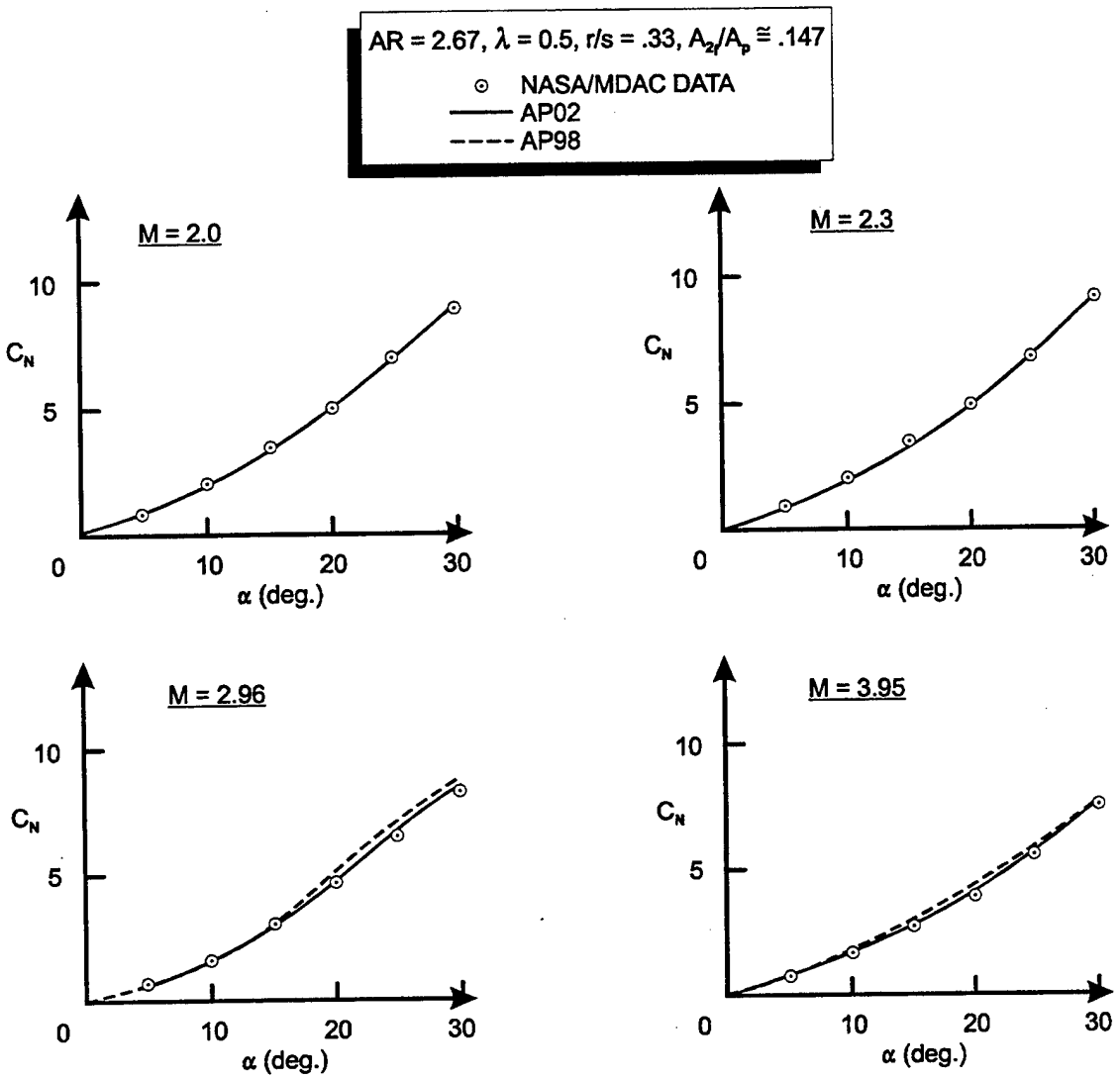

FIGURE 17. COMPARISON OF NASA/MDAC WING-BODY NORMAL FORCE WITH AP98 PREDICTIONS (FIN NO. 5) (Continued)

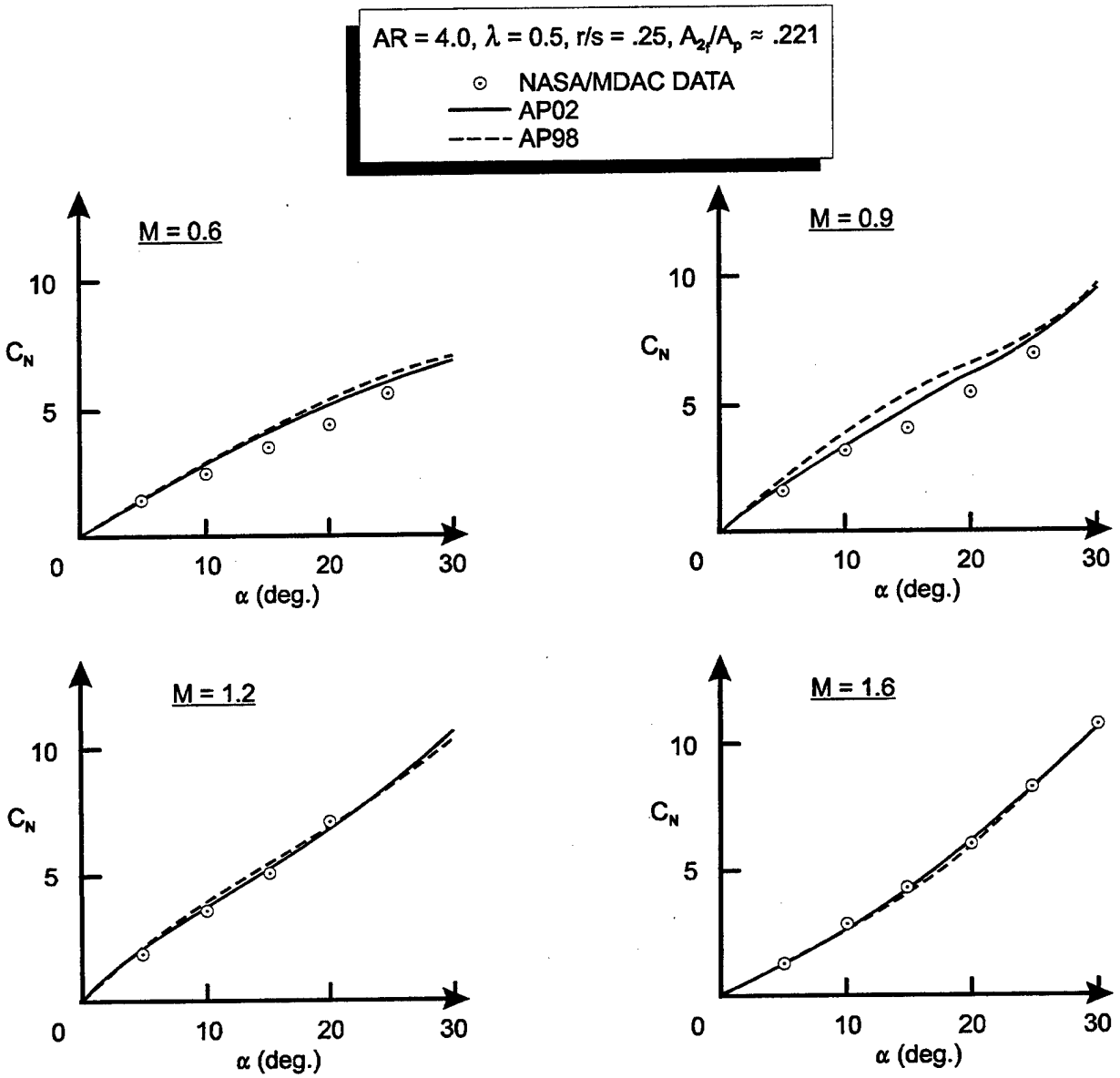

FIGURE 18. COMPARISON OF NASA/MDAC WING-BODY NORMAL FORCE WITH AP98 PREDICTIONS (FIN NO. 6)

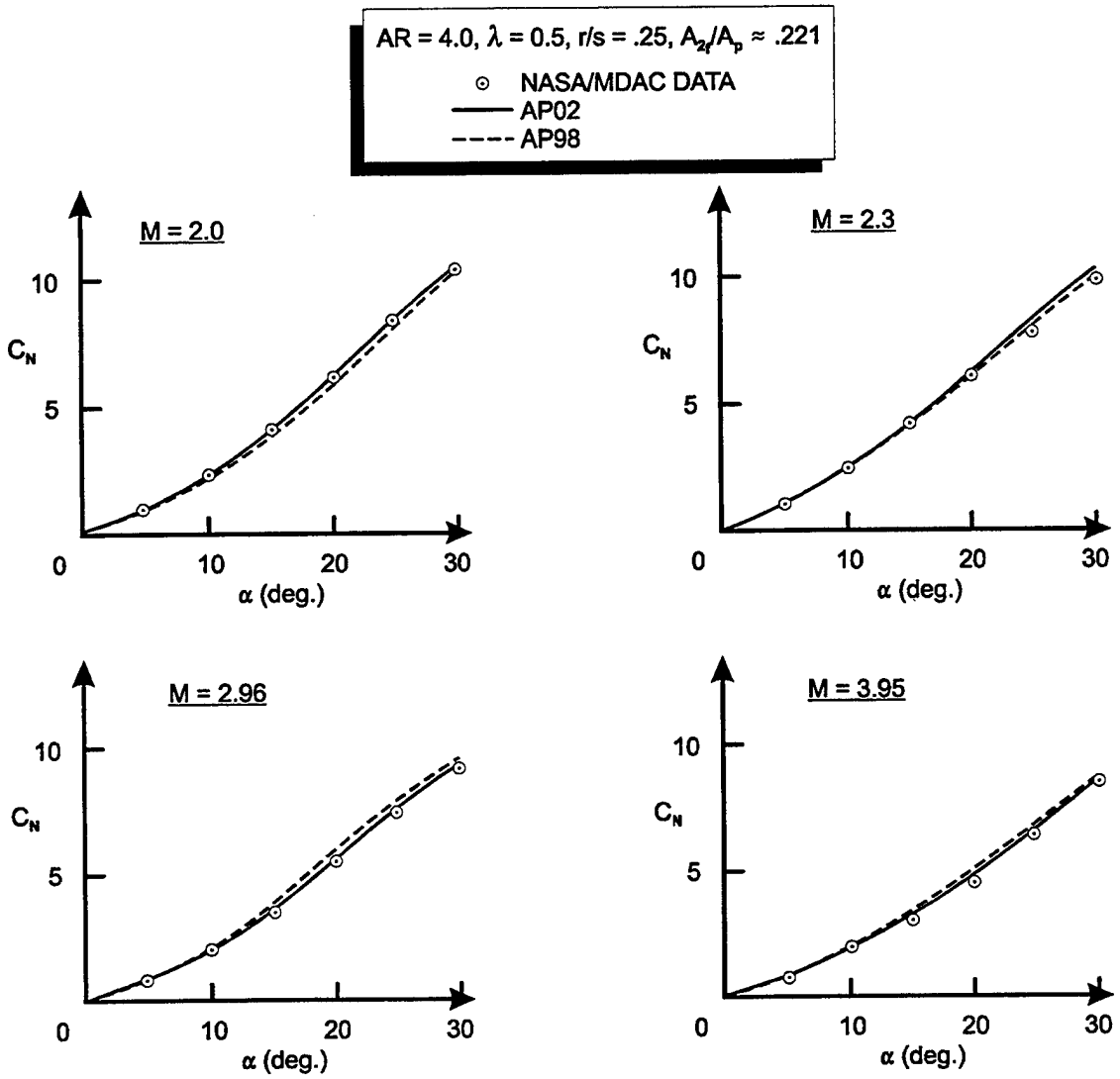

FIGURE 18. COMPARISON OF NASA/MDAC WING-BODY NORMAL FORCE WITH AP98 PREDICTIONS (FIN NO. 6) (Continued)

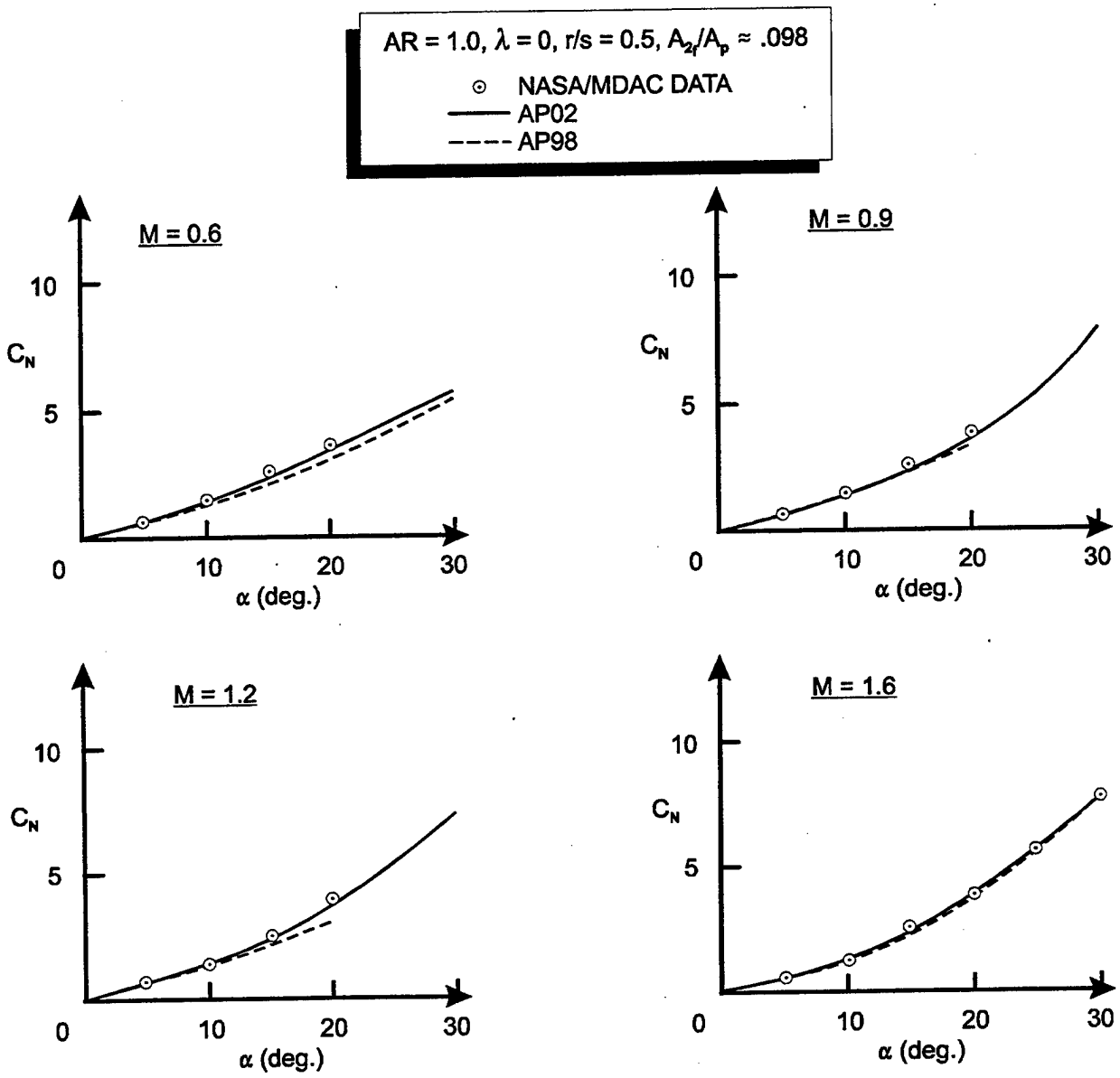

FIGURE 19. COMPARISON OF NASA/MDAC WING-BODY NORMAL FORCE WITH AP98 PREDICTIONS (FIN NO. 7)

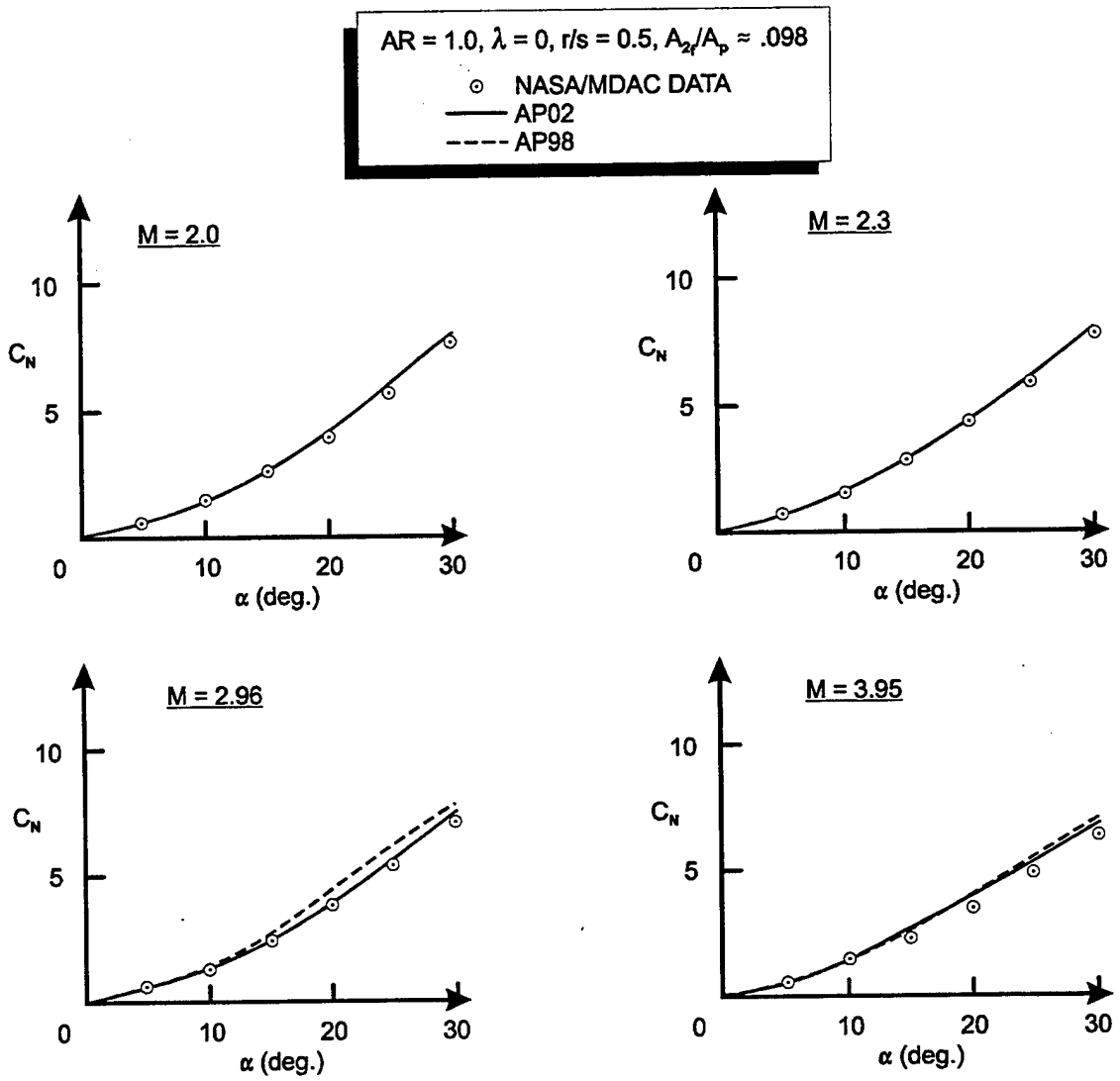

FIGURE 19. COMPARISON OF NASA/MDAC WING-BODY NORMAL FORCE WITH AP98 PREDICTIONS (FIN NO. 7) (Continued)

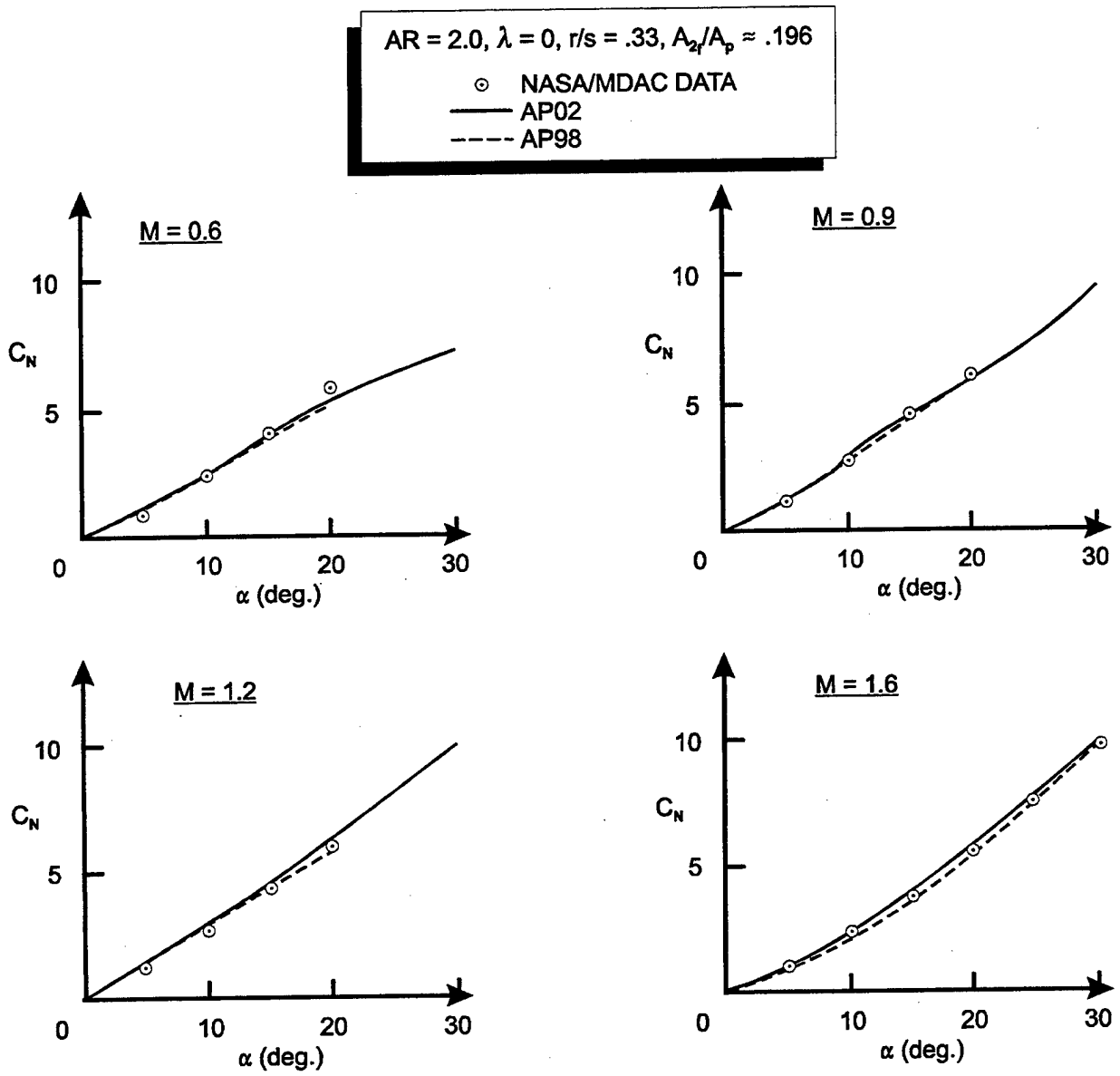

FIGURE 20. COMPARISON OF NASA/MDAC WING-BODY NORMAL FORCE WITH AP98 PREDICTIONS (FIN NO. 8)

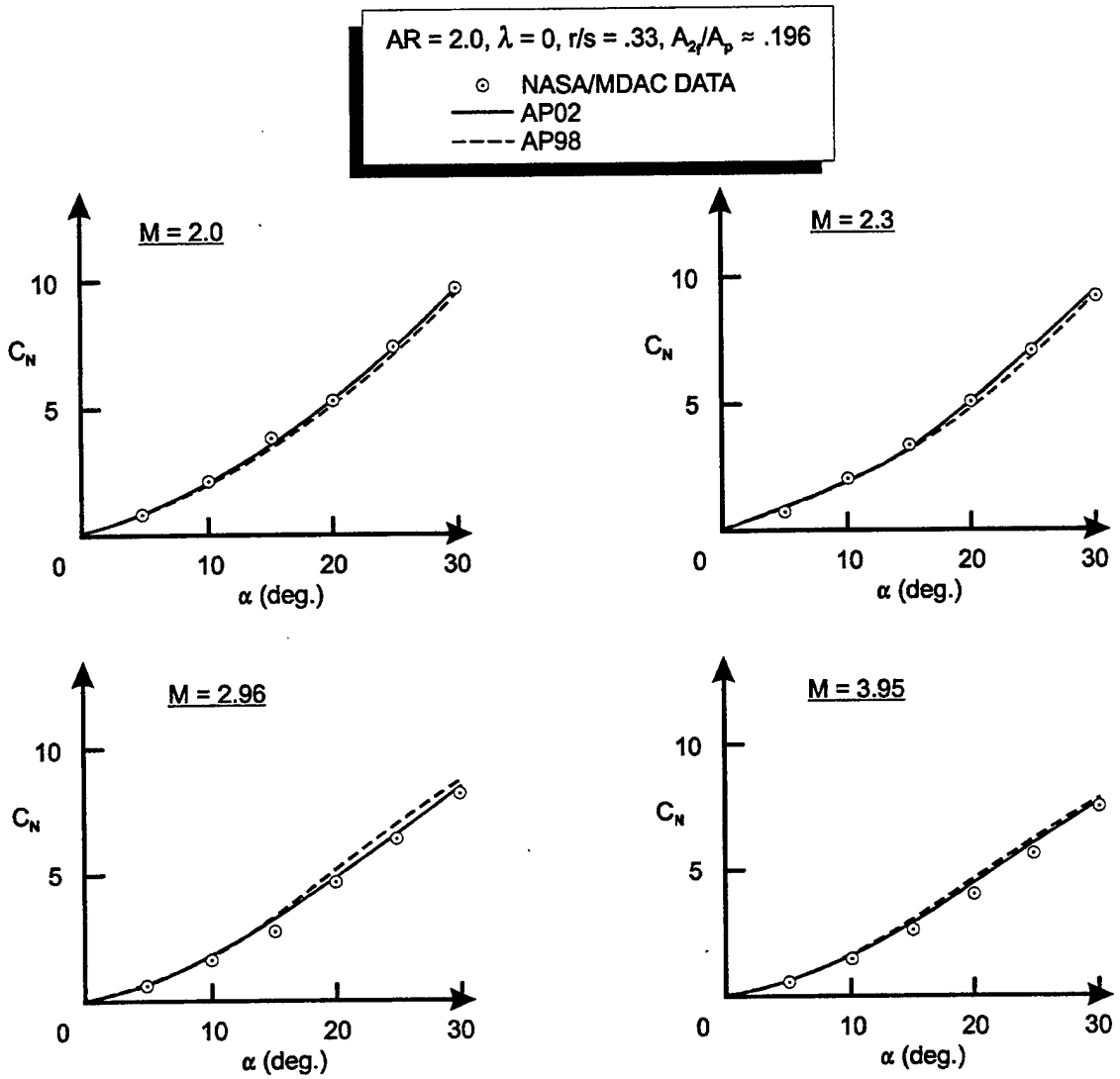

FIGURE 20. COMPARISON OF NASA/MDAC WING-BODY NORMAL FORCE WITH AP98 PREDICTIONS (FIN NO. 8) (Continued)

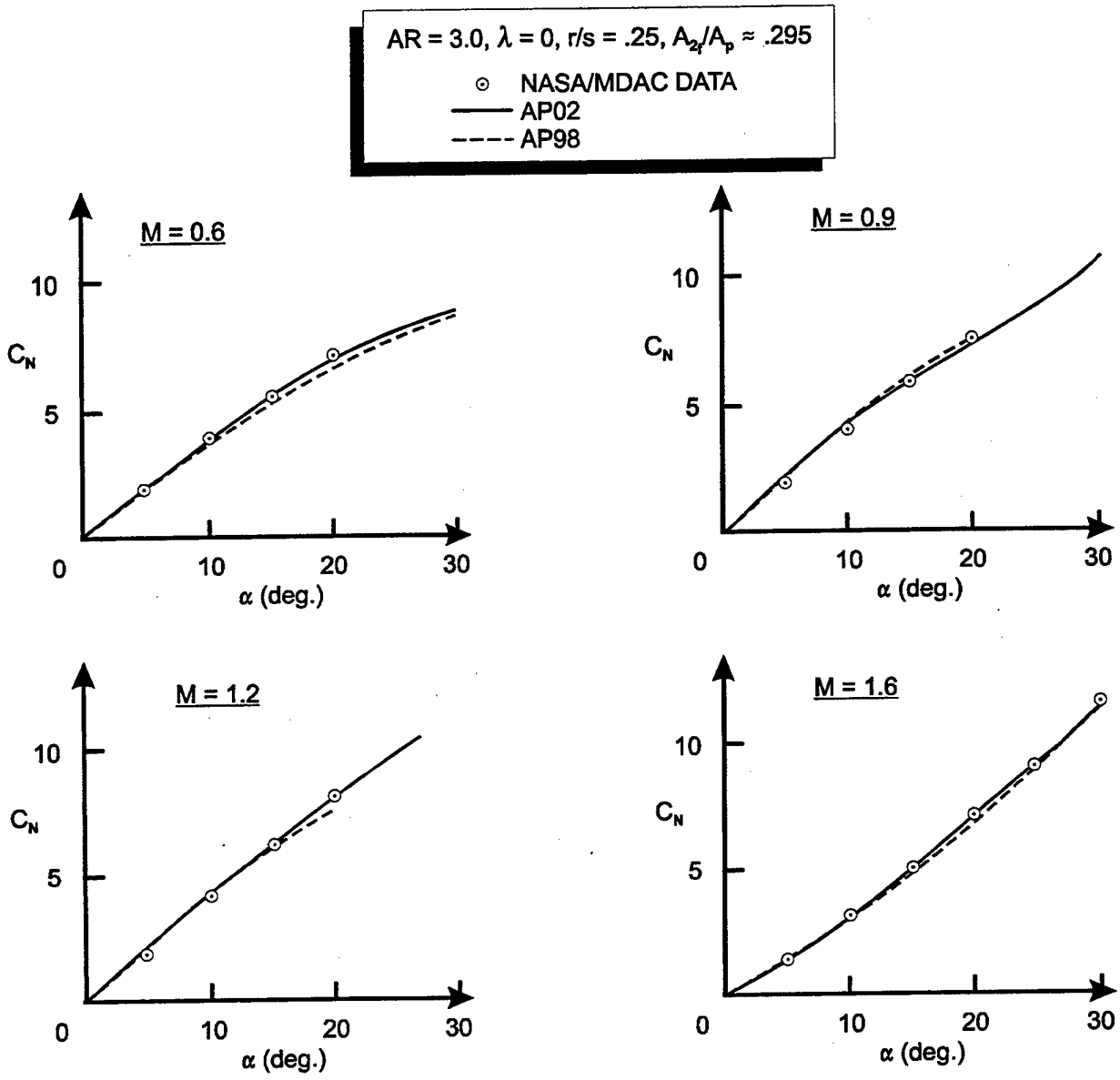

FIGURE 21. COMPARISON OF NASA/MDAC WING-BODY NORMAL FORCE WITH AP98 PREDICTIONS (FIN NO. 9)

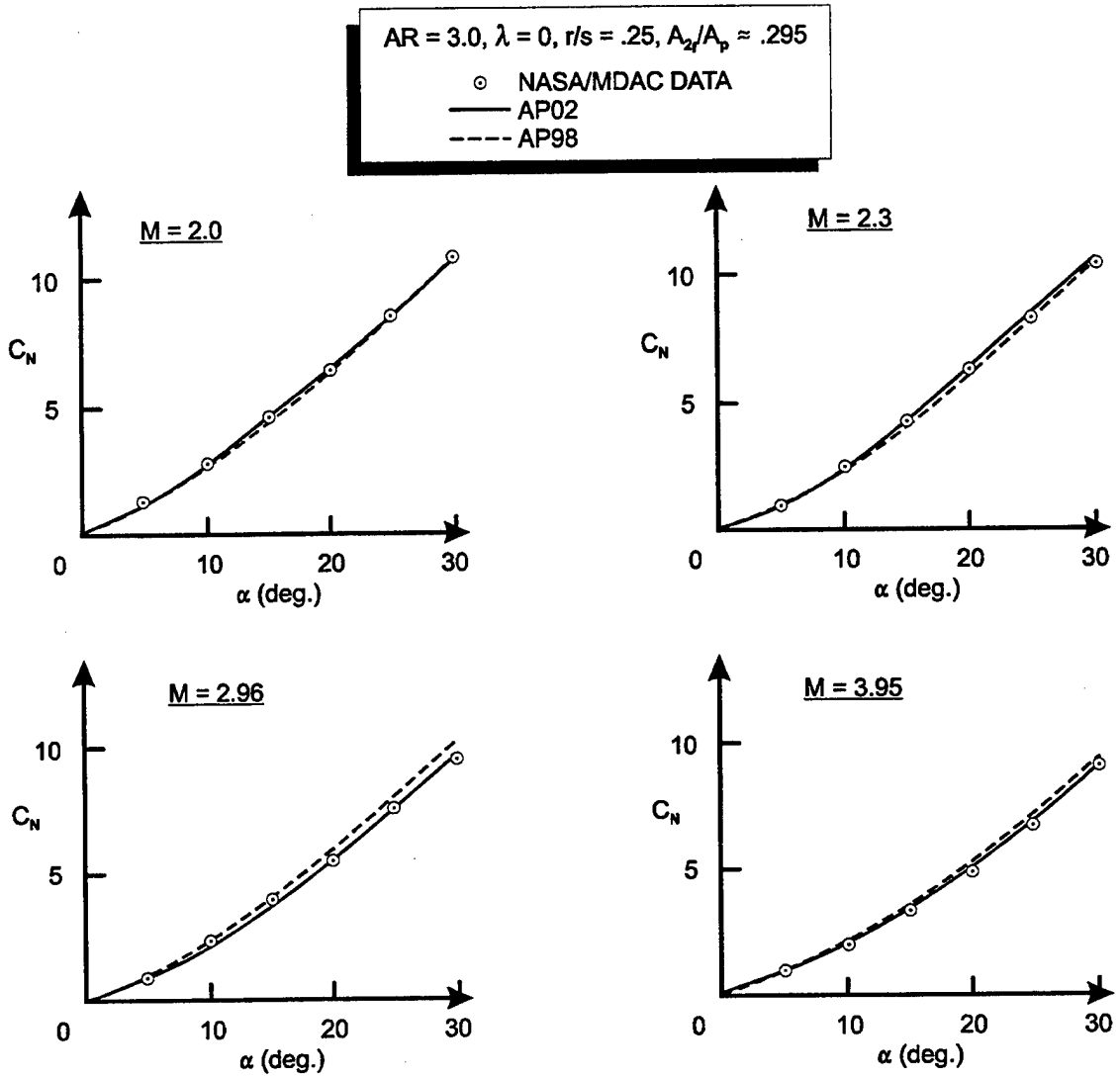

FIGURE 21. COMPARISON OF NASA/MDAC WING-BODY NORMAL FORCE WITH AP98 PREDICTIONS (FIN NO. 9) (Continued)

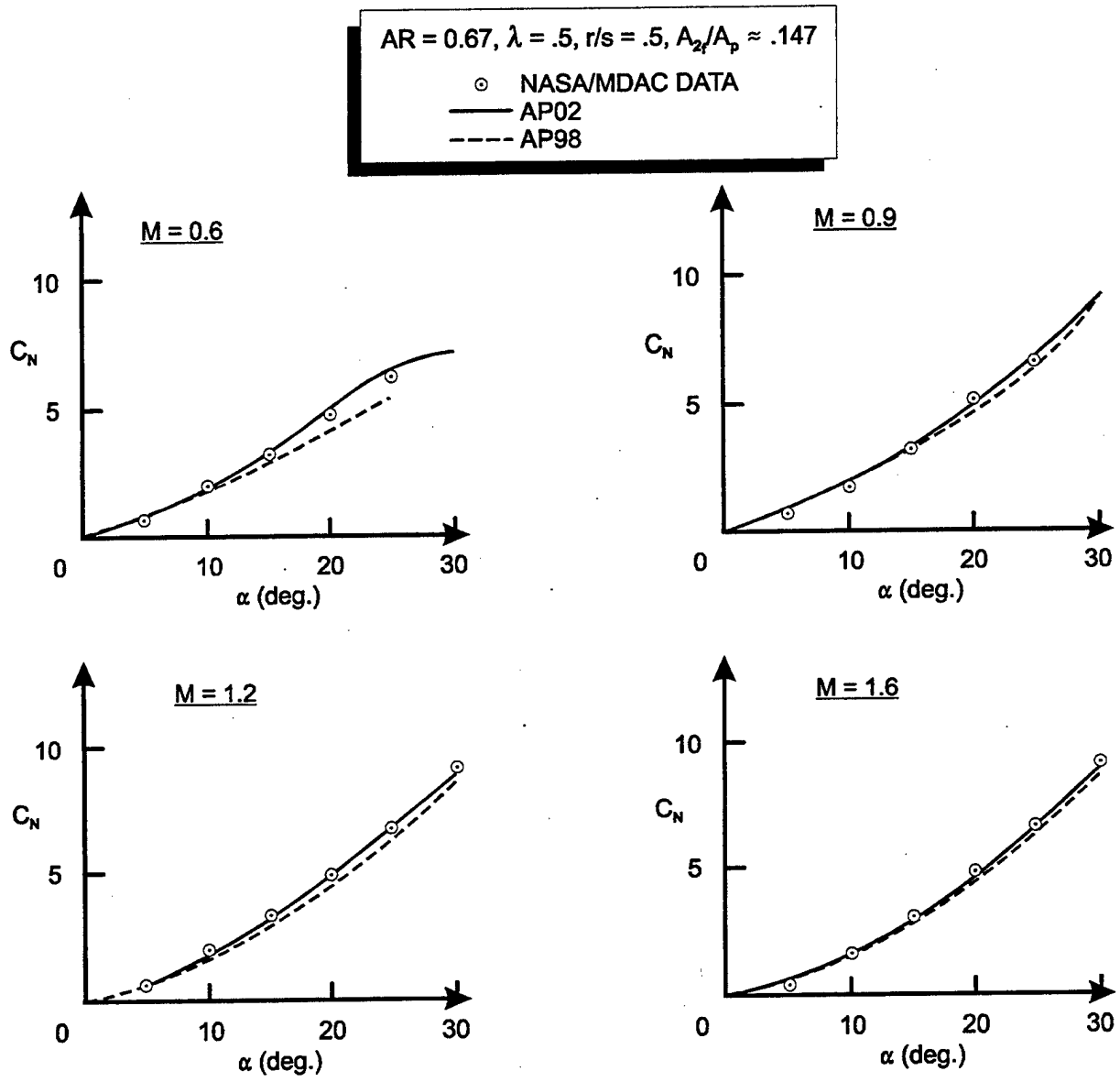

FIGURE 22. COMPARISON OF NASA/MDAC WING-BODY NORMAL FORCE WITH AP98 PREDICTIONS (FIN NO. 10)

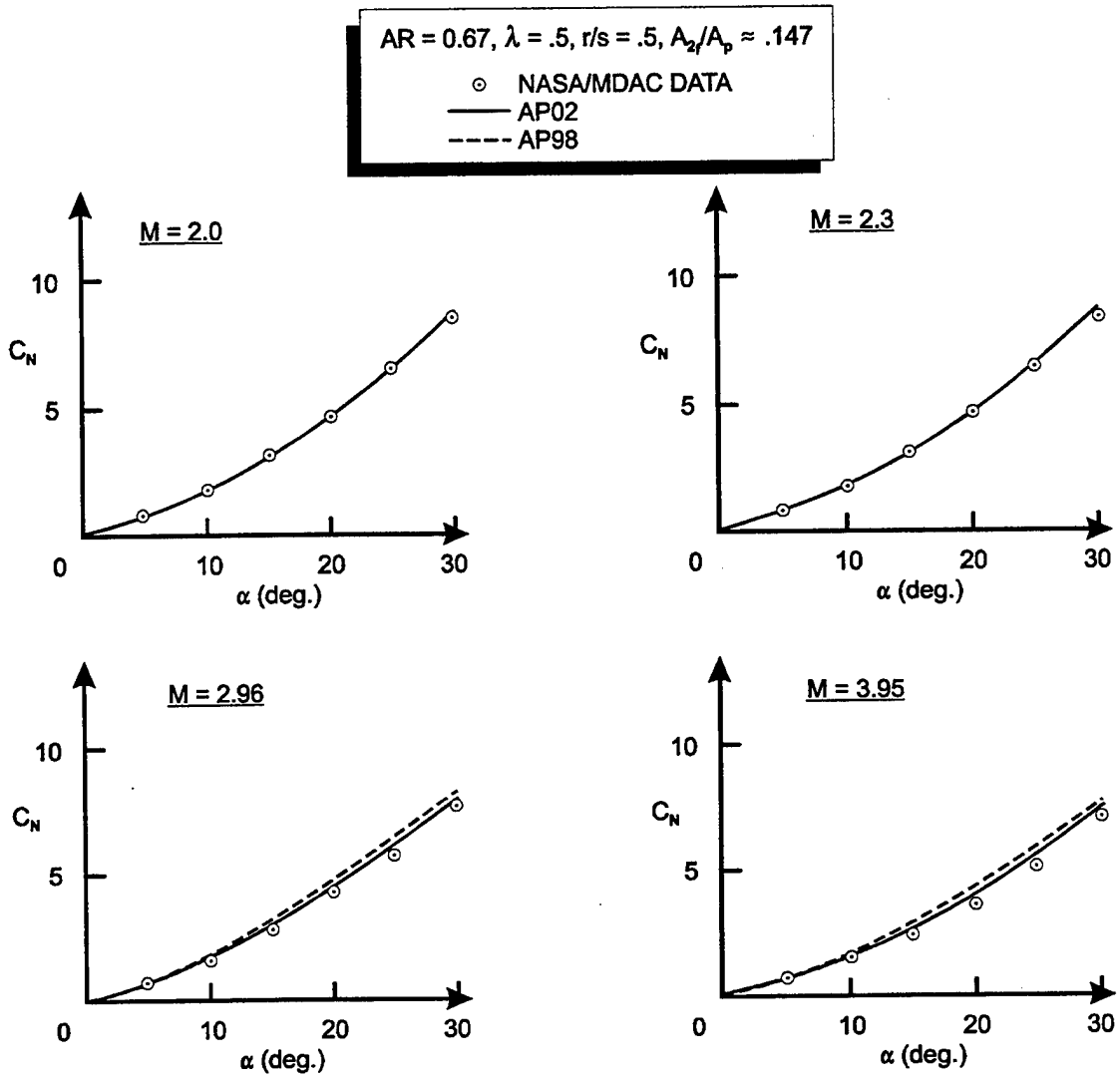

FIGURE 22. COMPARISON OF NASA/MDAC WING-BODY NORMAL FORCE WITH AP98 PREDICTIONS (FIN NO. 10) (Continued)

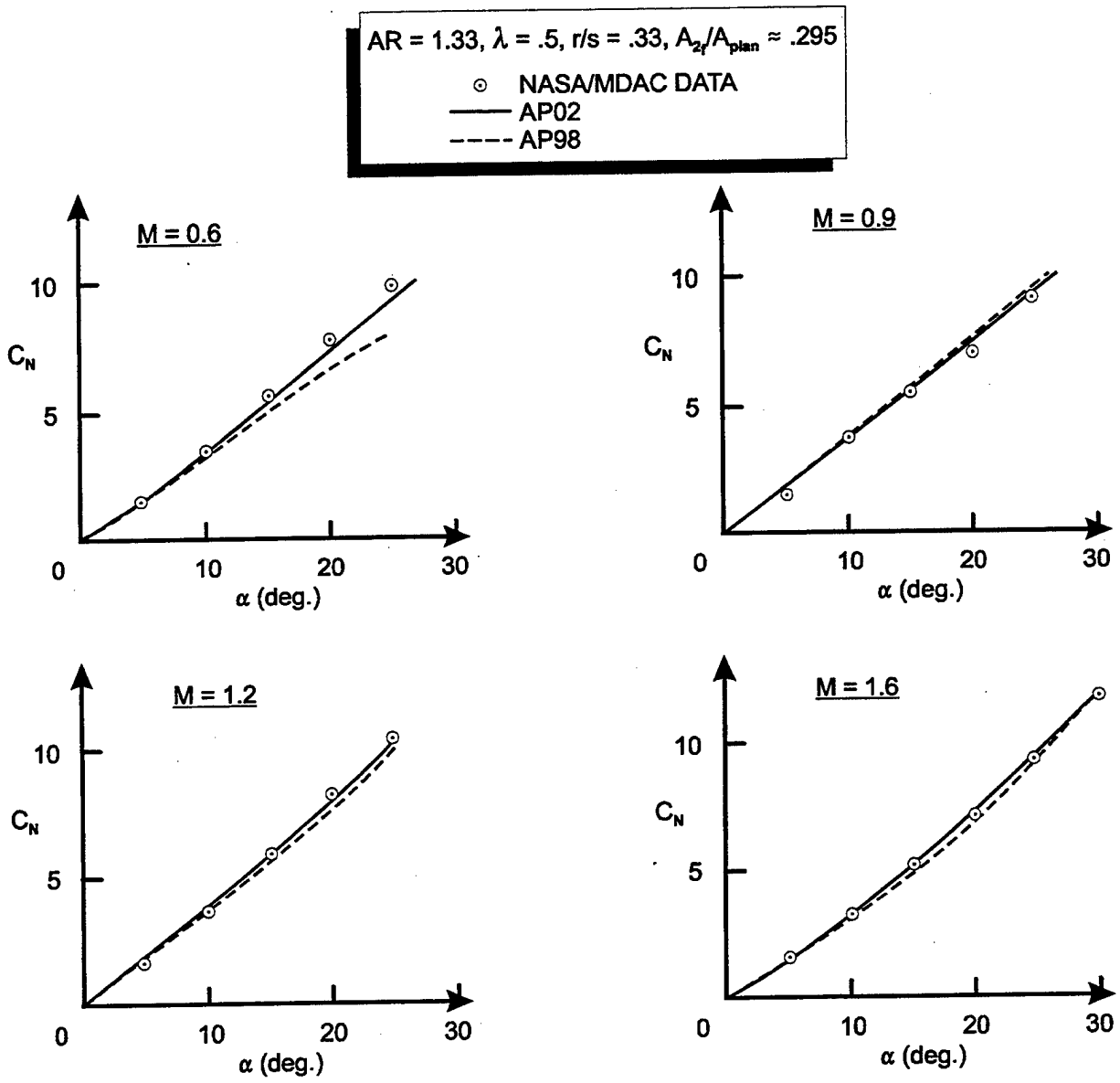

FIGURE 23. COMPARISON OF NASA/MDAC WING-BODY NORMAL FORCE WITH AP98 PREDICTIONS (FIN NO. 11)

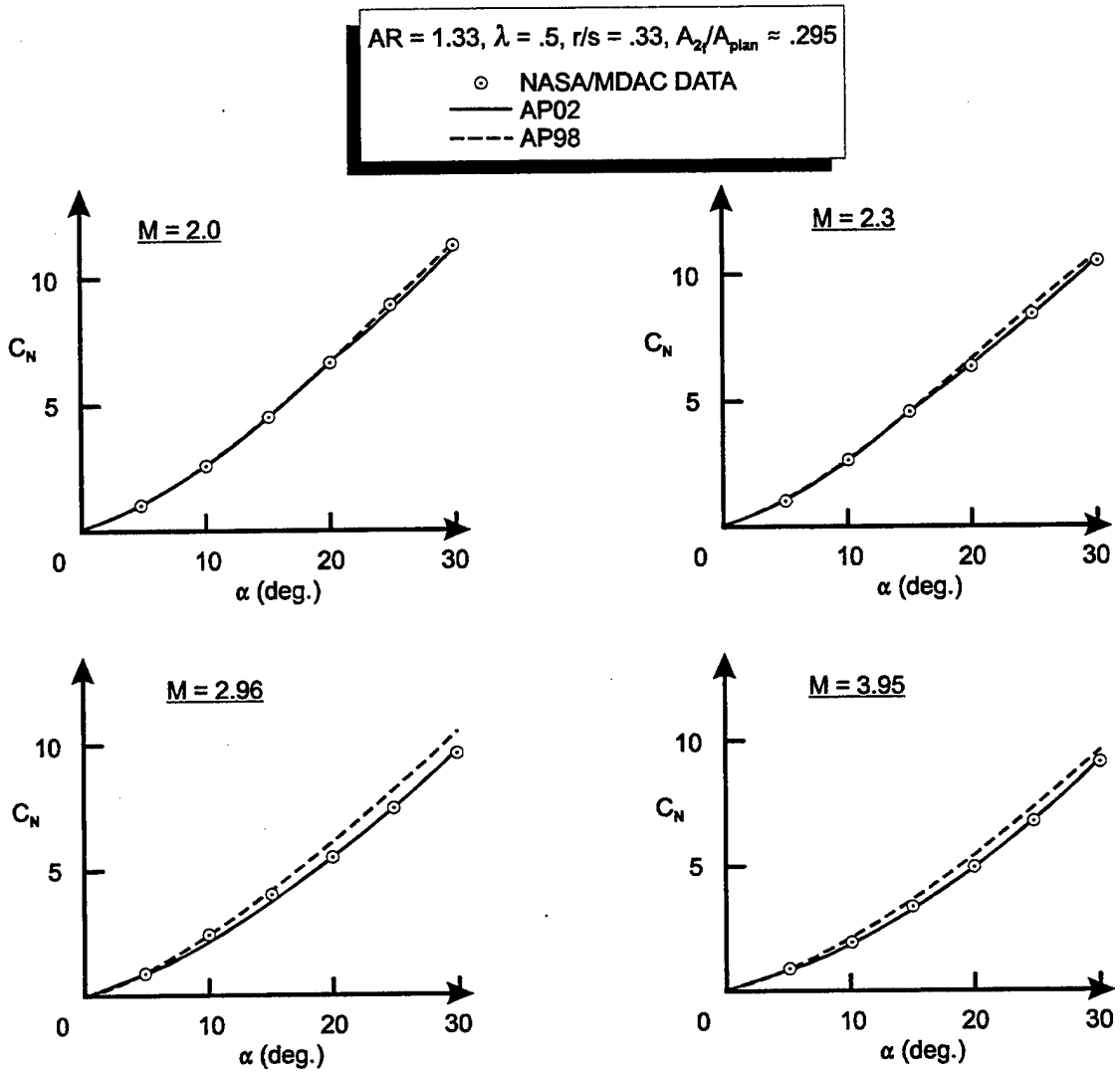

FIGURE 23. COMPARISON OF NASA/MDAC WING-BODY NORMAL FORCE WITH AP98 PREDICTIONS (FIN NO. 11) (Continued)

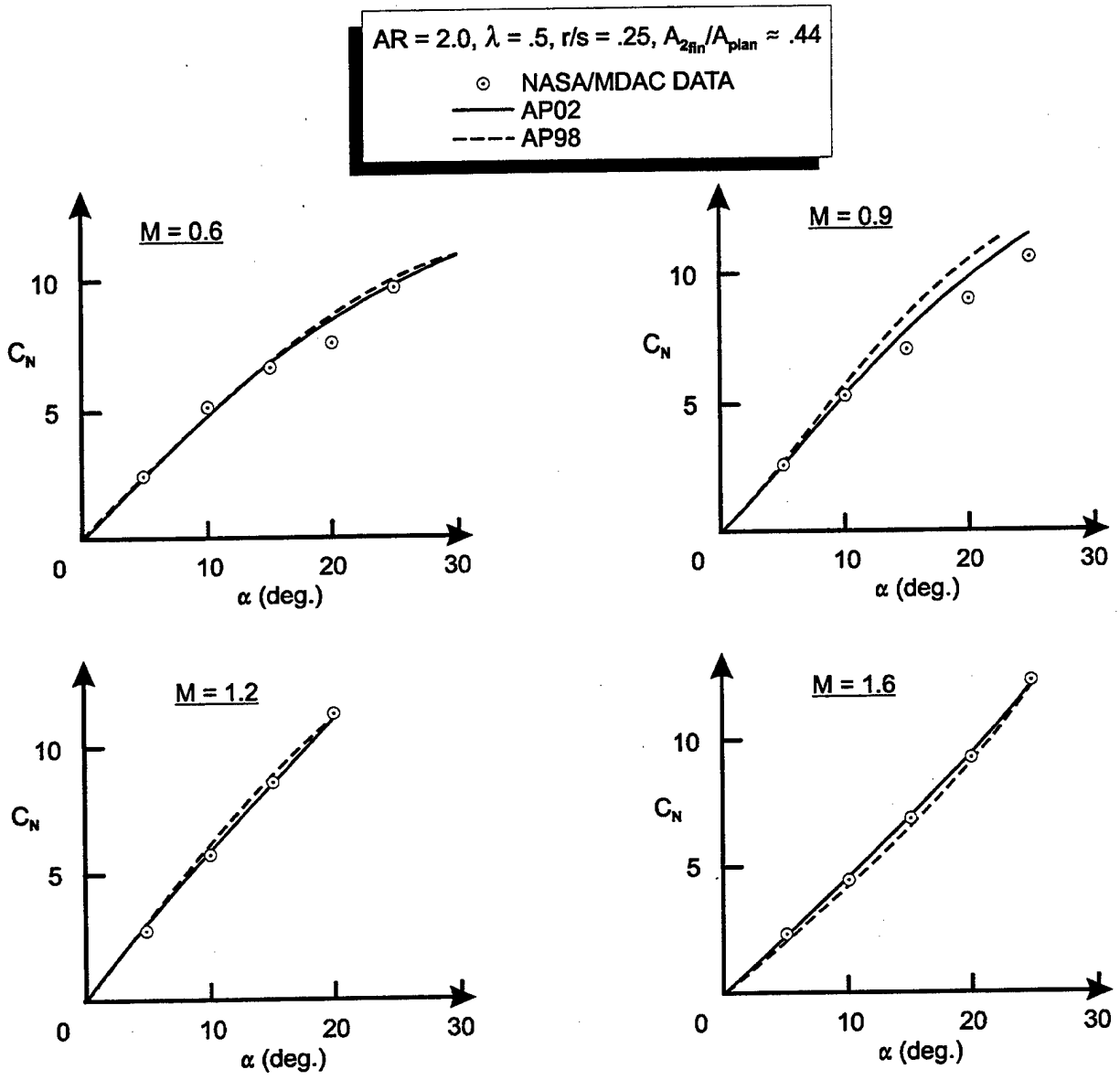

FIGURE 24. COMPARISON OF NASA/MDAC WING-BODY NORMAL FORCE WITH AP98 PREDICTIONS (FIN NO. 12)

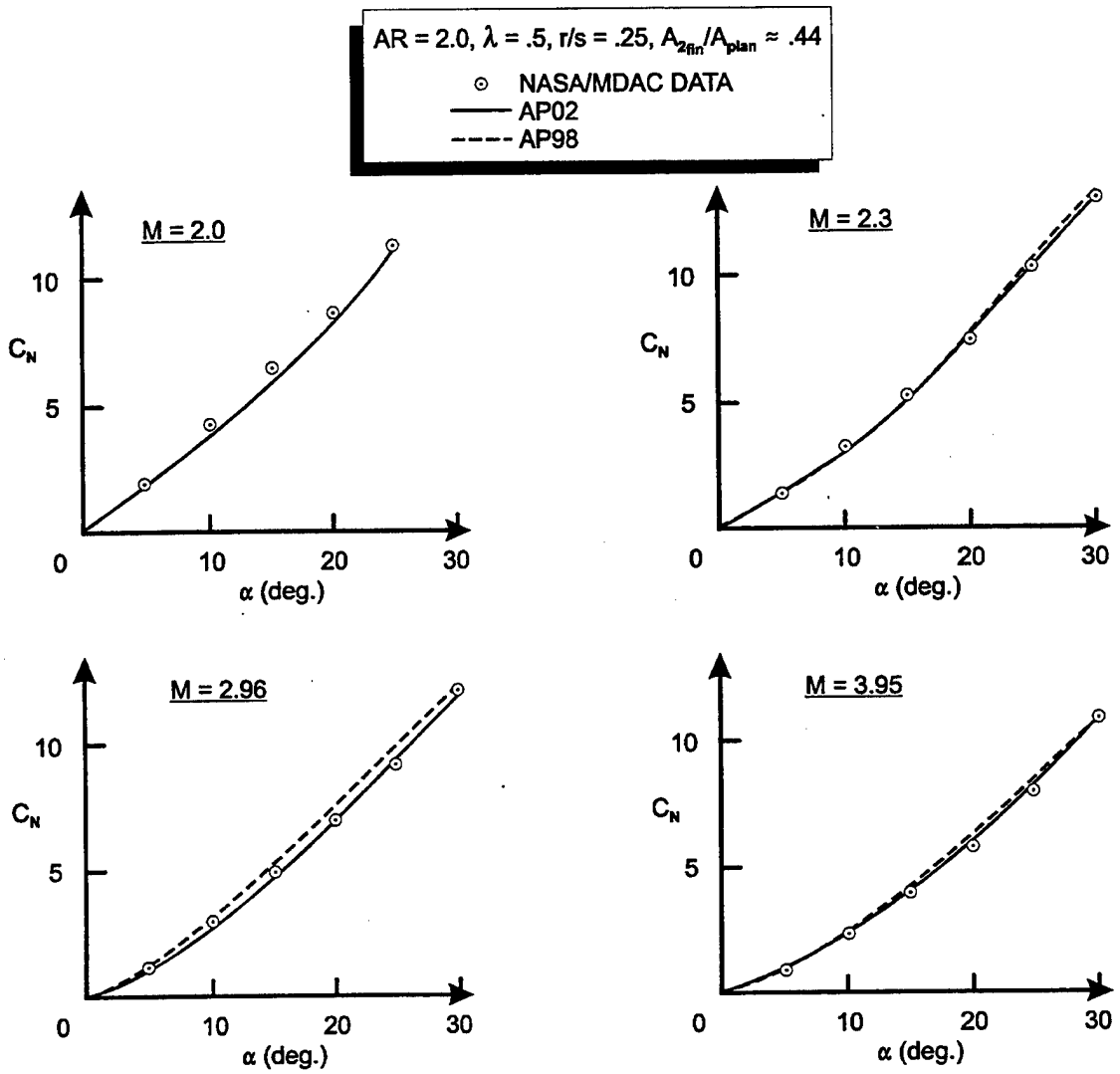

FIGURE 24. COMPARISON OF NASA/MDAC WING-BODY NORMAL FORCE WITH AP98 PREDICTIONS (FIN NO. 12) (Continued)

TABLE 27. AVERAGE NORMAL FORCE ERRORS OF AP02 COMPARED TO NASA/MDAC[7] DATA BASE ($\Phi = 0$)

MACH NO.	NO. POINTS	AVERAGE ERROR (PERCENT)
0.6	42	7.2
0.9	42	8.7
1.2	42	3.7
1.6	60	2.7
2.0	60	3.0
2.3	60	3.1
2.96	60	3.7
3.95	60	4.9
TOTALS	426	4.4

To check and see if the AP02 improvements have a positive or negative impact on predictions for the aerodynamics of the NASA Tri-Service data base,[4] Tables 28 and 29 were prepared. The Tri-Service data base consisted of Mach numbers 0.6, 0.8, 1.2, 1.5, 2.0, 2.5, 3.0, 3.5, and 4.5 with AOA up to 25 to 40 deg, depending on Mach number. Fins and body tested are shown in Figure 4. The highest aspect ratio fins were very small (AR = 4), so the data associated with those fins was not considered in the Tables 27 and 28 averages. Also, the aspect ratio 2.0 fin data was only considered above M = 1.5 in the averaging process. The overall average error for 442 data points in the $\Phi = 0$ deg roll is 3.4 percent. This compares to a value between 4 and 5 percent for the AP98. The $\Phi = 45$ deg roll results are presented in Table 29. Here, 362 data points were considered at the same AOA and Mach numbers as for the $\Phi = 0$ deg roll position. The average normal force error for each Mach number is less than 10 percent and the overall average for the entire data base is 3.5 percent. Reference 16 shows that the AP98 average accuracy for the $\Phi = 45$ deg roll is 6.2 percent for C_N and 1.2 percent of the body length for center of pressure.

Table 30 then combines the results for Tables 27 through 29 into an overall average. This overall average error is less than 4 percent, with the worst case averages being in subsonic and transonic flow, where matching the optimum critical crossflow Reynolds number is quite difficult. In scanning over the 1230 data points, it was seen that some worse-case errors can approach 30 percent in the subsonic region, even when we try to utilize the best crossflow Reynolds number for body-alone results. The flowfield changes when wings are added, so the best critical crossflow Reynolds number for the body alone may be different than the optimum value for the wing-body. Generally speaking, the worst-case errors at supersonic speeds are at low angle of attack where experimental data corrections for nonzero AOA were not made. Errors as high as 15 percent were seen. However, errors of this magnitude for a single data point were quite rare. It is seen that the improvements based on the Reference 7 data base carried over to the Reference 4 data base as well. Hence, the overall accuracy of the AP02 in predicting lifting characteristics of missile configurations should be slightly improved over the AP98.

TABLE 28. AVERAGE NORMAL FORCE ERRORS OF AP02 COMPARED TO NASA/TRI-SERVICE[4] DATA BASE ($\Phi = 0$)

MACH NO.	NO. POINTS	AVERAGE ERROR (PERCENT)
0.6	25	3.2
0.8	30	4.8
1.2	33	3.6
1.5	63	2.2
2.0	59	3.5
2.5	58	2.6
3.0	58	3.7
3.5	57	3.9
4.5	59	3.6
TOTALS	442	3.4

TABLE 29. AVERAGE NORMAL FORCE ERRORS OF AP02 COMPARED TO NASA/TRI-SERVICE[4] DATA BASE ($\Phi = 45$ DEG)

MACH NO.	NO. POINTS	AVERAGE ERROR (PERCENT)
0.6	22	4.8
0.8	23	7.5
1.2	27	3.8
1.5	49	3.0
2.0	49	3.5
2.5	48	2.5
3.0	49	3.2
3.5	46	3.7
4.5	49	2.7
TOTALS	362	3.5

TABLE 30. AVERAGE NORMAL FORCE ERRORS OF AP02 COMPARED TO COMBINED DATA BASES[4,7]

MACH NO.	NO. POINTS	AVERAGE ERROR (PERCENT)
0.6	89	5.5
0.8-0.9	95	7.2
1.2	102	3.7
1.5-1.6	172	2.6
2.0	168	3.3
2.3-2.5	166	2.8
2.96-3.0	167	3.6
3.5-3.95	163	4.2
4.5	108	3.2
TOTALS	1230	3.8

No average error on center of pressure was made because of time constraints. However, suffice it to say that the average center of pressure error for the AP98 on the NASA Tri-Service data base was less than 2 percent of the body length.[13] Improvements made in normal force should only improve these already excellent predictions. Likewise, no improvements in axial force were sought, as we were quite happy with the power-off predictions of axial force from the AP98. Improvements in power-on axial force will be addressed in a future report.

4.0 COMPARISON OF AP02 TO CONFIGURATIONS OUTSIDE THE REFERENCES 4 AND 7 DATA BASES

While the average accuracy comparisons of C_N to experiment of Tables 26 through 28 are impressive for a semiempirical code, the true measure of success is based on the ability to accurately predict aerodynamics on a wide variety of configurations outside the data bases upon which the empirical nonlinearities were derived. Several cases will be considered over a variety of flight conditions to make the determination of whether the improvements added to the AP02 are generically applicable to other missile configurations and if they improve the accuracy of aerodynamic estimation over the AP98. For this part of the validation effort, roll positions of both $\Phi = 0$ and 45 deg will be considered. Also, comparisons of the AP02 to the AP98 as well as to wind tunnel data will be given.

The first case considered is taken from Reference 17 and is a model of an older version of the SEASPARROW missile. A fairly extensive data base exists for this configuration. The configuration is shown in Figure 25, where the wings are used for control.

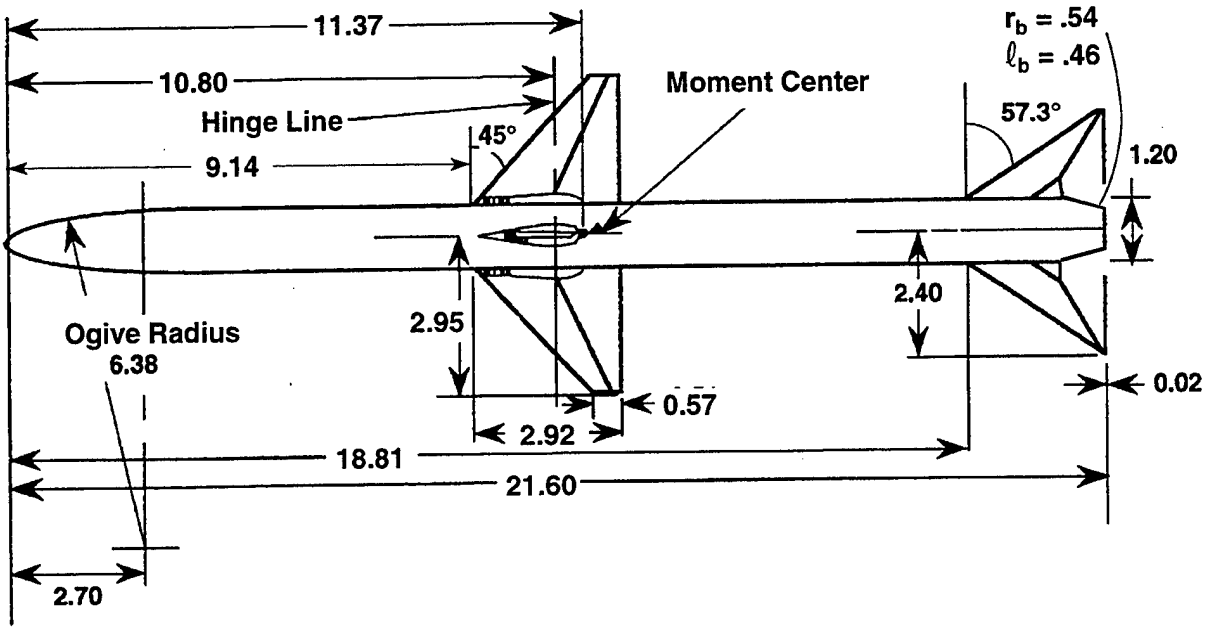

FIGURE 25. WING-BODY-TAIL CONFIGURATION USED IN VALIDATION PROCESS (ALL DIMENSIONS IN INCHES)

This configuration has a length of about 18 calibers with a tangent ogive nose 2.25 calibers in length. It has wings and tails of fairly high aspect ratios of 2.8 and 2.6 respectively. Data was taken at Mach numbers of 1.5 to 4.63 for AOAs to 40 deg and control deflections of 0 and 10 deg (at M of 1.5 and 2.0) and 0 to 20 deg (at M of 2.35 to 4.63). The data was taken at a Reynolds number of 2.5×10^6/ft and boundary layer trips were also used. The model had a hollow camber, and camber axial force measurements were given separately in Reference 20. These results were added to the forebody axial force measurements to compare with the AP98 and AP02.

Figure 26 shows the comparisons of the AP98 and AP02 to the data of Reference 17 for $\Phi = 0$ deg and $\Phi = 45$ deg. Figure 26A and 26B give C_A, C_N, and C_M for $M_\infty = 1.5$ at $\delta_W = 0$ and $\delta_W = 10$ deg at $\Phi = 0$ deg. In general, both the AP98 and AP02 give good comparisons to data. Figure 26C and 26D give similar results for $M_\infty = 2.87$, and Figure 26E and 26F, for $M_\infty = 4.6$. Overall, for this configuration, at $\Phi = 0$ deg roll, the AP02 and AP98 are about equal in overall accuracy comparisons. The worst case errors are for center of pressure at higher Mach number and AOA where the bow shock intersects the wing shocks. This nonlinear phenomenon is not modeled in the $\Phi = 0$ deg roll orientation at all. For the $\Phi = 45$ deg roll, the center of pressure shift, Equation (10), partially accounts for this phenomenon, but not entirely. Center of pressure errors approach 0.6 caliber or 3 percent of the body length at $M_\infty = 4.6$ and $\alpha = 40$ deg. The other point is that the normal force predicted by the AP02 for combined α and δ_W is better than the AP98 at $M_\infty = 4.6$, whereas the opposite is true for the axial force at high AOA. The reason for this phenomenon has to do with the fact that the wing-alone normal force tables were

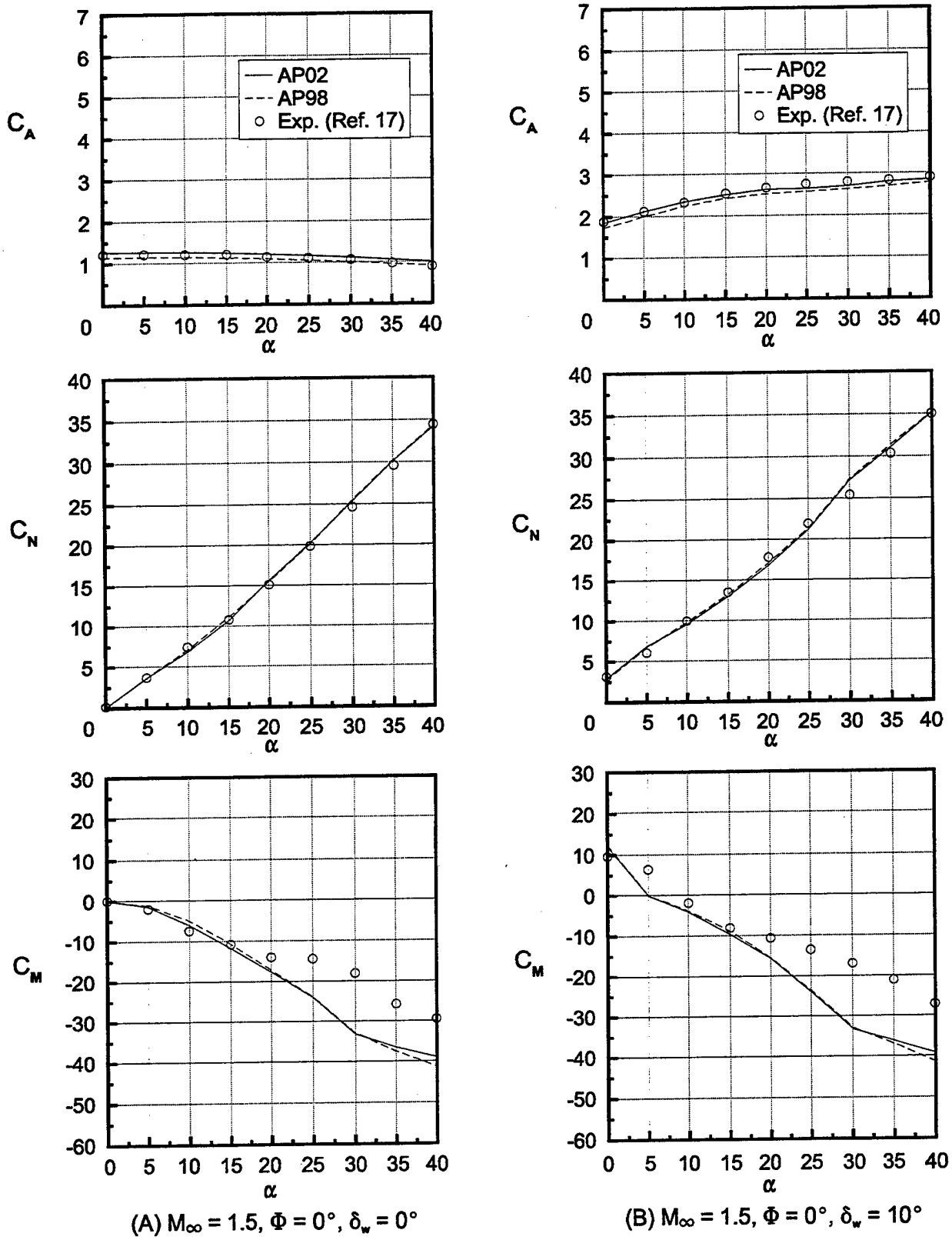

FIGURE 26. COMPARISON OF EXPERIMENT AND THEORY FOR C_A, C_N AND C_M FOR FIGURE 25 WING CONTROL CASE

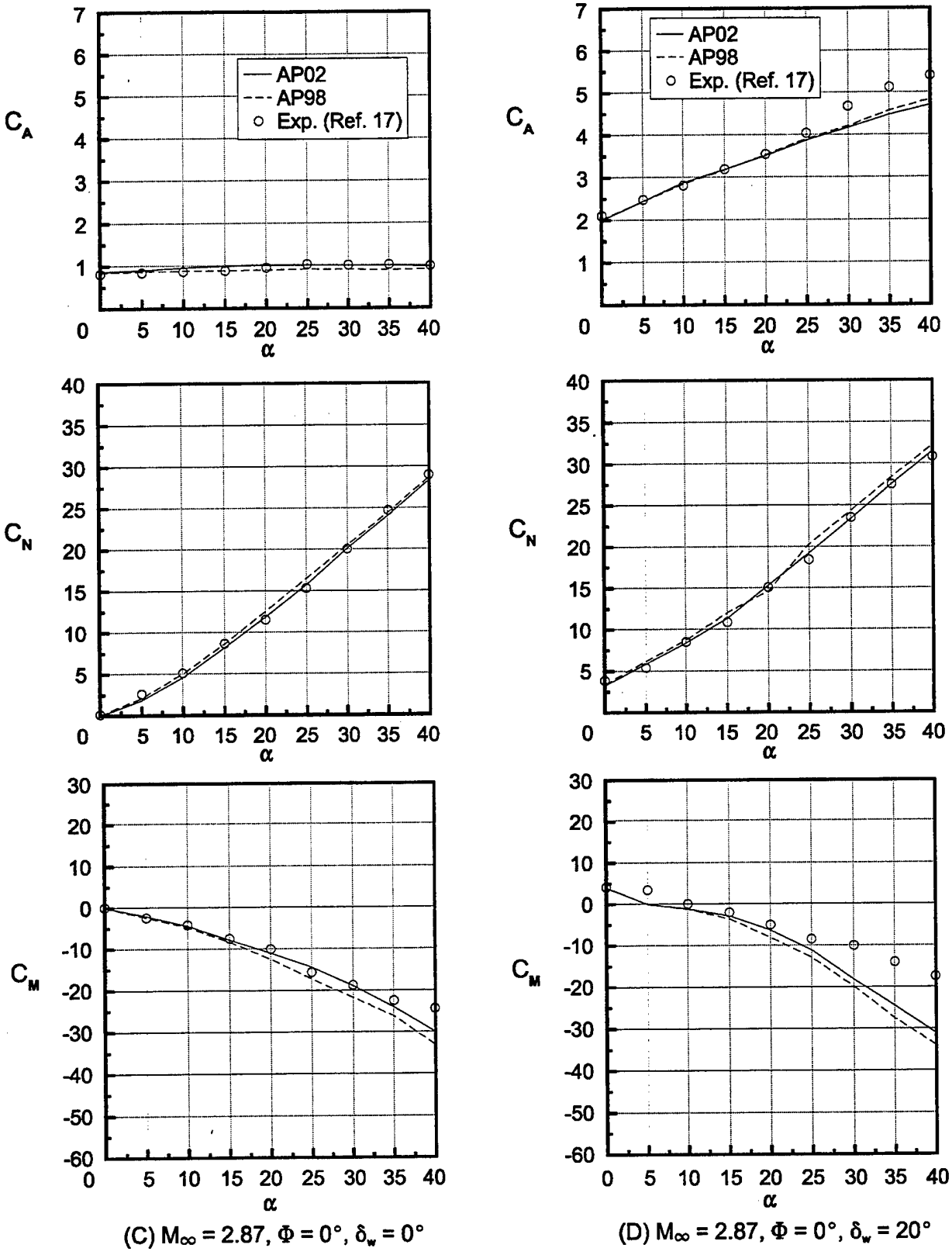

FIGURE 26. COMPARISON OF EXPERIMENT AND THEORY FOR C_A, C_N AND C_M FOR FIGURE 25 WING CONTROL CASE (Continued)

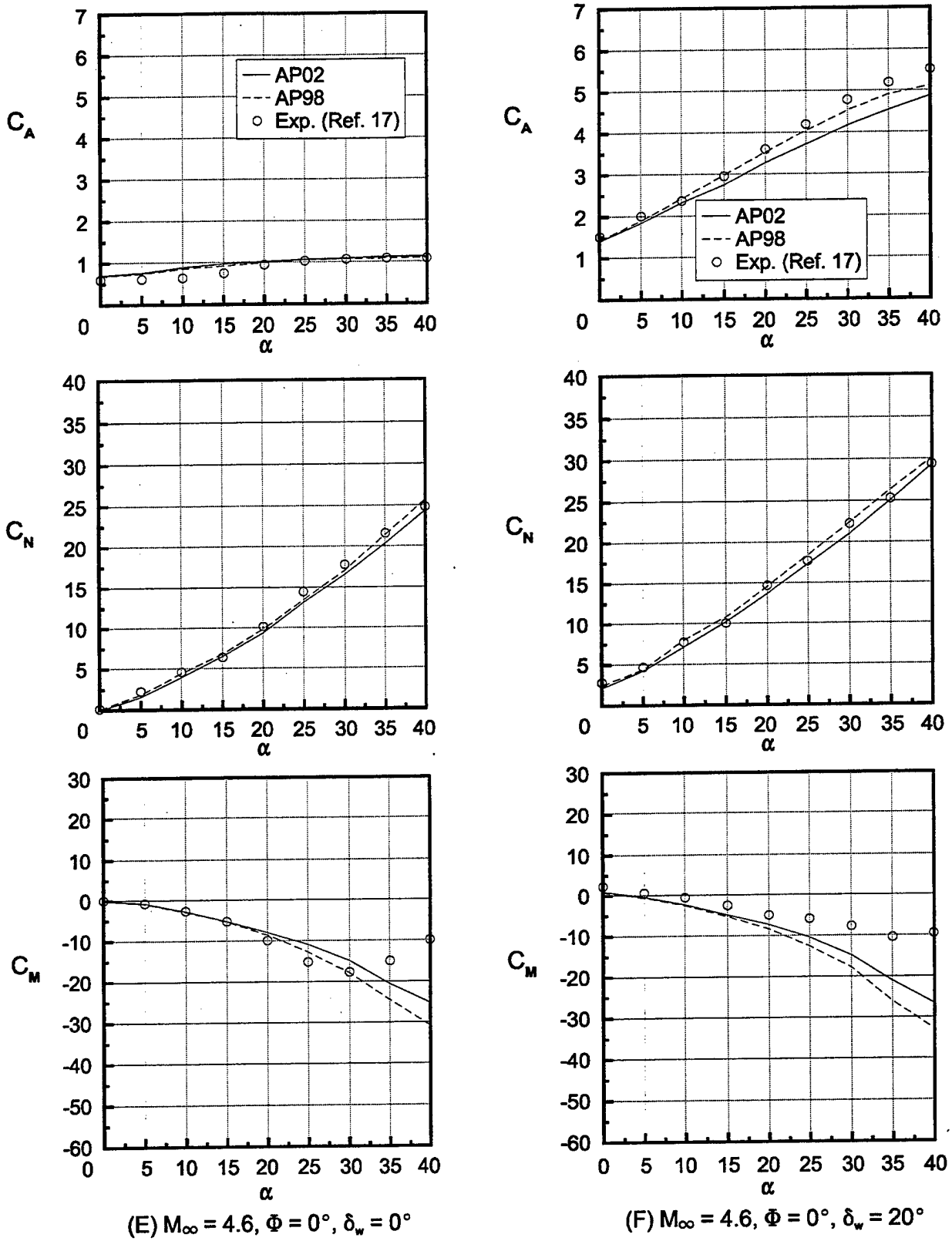

FIGURE 26. COMPARISON OF EXPERIMENT AND THEORY FOR C_A, C_N AND C_M FOR FIGURE 25 WING CONTROL CASE (Continued)

decreased slightly at $\alpha = 60$ deg for the AP02. This had the effect of lowering the configuration normal force, to be more in line with experimental data, but moving the axial force at combined α and δ_W away from the data (see Figure 26F).

Figures 26G and 26H present $M_\infty = 1.5$ results of theory compared to experiment for $\Phi = 45$ deg roll. Figures 26G and 26H give C_A, C_N, and C_M for $M = 1.5$ and $\delta_W = 0$ and 10 deg. Figures 26I and 26J give similar results for $M_\infty = 2.87$ and $\delta_W = 0$ and 20 deg, and Figures 26K and 26L give results for $M_\infty = 4.6$ and $\delta_W = 0$ and 20 deg. Figure 26L shows the same phenomena as Figure 26F: that is, with the lowering of C_{N_w} at $\alpha = 60$ deg in Table 5 to be more in line with the Stallings data,[5] improvements in normal force coefficient prediction are realized, but at the expense of axial force coefficient prediction. Note that reasonably good agreement is obtained between experimental data and both the AP98 and AP02 for all static aerodynamics at all three Mach numbers and for all control deflections. Here, the worst-case center of pressure error is less than 3 percent of the body length.

In general, for the configuration of Figure 25, the AP02 average errors show only slight improvements over the AP98. This is primarily because the AP98 comparisons to data were already extremely good and the changes to the AP98 methodology based on the Reference 7 data base were minor for this configuration. In fact, while C_N and C_M are predicted slightly better with the AP02 than with the AP98, the axial force at combined α and δ_W is slightly worse with the AP02 than with the AP98.

The second configuration is taken from Reference 18 and is a canard-body-tail missile configuration. It is 22.2 calibers in length, and the nose is hemispherical. The tail surfaces are fairly large, with aspect ratio 0.87, and fairly thick, with truncated trailing edges. The canards are aspect ratio 1.73. The configuration is shown in Figure 27A. The hangers which are on the wind tunnel model were not modeled by the APC. Tests were conducted for $M_\infty = 0.2$ to 4.63, AOA of 0 to 20 deg, control deflections of 0 to 20 deg, roll of 0 to 45 deg, R_N/ft of 2×10^6 for a model with boundary layer trips. Base pressure values as a function of M_∞ and AOA were given in Reference 18, and these values were added to the axial force information so total axial force values could be shown.

It should be pointed out that the tail thickness in Figure 27A is less than that of Figure 32A in Reference 1. Reference 1 incorrectly used the value of 0.236 in. for the tail thickness, versus the correct value of 0.109 in. as shown in Figure 27A. This larger value of thickness was the primary source of the overprediction in axial force coefficient in Reference 1 using the AP98. The correct value of tail thickness was used for both the AP98 and AP02 computations in this report.

Figure 27B gives the comparison of theory and experiment for $\Phi = 0$ deg roll for both 0 and 20 deg control deflections. Results are shown in terms of C_A, C_N, and C_M versus Mach number for $\alpha = 20$ deg. Viewing Figure 27B, it is seen that the AP98 and AP02 both give good agreement to data. In comparing the AP02 to the AP98 and experiment, it is seen that the AP02 shows some improvement in prediction of normal force and pitching moment coefficients compared to the AP98 for the following conditions: (1) Mach numbers less than 0.9 and (2) Mach numbers greater than 2.1 for normal force coefficient. For the intermediate Mach

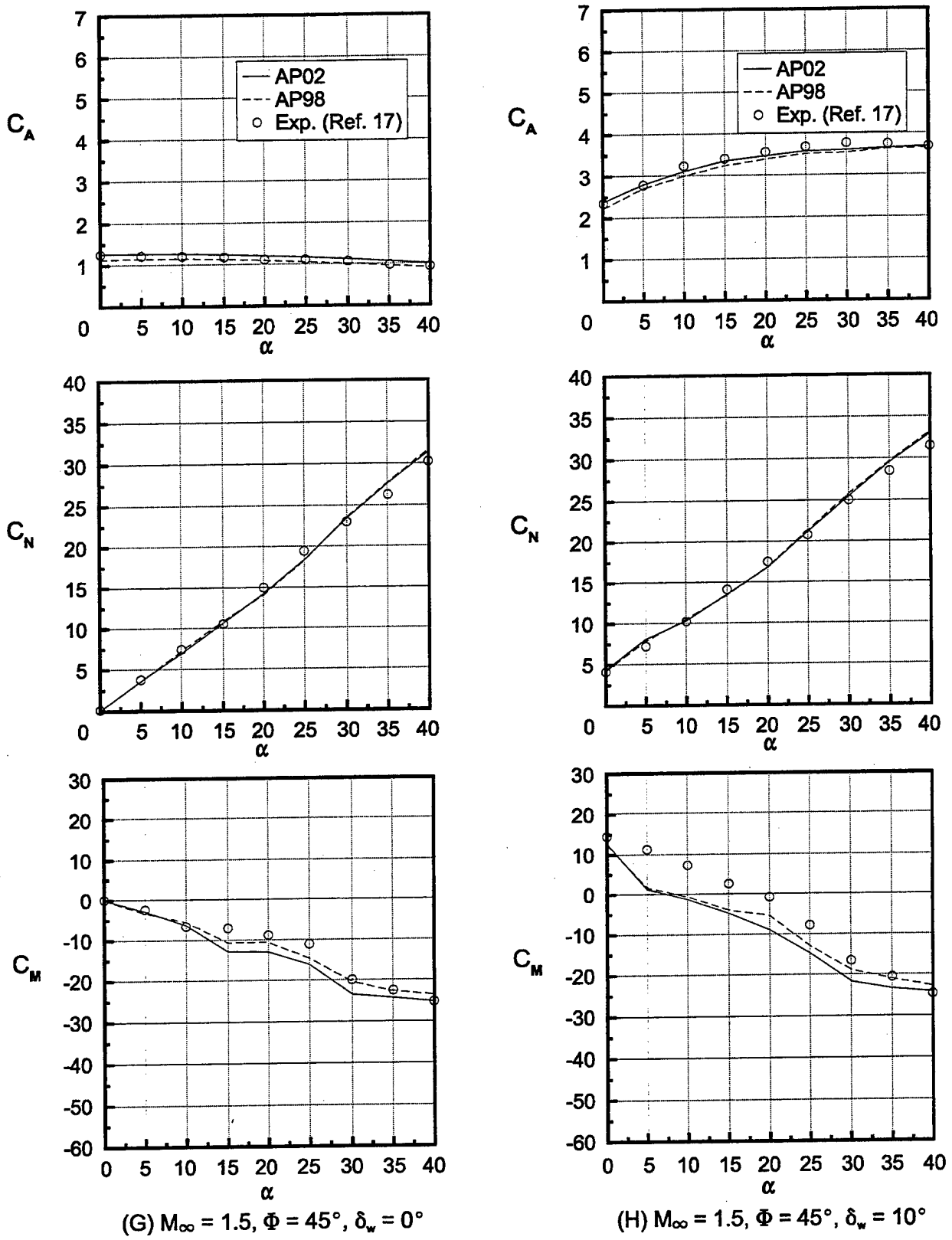

FIGURE 26. COMPARISON OF EXPERIMENT AND THEORY FOR C_A, C_N AND C_M FOR FIGURE 25 WING CONTROL CASE (Continued)

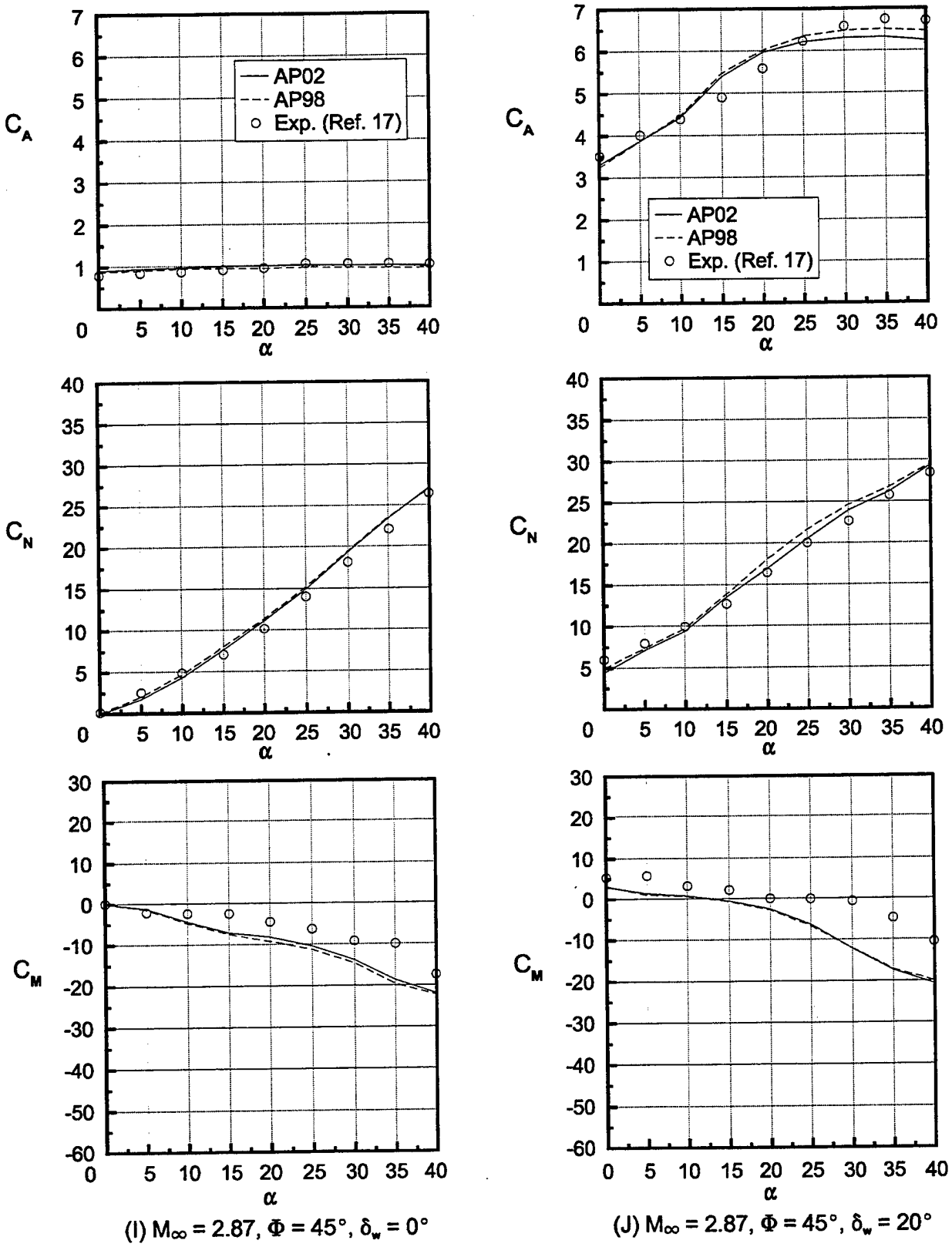

FIGURE 26. COMPARISON OF EXPERIMENT AND THEORY FOR C_A, C_N AND C_M FOR FIGURE 25 WING CONTROL CASE (Continued)

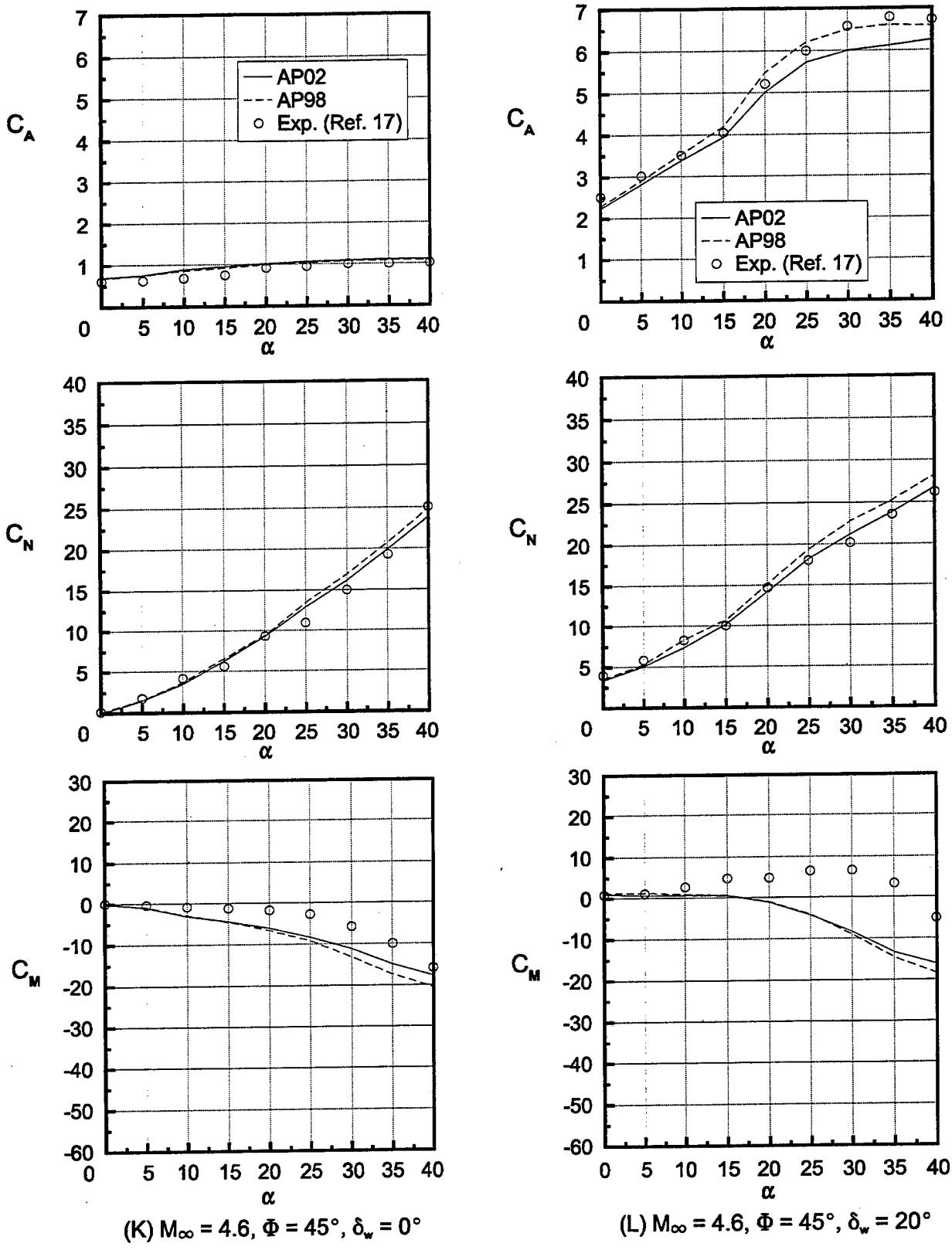

FIGURE 26. COMPARISON OF EXPERIMENT AND THEORY FOR C_A, C_N AND C_M FOR FIGURE 25 WING CONTROL CASE (Continued)

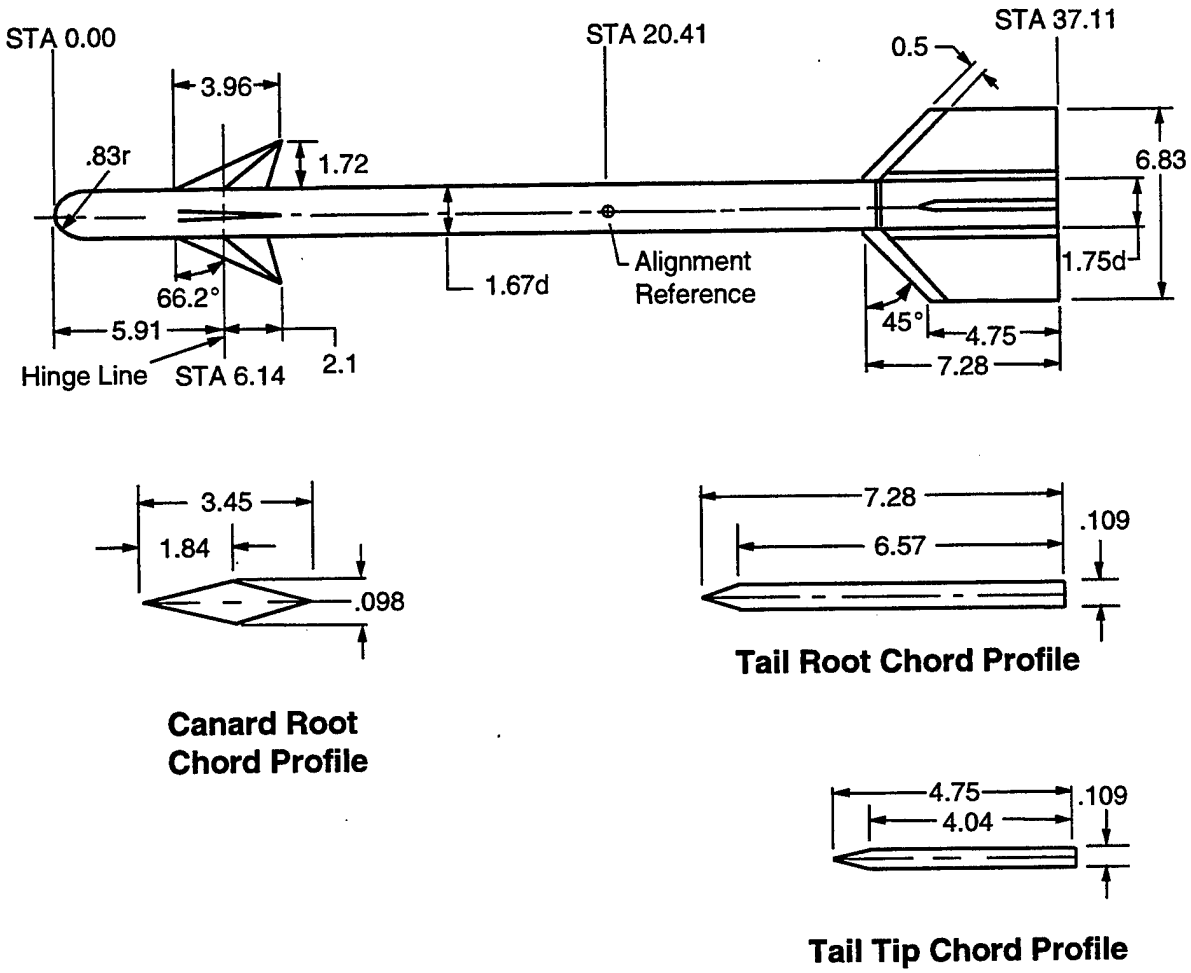

FIGURE 27A. CANARD-BODY-TAIL CONFIGURATION WITH HEMISPHERICAL NOSE[18]

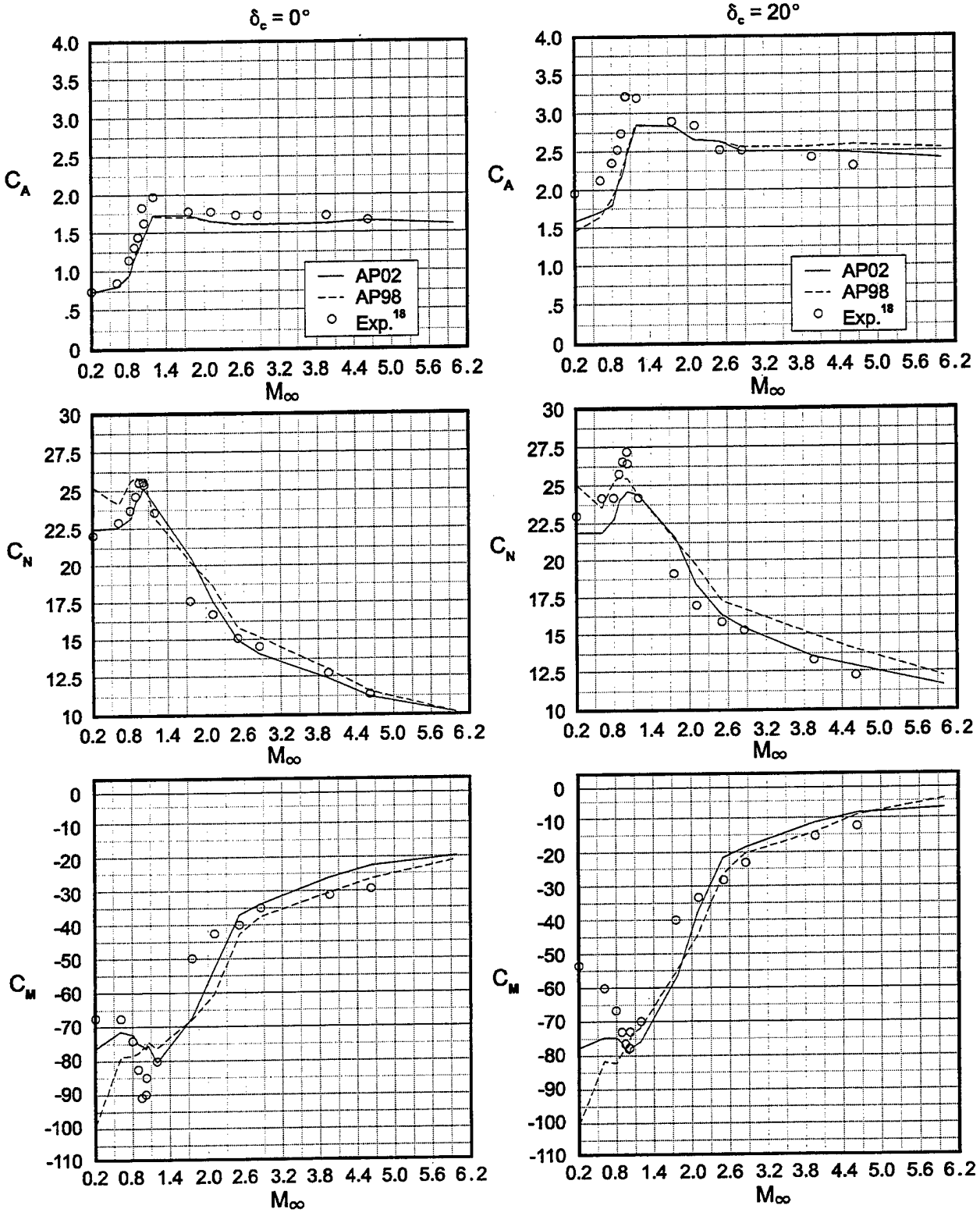

FIGURE 27B. C_A, C_N AND C_M VERSUS MACH NUMBER FOR CONFIGURATION OF FIGURE 27A ($\Phi = 0$, $\alpha = 20$ DEG)

numbers, prediction accuracy of the two versions of the APC is comparable. Axial force prediction accuracy for this configuration of the two codes is also comparable, since only minor changes were made to the AP02 with respect to axial force estimation.

The $\Phi = 45$ deg roll comparisons of C_A, C_N, and C_M for $\alpha = 20$ deg and $\delta_C = 0$ and 20 deg are shown in Figure 27C. In general, the AP02 gives better normal force coefficient predictions compared to data than does the AP98. Pitching moment coefficients predicted by the AP02 are also slightly better than those predicted by the AP98, although the improvement is not as great as for the normal force coefficient. Again little difference in axial force coefficient is seen between the AP02 and AP98.

To summarize the second validation case considered, it is seen that the improvement in normal force prediction accuracy of the AP02 based on the more recent data base of Reference 7 carried over to the Figure 27A configuration. For the 56 data points of Figures 27B and 27C (14 Mach numbers, 2 roll orientations, and 2 control deflections), the average normal force error was reduced from 7.9 percent using the AP98 to 4.2 percent using the AP02. This is a reduction in the normal force prediction error of over 40 percent. Some slight improvement in pitching moment, center of pressure, and axial force was also observed for the AP02 compared to the AP98. However, these improvements were not nearly as large as for normal force coefficient.

The third configuration was tested by Jorgensen.[19] The configuration is shown in Figure 28A and consists of a wing-body and wing-body-tail. Both the wings and tails are fairly large in surface area and aspect ratio. Figure 28B gives the normal force coefficient comparison between the AP98, the AP02, and experiment for the wing-body case at Mach numbers of 0.6, 0.9, 1.5, and 2.0 and AOA to 60 deg. The AP02 provides only slight overall average accuracy improvement over the AP98. Both predictions fall well below the average accuracy goal of ± 10 percent. Figure 28C gives both the normal force and center of pressure comparisons for the wing-body-tail case of Figure 28A. Again, the AP02 shows only slight improvement over the AP98 compared to experiment.

The fourth case considered in the evaluation of the improved empirical constants developed for the nonlinear aerodynamic terms of the normal force Equation (1) is taken from Reference 20 and is shown in Figure 29A.

The wind tunnel model was about 22 calibers in length with a sharp nose of 2.25 calibers. The canards had an aspect and taper ratio of 2.0 and 0.3 respectively. Various tail fin spans were considered. This model was tested at Mach numbers 1.6 to 3.5 at AOA to about 18 to 20 deg. It had a boundary layer trip present and was tested at a R_N/ft of 2.0×10^6. Reference 20 gave separate values of base axial force coefficient, which were added to the axial force values given in the reference to compare to the AP98 and AP02 computations. To compare the experimental data to theory, Mach numbers of 2.5 and 3.5 are selected at roll angle 45 deg. Also, values of the tail-to-canard semispan of 0.47 and 1.25 are considered. Figures 29B and 29C present the comparison of theory to experiment for $b_t/b_c = 0.47$ and $b_t/b_c = 1.25$ at Mach numbers of 2.5 and 3.5, respectively, for C_A, C_N, and C_M.

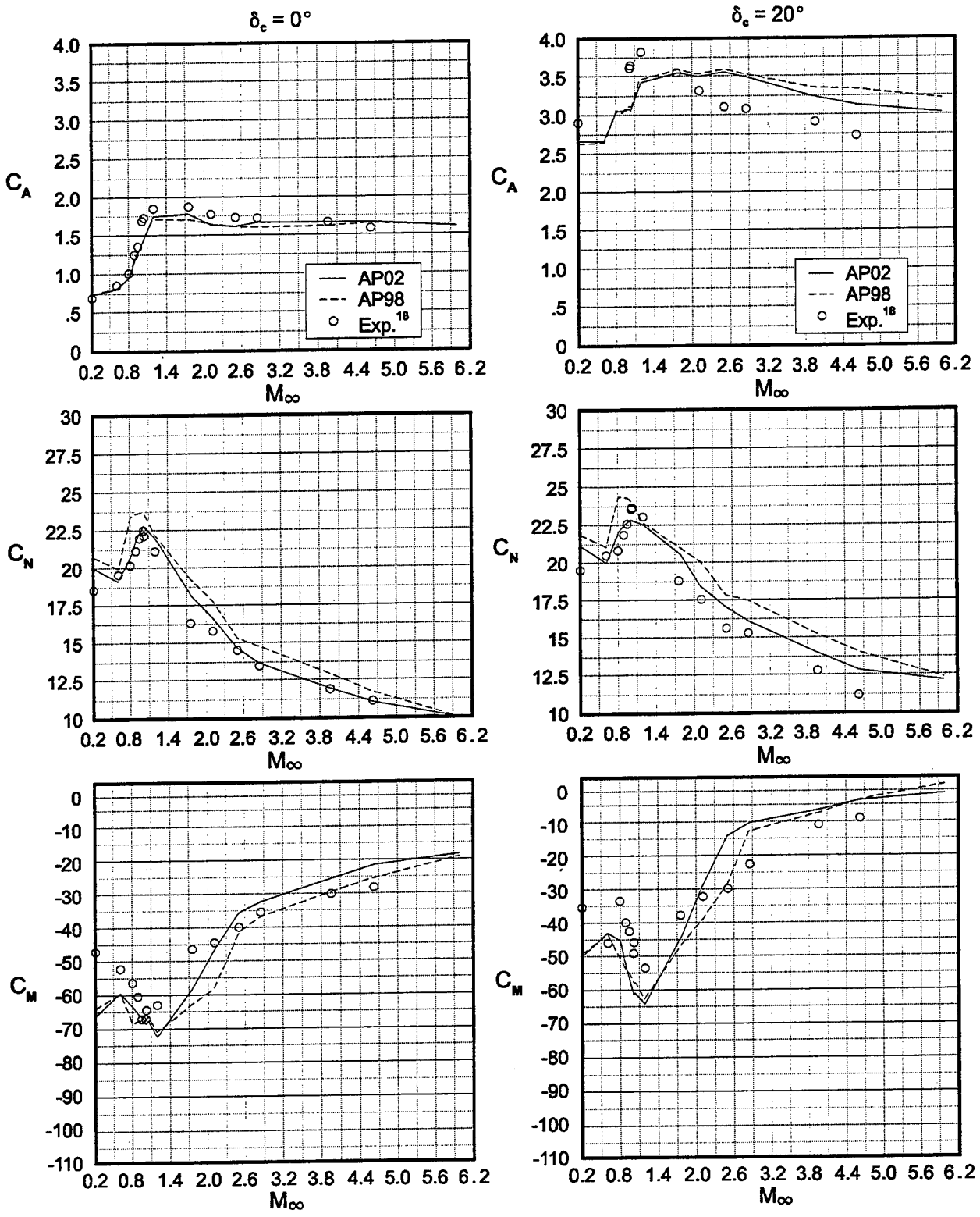

FIGURE 27C. C_A, C_N AND C_M VERSUS MACH NUMBER FOR CONFIGURATION OF FIGURE 27A ($\Phi = 45$, $\alpha = 20$ DEG)

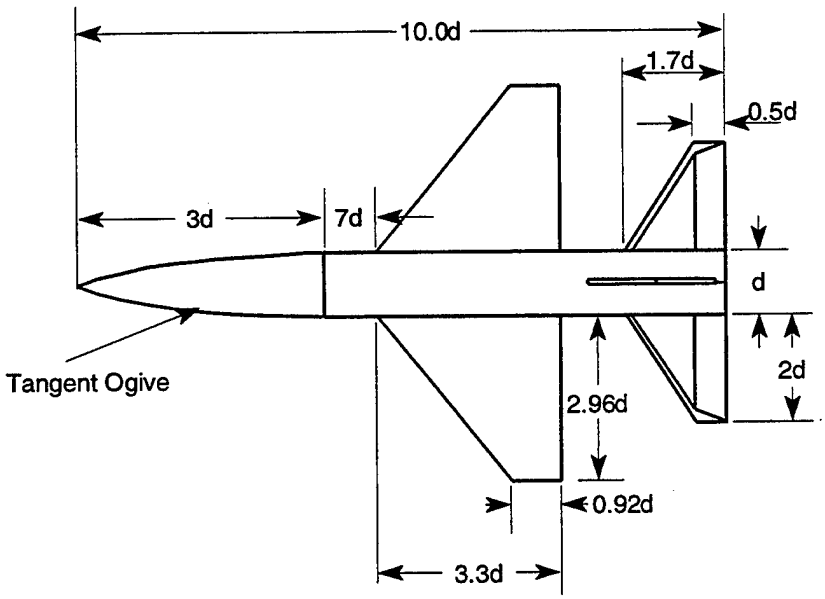

PARAMETERS

$(AR)_T = 3.64$	$\lambda_T = .29$	d = 2.6 in.
$(AR)_W = 2.81$	$\lambda_T = .28$	

FIGURE 28A. WING-BODY AND WING-BODY-TAIL CONFIGURATIONS USED FOR COMPARING AP98 TO EXPERIMENT AND AP02

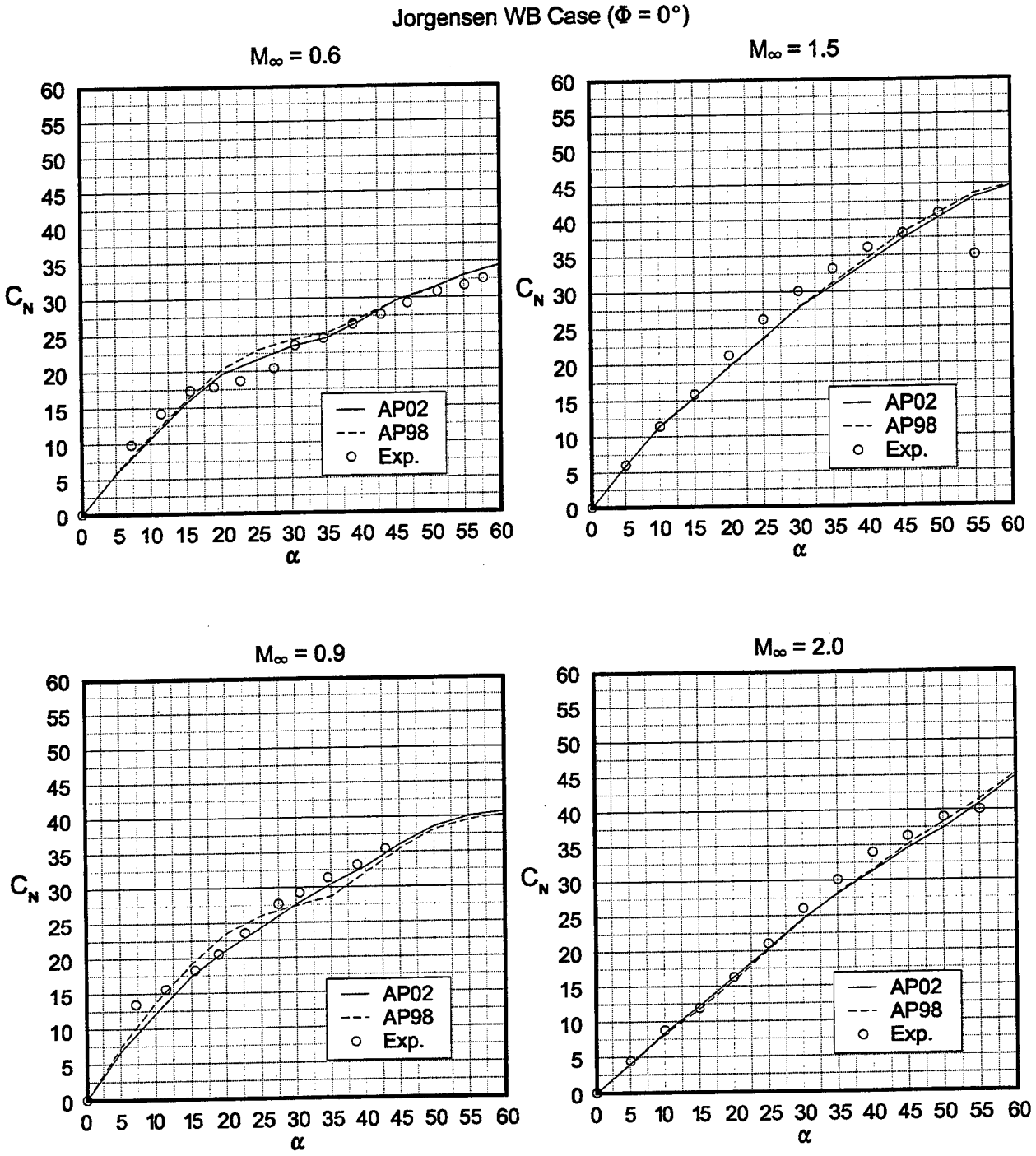

FIGURE 28B. NORMAL FORCE COEFFICIENT COMPARISONS FOR WING-BODY CONFIGURATION OF FIGURE 28A

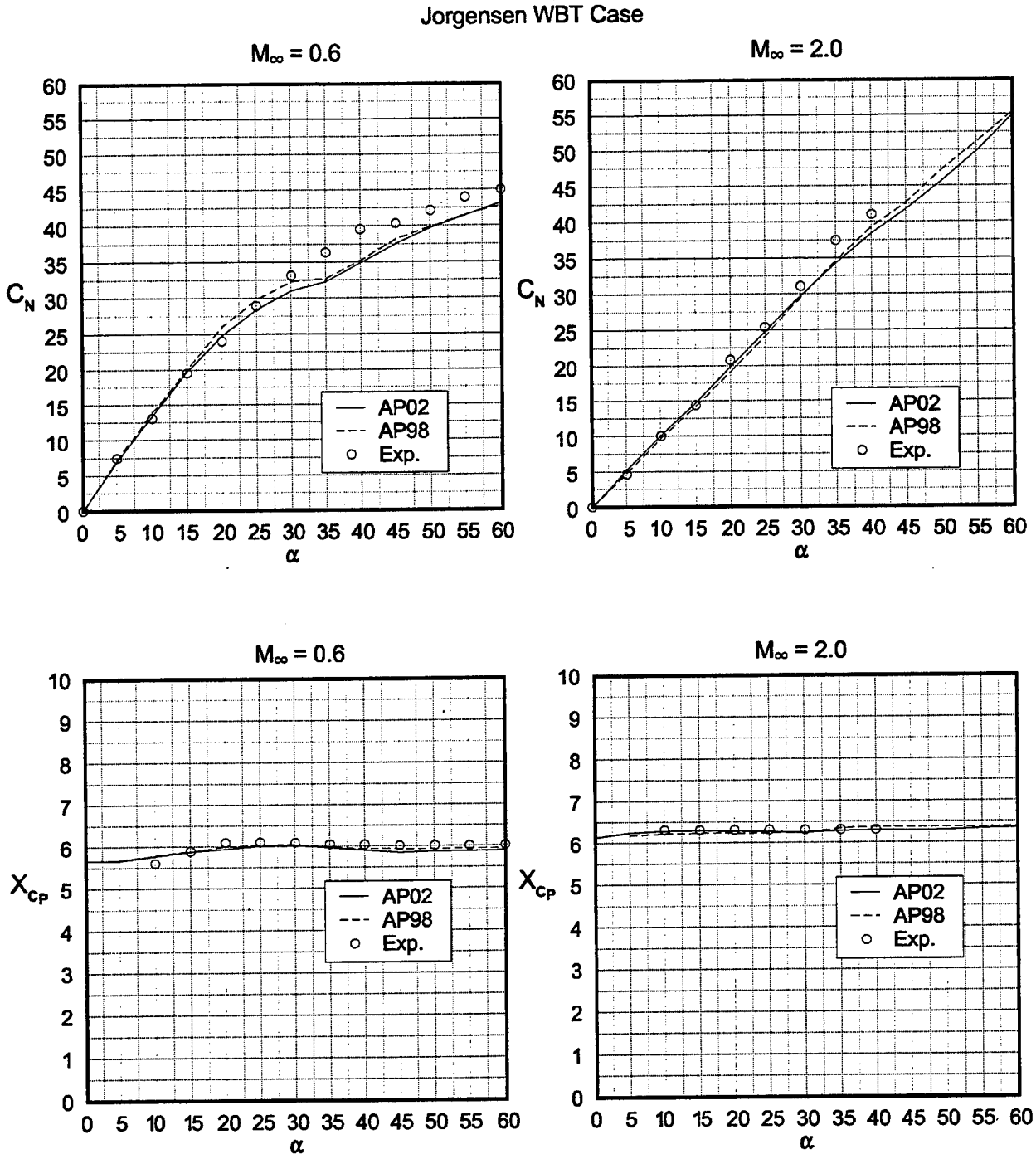

FIGURE 28C. NORMAL FORCE COEFFICIENT AND CENTER OF PRESSURE COMPARISONS FOR WING-BODY-TAIL CONFIGURATION OF FIGURE 28A

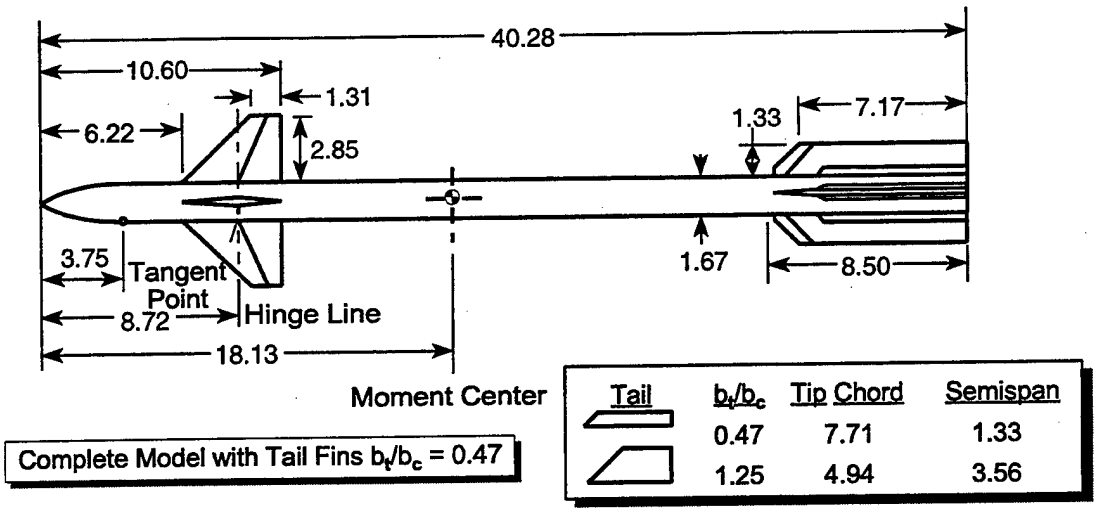

FIGURE 29A. CANARD-BODY-TAIL CONFIGURATION WITH VARYING TAIL SPAN (FROM REFERENCE 20) (ALL DIMENSIONS IN INCHES)

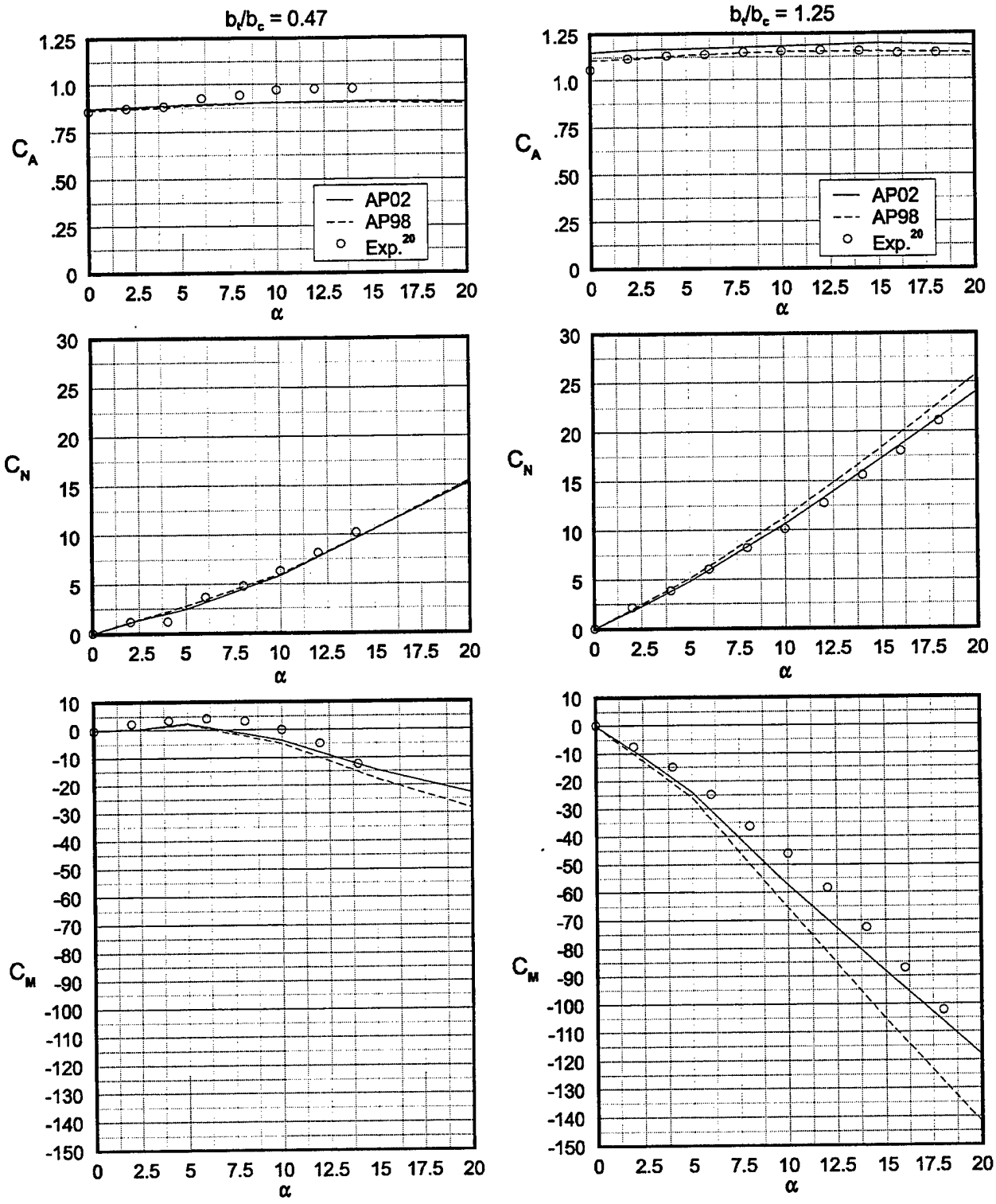

FIGURE 29B. COMPARISON OF THEORY AND EXPERIMENT FOR CONFIGURATIONS OF FIGURE 29A (Φ = 45 DEG, M_∞ = 2.5)

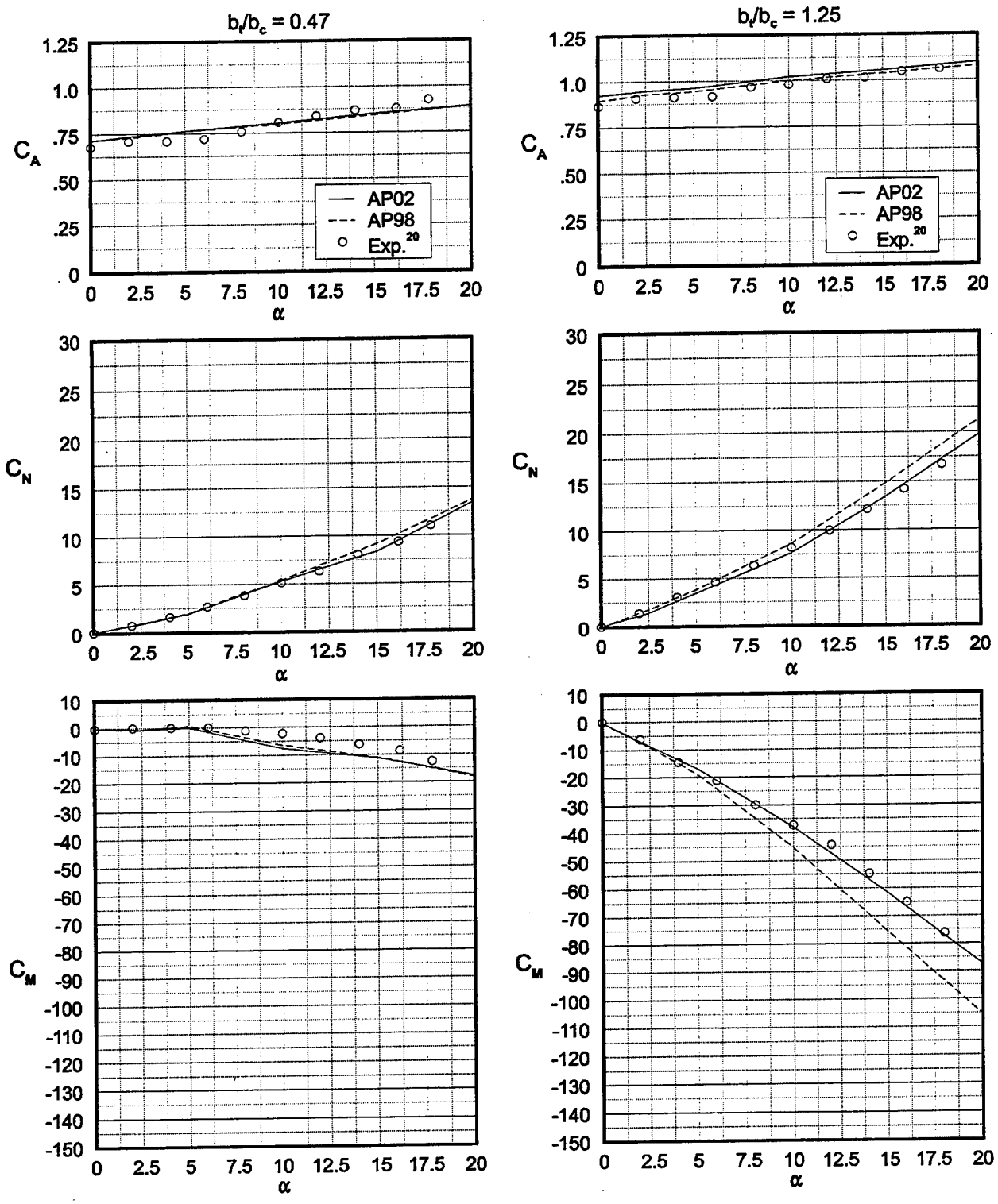

FIGURE 29C. COMPARISON OF THEORY AND EXPERIMENT FOR CONFIGURATIONS OF FIGURE 29A (Φ = 45 DEG, M_∞ = 3.5)

In examining Figures 29B and 29C, it is seen that the AP02 and AP98 both give excellent agreement with experiment for the $b_t/b_c = 0.47$ case. However, for the $b_t/b_c = 1.25$ case, the AP02 shows significant improvement over the AP98 in both C_N and C_M at both M = 2.5 and M = 3.5. Average normal force coefficient and center of pressure errors were reduced by a factor of two or more for this case with the AP02 compared to the AP98 and experiment.

The next set of wind tunnel data considered for comparison purposes is taken from Reference 21. Body-alone, body-tail, and wing-body-tail configurations were all a part of this test series. Figure 30A shows one of the configurations tested and considered here for validation of the AP02 results. The model is 13.5 calibers in length with a 1.5 caliber tangent ogive nose. The wing surfaces are fairly large, with thickness of $t/c_r = 0.0178$ and wedge angles of 15 deg on the leading and trailing edges. The tail surfaces have thickness of $t/c_r = 0.05$ and wedge angles of 20 deg. The tests were conducted at Mach numbers 0.7 to 3.08 with Reynolds number varying from about 2×10^6 to 4.6×10^6 per foot. The smooth model without boundary layer trip option was used for the AP02 and AP98 calculations. AOA to 25 deg were considered in the wind tunnel test. For comparison purposes, normal force and pitching moments are compared to data at $M_\infty = 1.42$ and 3.08 for the $\Phi = 0$ deg roll orientation. Figure 30B presents these results. As seen in the figure, both the AP02 and AP98 give quite acceptable comparisons to data, with the AP02 giving slightly better comparisons for normal force coefficients. The pitching moment prediction of the AP02 and AP98 are about equal for this configuration at the conditions considered, with the AP02 being slightly better at $M_\infty = 3.08$ and the AP98 slightly better at $M_\infty = 1.42$. Both versions of the APC give aerodynamics well within the accuracy goals. Reference 21 also gives axial force information where the base pressure has been subtracted out. Unfortunately, only a side camber tap was used, so the AOA information was not believed to be accurate. Hence, no axial force comparisons with AOA are shown.

Figure 31 shows a sixth case considered. This case has the same body (12.33-caliber tangent ogive-cylinder with a 3-caliber nose) as that tested at Langley.[4] However, dorsals of aspect ratio 0.1 and tail surfaces of aspect ratio 2.0 have been added. Mach numbers considered are 4.5 and 10.0. This case was originally defined[13] to allow computations to be performed with a full Euler solver[22] at high Mach number, since wind-tunnel data above Mach 4.6 appeared to be lacking. Figure 31B shows the comparison of the ZEUS[22] computations for normal force and center of pressure with the AP98 and AP02 results for the body-tail configuration, and Figure 31C shows the same comparisons for the body-dorsal-tail case of Figure 31A. ZEUS[22] computations are here used as the truth model, although the full Euler solution also has some small errors in comparison to wind tunnel data, based on past experience. ZEUS computations are shown only for $\alpha = 1$, 10, 20, and 30 deg. It is seen that both the AP98 and AP02 give good comparisons to the ZEUS computations, and the overall average comparisons to the ZEUS computations for the AP98 and AP02 are about the same.

The cases considered to this point in the results and discussion are cases that lie within the parameter space of the Reference 7 data base except for the Figure 31 configuration. Since Tables 6 through 26 are used at all Mach numbers and the Reference 7 data base only goes down to $M_\infty = 0.6$, it was decided to adjust the empirical constants in the tables based on several configurations outside the Reference 7 data base for Mach numbers near zero. The first low Mach number case is shown in Figure 32A and is taken from Reference 23. This configuration

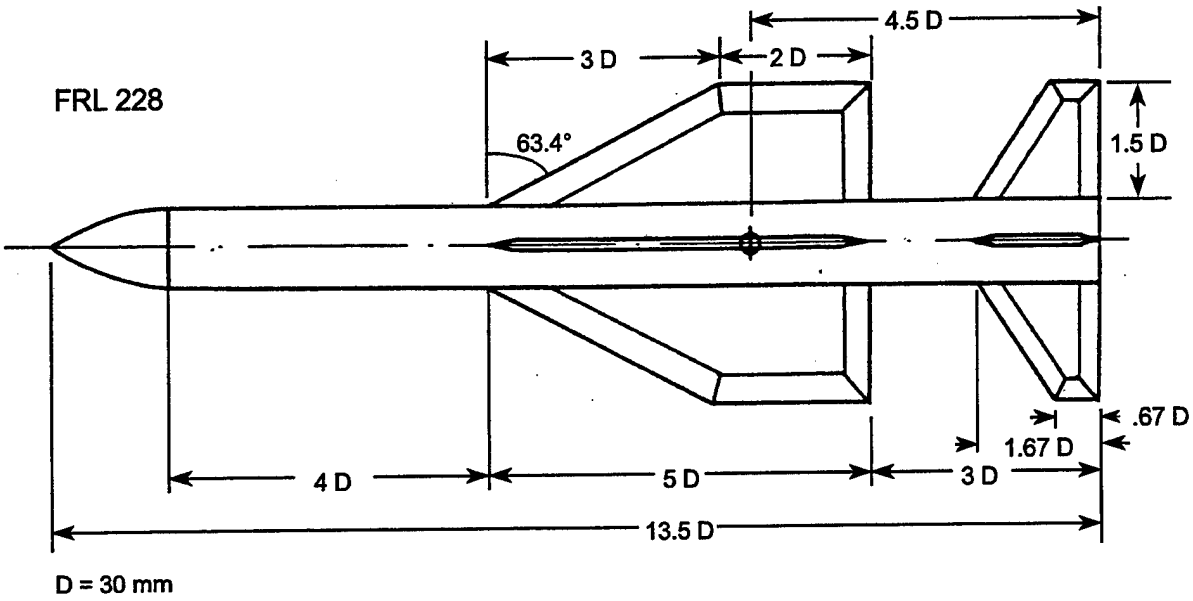

FIGURE 30A. WING-BODY-TAIL CONFIGURATION CONSIDERED FOR VALIDATION WITH AP02 AND AP98 (REFERENCE 21)

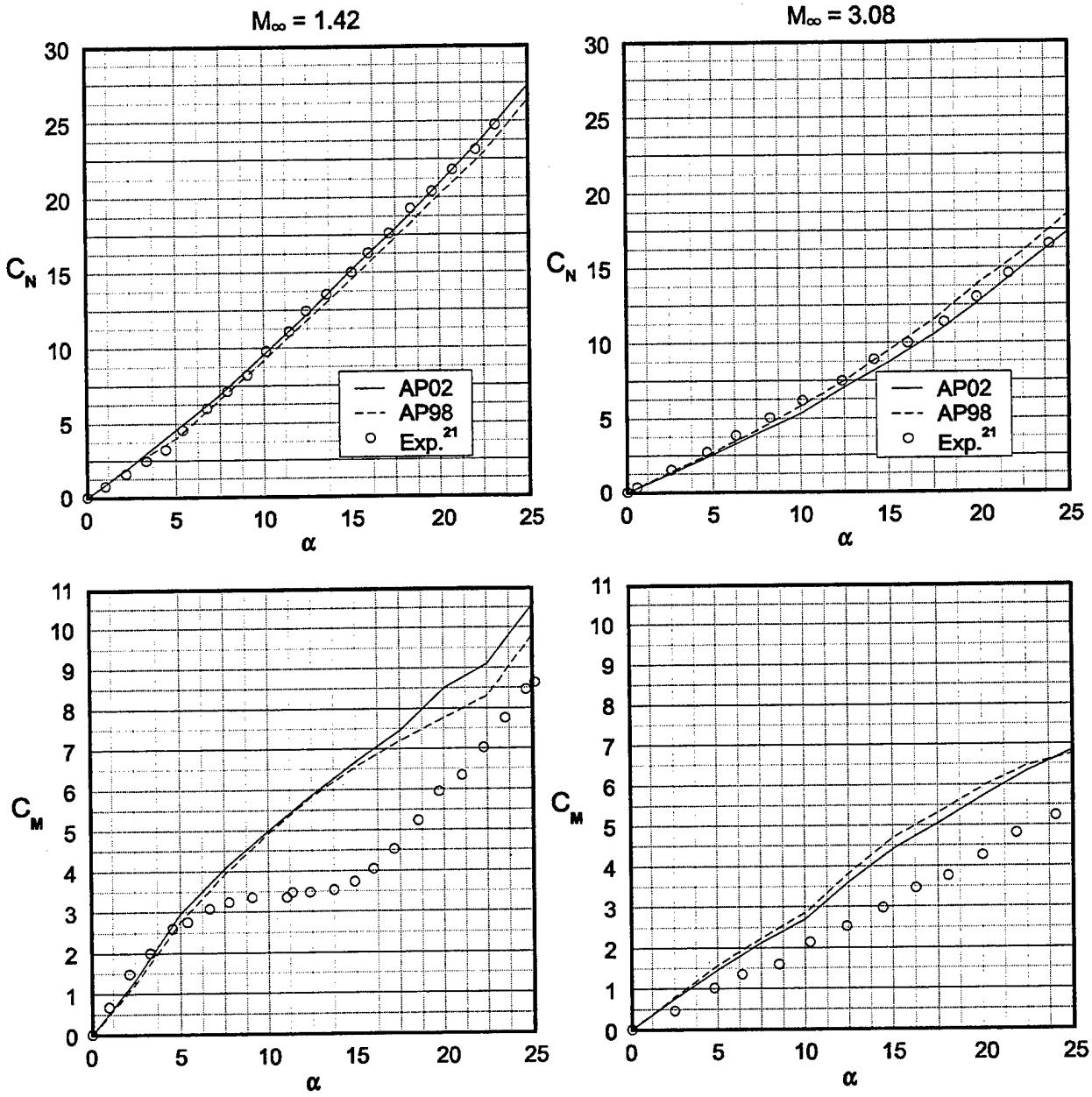

FIGURE 30B. NORMAL FORCE AND PITCHING MOMENT COMPARISONS OF THEORY AND EXPERIMENT FOR FIGURE 30A CONFIGURETION (Φ = 0 DEG)

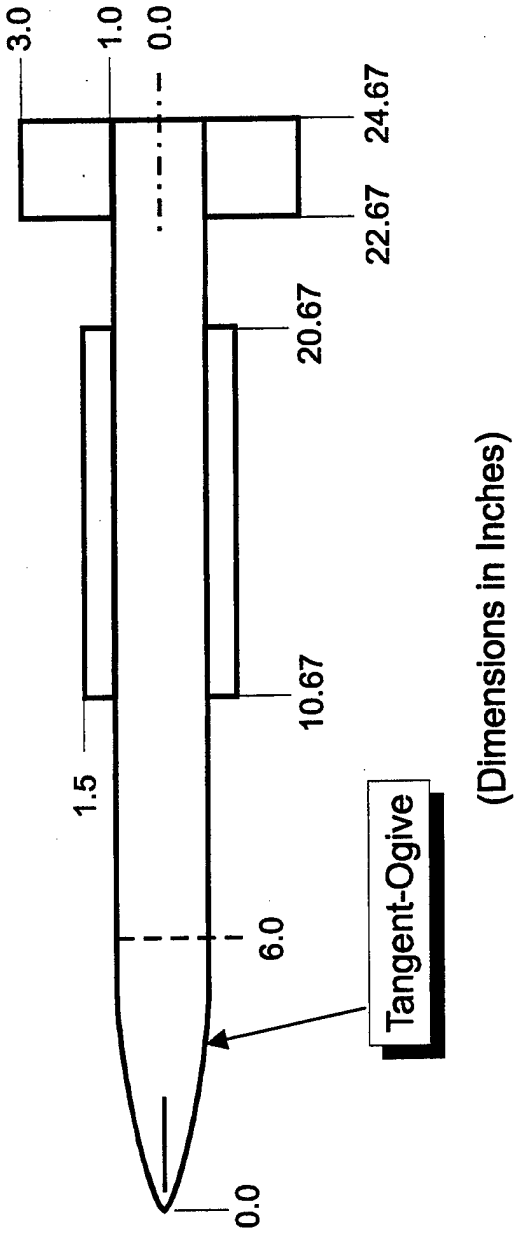

FIGURE 31A. BODY-DORSAL-TAIL CONFIGURATION USED FOR COMPARING ZEUS, AP02, AND AP98 COMPUTATIONS

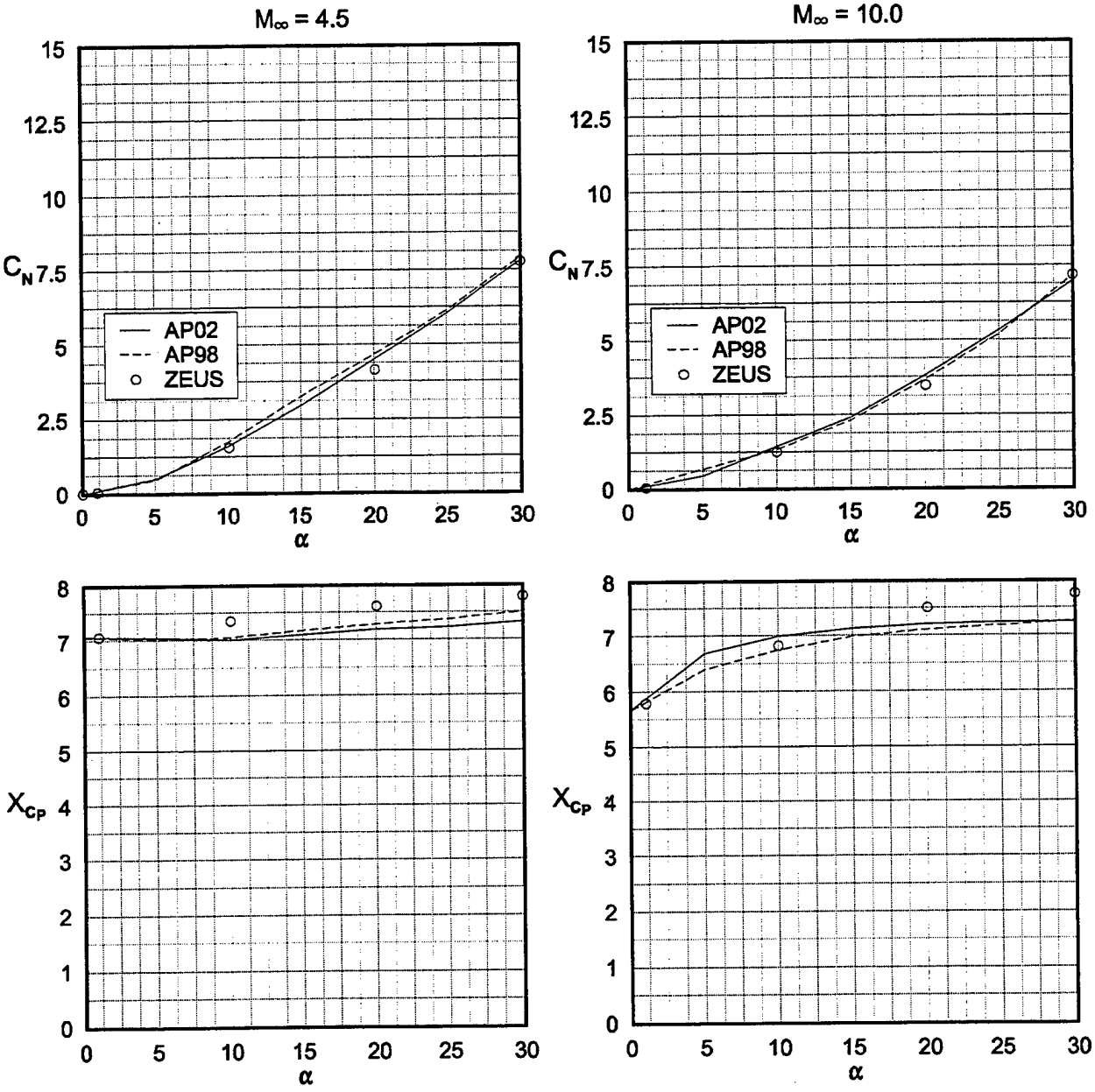

FIGURE 31B. NORMAL FORCE COEFFICIENT AND CENTER OF PRESSURE COMPARISONS OF THREE ANALYTICAL METHODS FOR BODY-TAIL OF FIGURE 31A

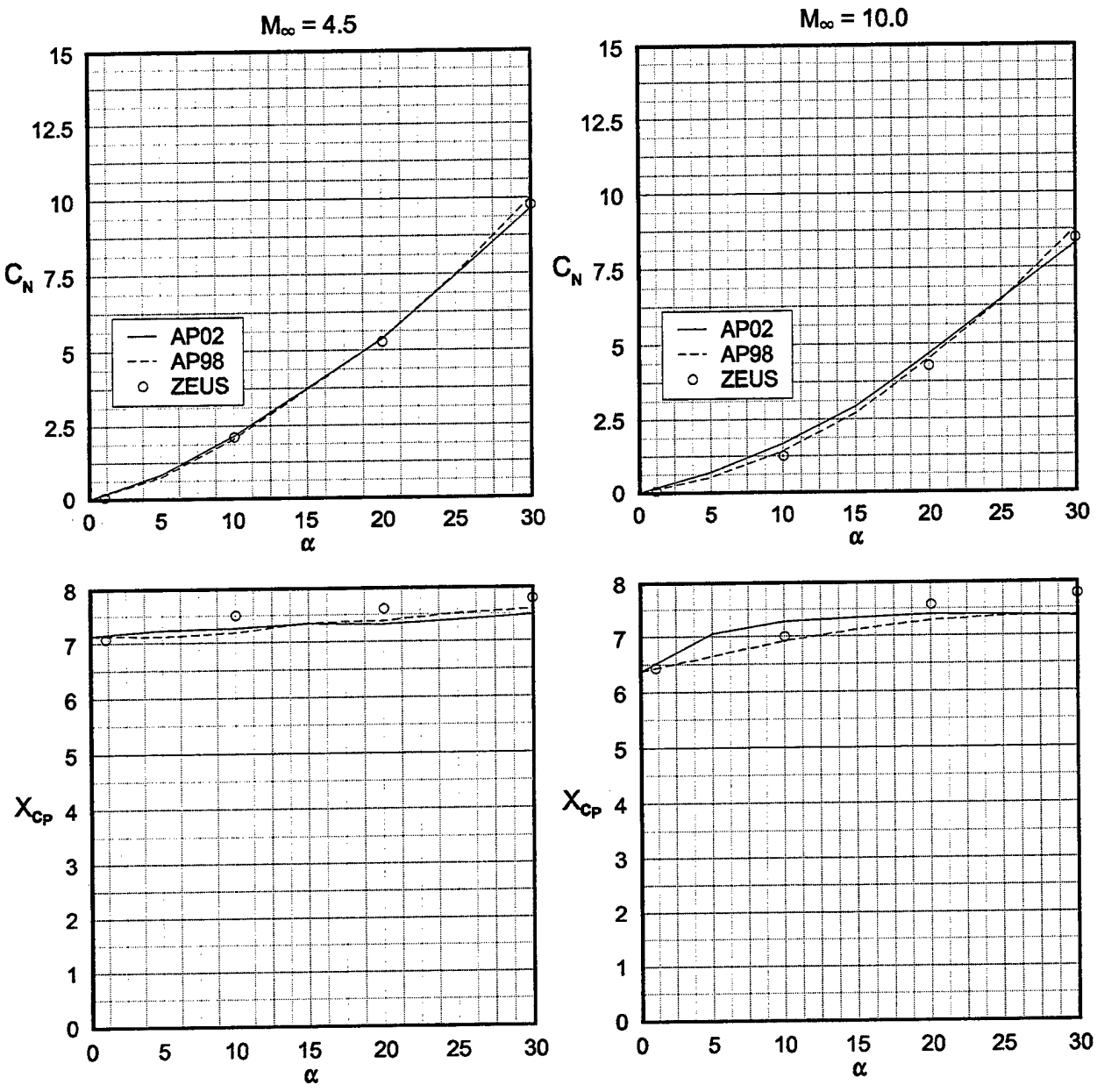

FIGURE 31C. NORMAL FORCE COEFFICIENT AND CENTER OF PRESSURE COMPARISONS OF THREE ANALYTICAL METHODS FOR BODY-DORSAL-TAIL CONFIGURATION OF FIGURE 31A

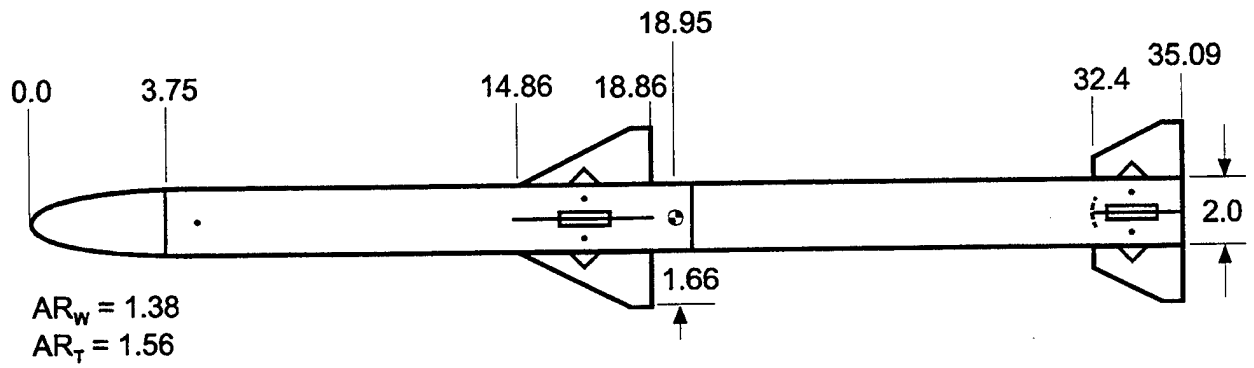

FIGURE 32A. MMPT CONFIGURATION TESTED AT M_∞ = 0.2 (FROM SMITH, SALAZAR et al.[23])

is 17.5 calibers in length and has a 1.88-caliber tangent-ogive nose. It has aspect ratio 1.38 wings located near the point where moments are taken, and aspect ratio 1.56 tail surfaces located flush with the base. Axial force, normal force, and pitching moment coefficients predicted by the AP98 and the modified AP98, or AP02, are compared to the Reference 23 experimental data in Figure 32B. Results are given for the Φ = 0 deg roll plane only. Reference 23 also stated that axial force measurements could have significant errors due to use of a sting designed for large normal forces at high AOA. In viewing Figure 32B, it is seen that both the AP02 and AP98 give good predictions of normal force and pitching moment coefficients compared to experiment. Axial force coefficient predictions for the AP02 and AP98 are identical and follow the trends one would expect, although discrepancies with experiment exist because of the balance used for measurements. In a quantitative sense, the average normal force coefficient error of the AP98 was 7.4 percent for the 10 AOAs considered. The AP02 reduced this average error to 5.0 percent or about a one-third reduction in average error.

The next low Mach number case is shown in Figure 33, and the test data was given in a report by Howard and Dunn.[24] This configuration has dorsals that have an aspect ratio of 0.12 and tail surfaces that have an aspect ratio of 4.0. The exact configuration illustrated at the top of Figure 33 is not within the allowable constraints for fin planform required by the APC. Therefore, a modified version of the fin planforms is required, one that meets the constraints of the APC. This configuration is shown in the middle of Figure 33. Note that the parameters that were held constant for the fin planforms were area, aspect ratio, span, taper ratio, leading-edge sweep angle, and location of the geometric centroid of the planform area. The Howard and Dunn[24] work gave only normal force as a function of AOA. The AP02 and AP98 results are also shown at the bottom of Figure 33. Quite acceptable agreement is obtained with the AP02 compared to experiment, even at high AOA. The AP98 and AP02 are somewhat lower than the data suggest at high α. However, part of this underprediction is suspected to be the tendency of a base-mounted sting to give larger-than-true normal forces at subsonic Mach numbers.[25,26] In making this statement, sting interference effects were assumed to be unaccounted for in Reference 24. Comparing the results of the AP02 to the AP98 in a quantitative sense, the average normal force error of the AP98 for 34 data points is 10.7 percent, whereas the average normal force error of the AP02 is 6.0 percent. This 6.0 percent error is based on 34 data points at both the Φ = 0 and Φ = 45 deg roll orientations.

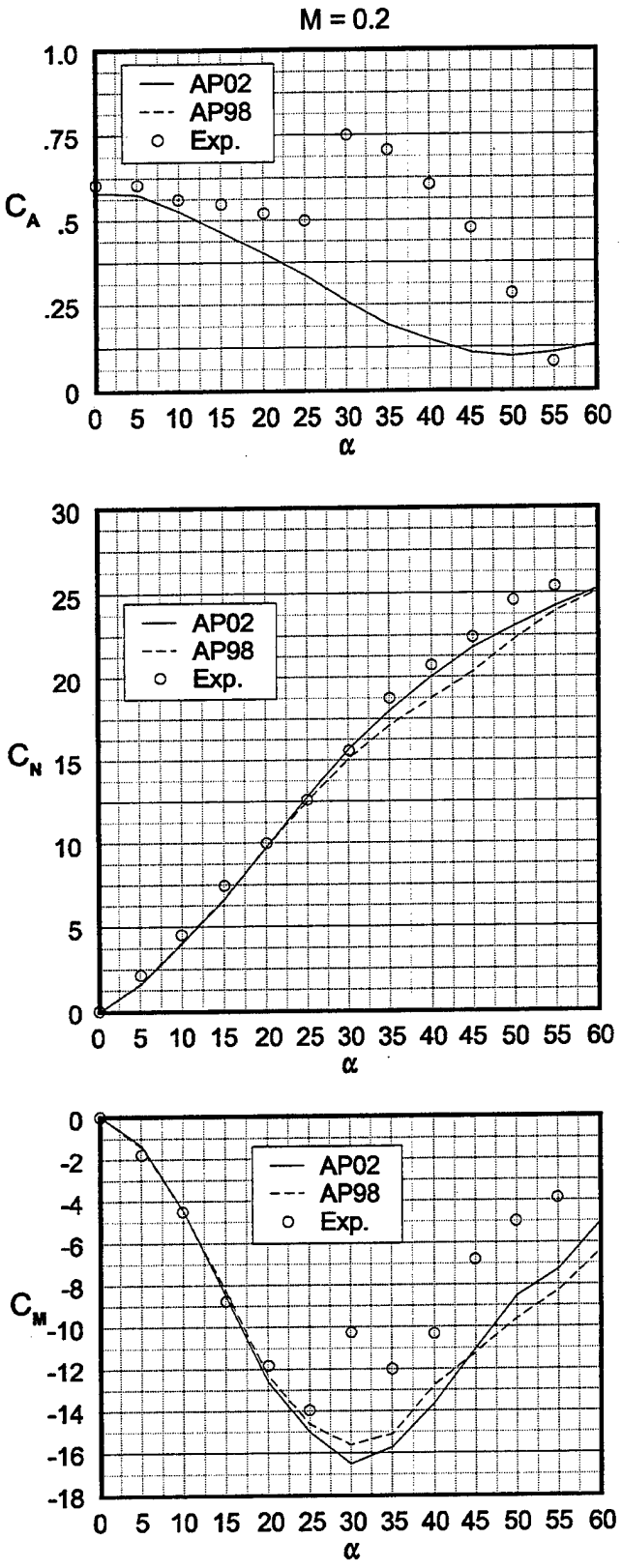

FIGURE 32B. COMPARISON OF STATIC AERODYNAMIC COEFFICIENTS BETWEEN EXPERIMENT AND PREDICTIONS FOR FIGURE 32A CONFIGURATION (Φ = 0 DEG, M_∞ = 0.2)

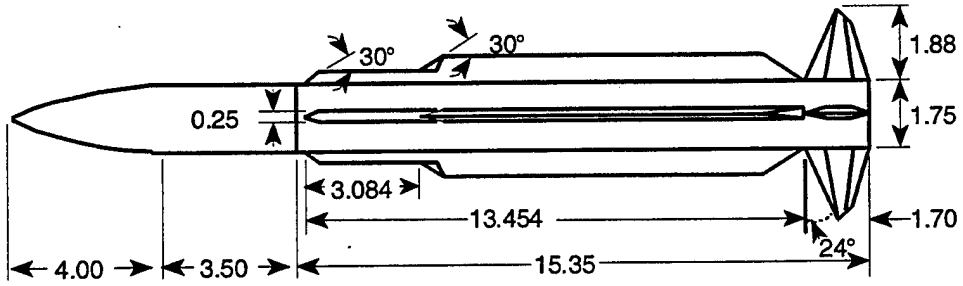

Configuration Tested in Wind Tunnel (from Ref. 34)
(All Dimensions in Inches)

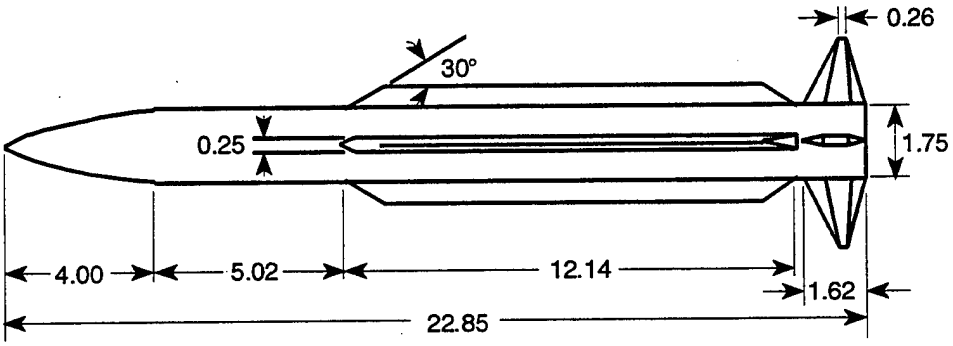

Modified Configuration Used in AP98 and AP02 Computations

Parameters for Both Models

$(AR)_T = 4.0$ $b_t = 3.76$ in. $\lambda_T = 0.16$ $(\Lambda_{LE})_T = 24°$ $A_T = 3.54$ in.^{2}

$(AR)_D = 0.12$ $b_D = 1.32$ in. $\lambda_D = 0.77$ $(\Lambda_{LE})_D = 60°$ $A_D = 14.2$ in.^{2}

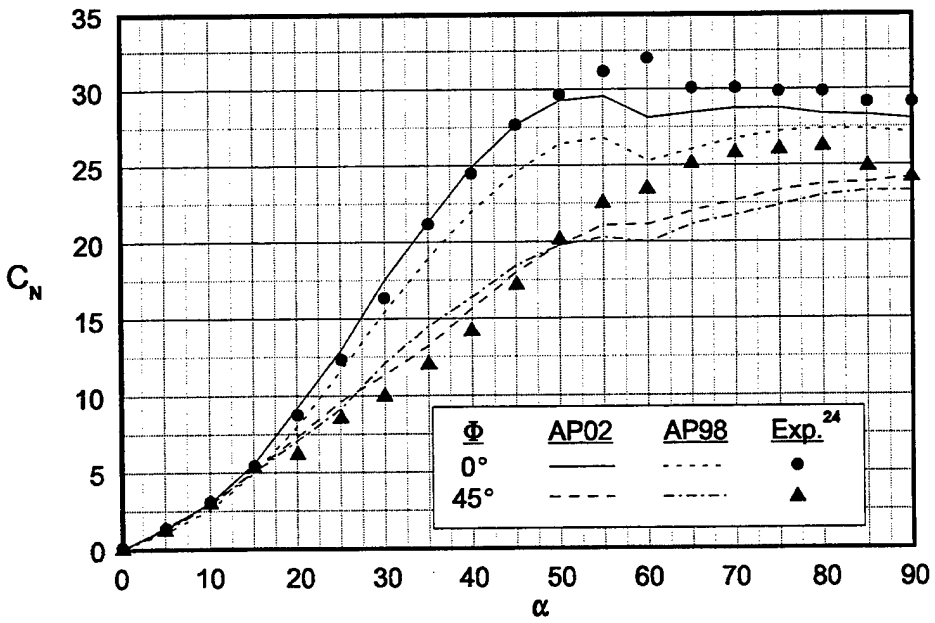

FIGURE 33. NORMAL FORCE COEFFICIENT COMPARISON OF THEORY AND EXPERIMENT ($M_\infty = 0.1$)

The last case considered for the low Mach number validation of the refined nonlinear empirical constants of Tables 6 through 26 is shown in Figure 34A. It was also tested[27] in the Naval Postgraduate School wind tunnel in Monterey, California. This case is a canard-controlled configuration with aspect ratio 1.59 canard and 0.9 tail surfaces (see Figure 34A). The body is 22.6 calibers in length. Data are available for $M_\infty = 0.2$ up to 45 deg AOA and for control deflections of the canards of −20 deg, 0 deg, and +20 deg for both $\Phi = 0$ and 45 deg roll. Results will be presented here for only the 0 deg control deflection case at roll of both 0 and 45 deg. Figure 34B presents axial, normal, and pitching moment coefficient comparisons of the AP02 and AP98 to experimental data[27] for $\Phi = 0$ deg roll. The same comment applies here as to the previous case with respect to wind tunnel accuracy of axial force measurements using a sting balance system designed for measurement of high AOA normal force loads. In fact, even the normal force loads at low AOA are suspect since both the 0 and 5 deg AOA loads are negative. In general, the AP02 has slightly improved average normal force predictions compared to experimental data between AOA 10 deg and 45 deg and the AP98. The AP98 and AP02 give about equal results for pitching moment coefficients. The $\Phi = 45$ deg roll results are shown in Figure 34C. Again, the AP02 gives slightly improved results for normal force predictions compared to the AP98, with pitching moment predictions being about equal. Quantitatively, the AP02 and AP98 give average normal force prediction errors of about 6.8 percent and 8.2 percent respectively for the 25 data points at $\alpha = 10$ to 45 deg and roll of 0 and 45 deg.

5.0 SUMMARY AND CONCLUSIONS

To summarize, the nonlinear empirical constants used in the APC to predict nonlinear normal force and pitching moments on missile configurations at high AOA have been refined based on a more recent missile-component, wind-tunnel data base.[7] In comparing the new aerodynamic predictions of the revised code (AP02) to the latest released version of the APC (AP98) the following conclusions were drawn:

(1) The refined nonlinear empirical coefficients reduced the average normal force error of the AP02 compared to the AP98 for the NASA/MDAC[7] data base by over a third (7.0 percent average to 4.4 percent average error based on 426 data points)

(2) In comparing the new AP02 to the AP98 for the older NASA Tri-Service Data Base,[4] it was seen that the improvements made to the empirical constants also gave improvements in accuracy of normal force coefficient for this data base as well. Average normal force errors were reduced from 4 to 5 percent for the AP98 to 3.4 percent for the AP02. This also represents close to a one-third reduction in average normal force coefficient errors.

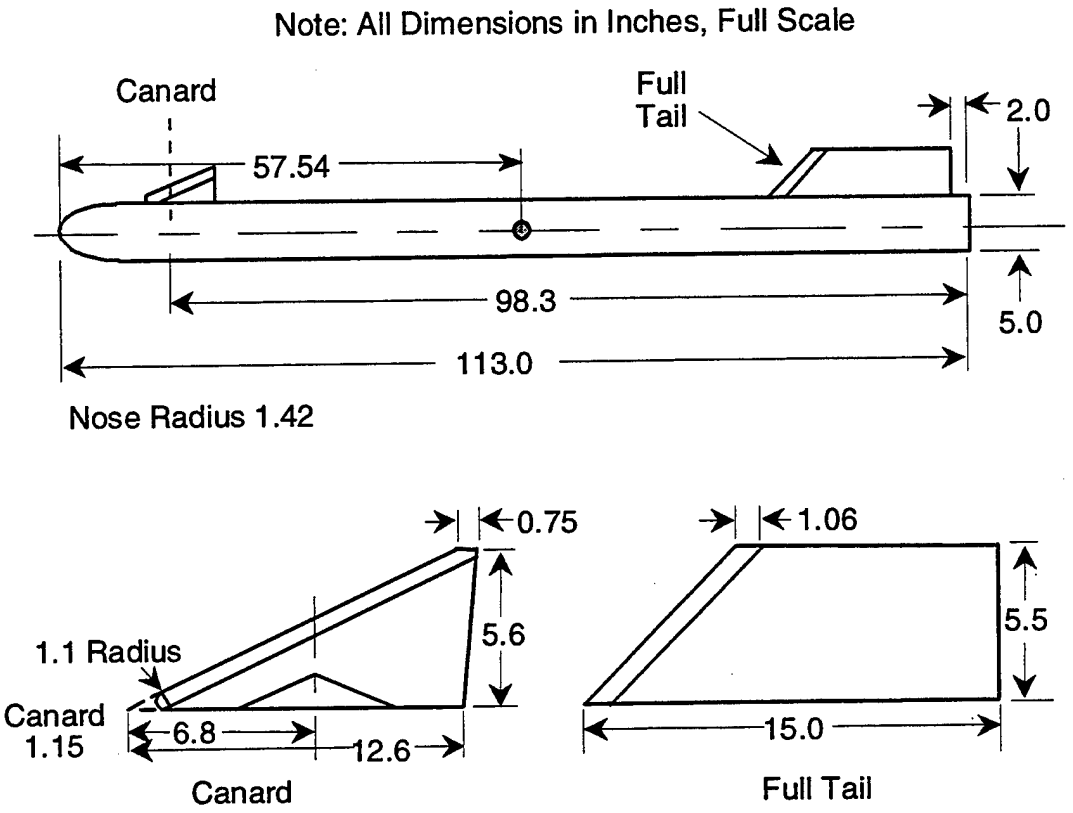

FIGURE 34A. CANARD-CONTROLLED MISSILE CONFIGURATION[27]

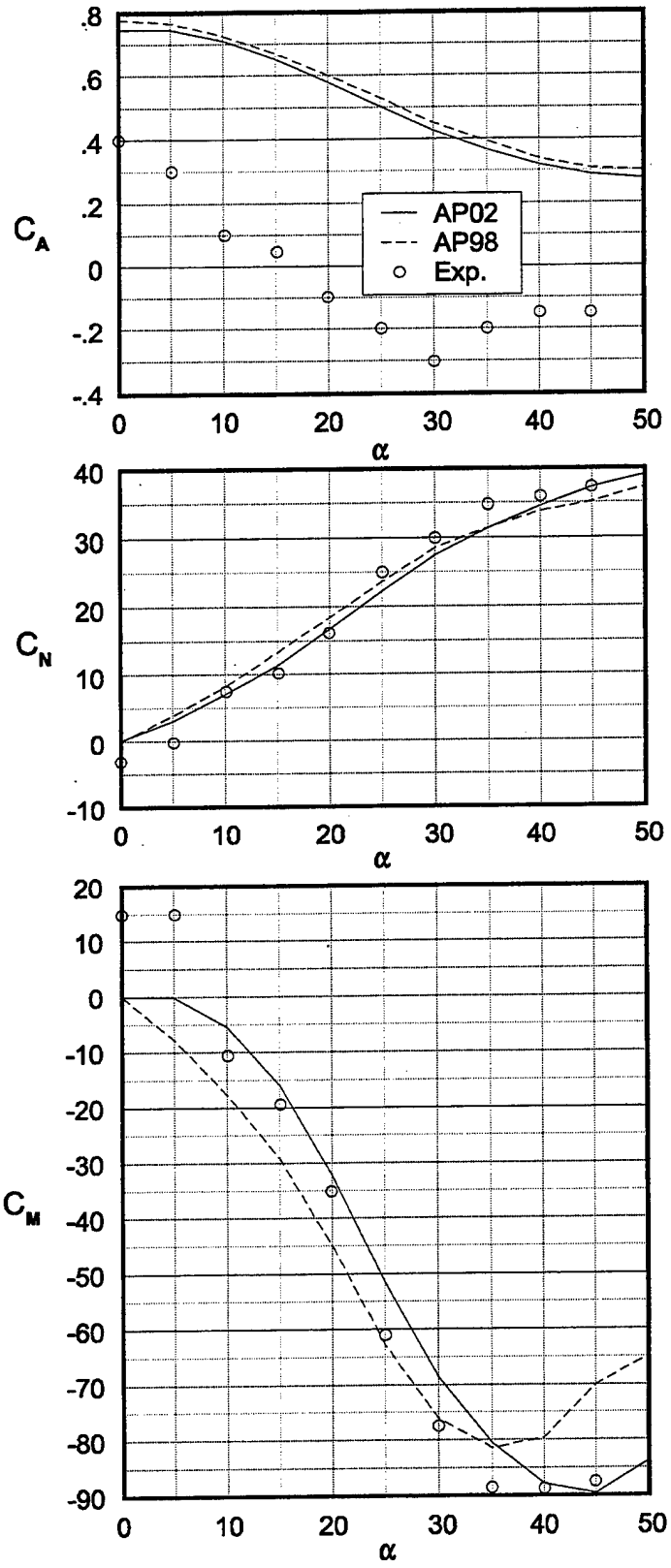

FIGURE 34B. COMPARISON OF AXIAL, NORMAL AND PITCHING MOMENT COEFFICIENTS BETWEEN EXPERIMENT, AP02, AND AP98 FOR FIGURE 34A CONFIGURATION (Φ = 0 DEG, M_∞ = 0.2)

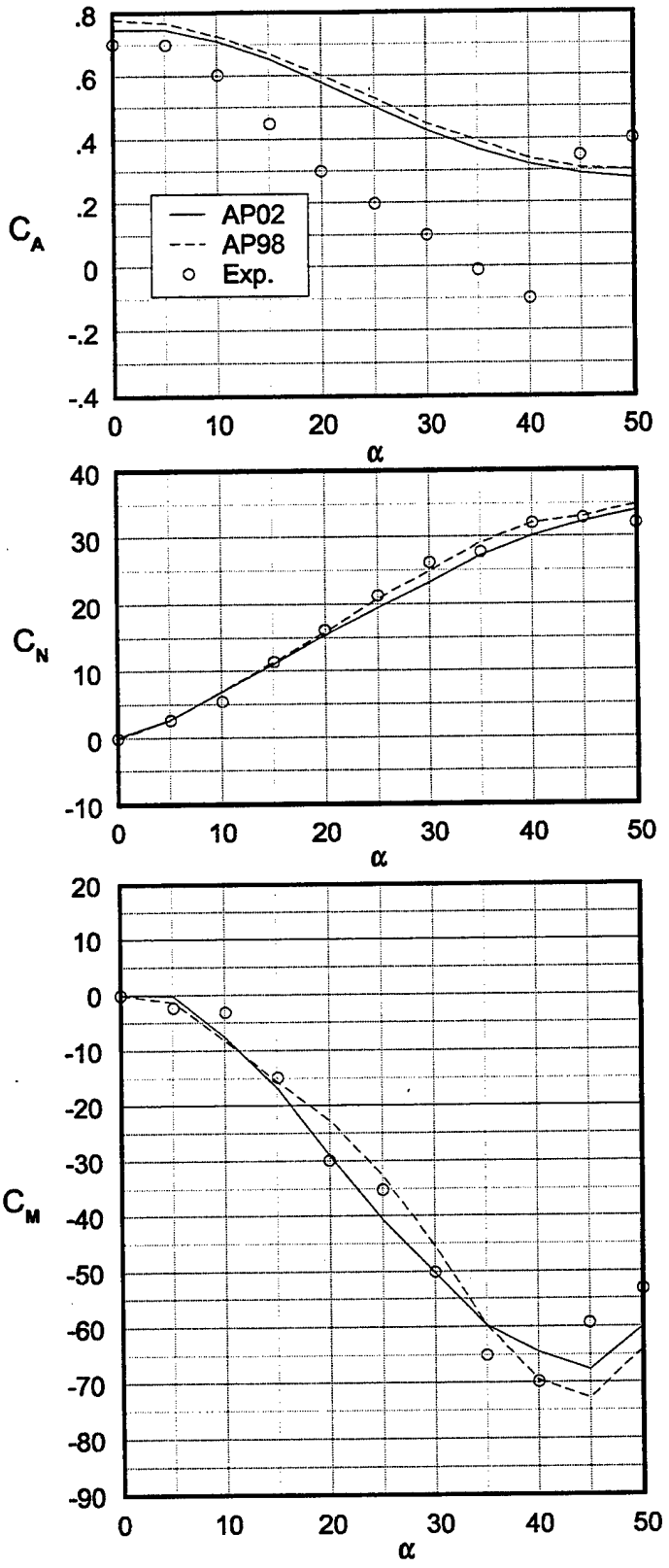

FIGURE 34C. COMPARISON OF AXIAL, NORMAL AND PITCHING MOMENT COEFFICIENTS BETWEEN EXPERIMENT, AP02, AND AP98 FOR FIGURE 34A CONFIGURATION (Φ = 45 DEG, M_∞ = 0.2)

(3) No quantitative assessment was made of center of pressure (or pitching moment) improvements. However, in viewing the results qualitatively, it is believed a slight overall improvement was realized by the improved normal force loads. In addition, an error in the center of pressure shift at roll of 45 deg was corrected in the AP02, also adding some slight improvement in center of pressure predictions.

(4) In comparing the AP02 to the AP98 on nine wing-body-tail configurations outside of the missile component data bases upon which the nonlinear empirical constants were derived, it was found that in general, the improvements in average normal force error of the AP02 were seen here as well. The average improvements range from only a slight improvement on one case to over 40 percent reduction in error for the best case. Overall, it is guessed that the average normal force error was reduced by about 20 to 25 percent from the AP98 to the AP02.

(5) While the overall accuracy improvement in normal force coefficient is based on averages, one can still find a single data point error on either the AP98 or AP02 where the error is as high as 35 percent. These worst-case data points usually occur at subsonic or transonic speeds where it is very difficult to predict the correct value of critical crossflow Reynolds number and Mach number.

(6) No assessment of axial force or control deflection errors were made since no changes were implemented into the AP02 compared to the AP98.

(7) Based on the overall improvement in normal force using the refined nonlinear constants of this report, these improvements will be a part of the next version of the aeroprediction code that will be transitioned to users in Fiscal Year 2002.

6.0 REFERENCES

1. Moore, F. G.; McInville, R. M.; and Hymer, T., *The 1998 Version of the NSWC Aeroprediction Code: Part I – Summary of New Theoretical Methodology*, NSWCDD/TR-98/1, Apr 1998.

2. Moore, F. G.; McInville, R. M.; and Robinson, D. I., *A Simplified Method for Predicting Aerodynamics of Multi-Fin Weapons*, NSWCDD/TR-99/19, Mar 1999.

3. Hymer, T. C.; Downs, C.; and Moore, F. G., *Users Guide for an Interactive Personal Computer Interface for the 1998 Aeroprediction Code (AP98)*, NSWCDD/TR-98/7, Jun 1998.

4. NASA Langley Research Center Tri-Service Missile Data Base, transmitted from NASA/LRC Jerry M. Allen to NSWCDD, 5 Nov 1991 (formal documentation of data base in process).

5. Stallings, R. L., Jr. and Lamb., *Wing-Alone Aerodynamic Characteristics for High Angles of Attack at Supersonic Speeds*, NASA Technical Paper 1989, Jul 1981.

6. Baker, W. B., Jr., *Static Aerodynamic Characteristics of a Series of Generalized Slender Bodies With and Without Fins at Mach Numbers from 0.6 to 3.0 and Angles of Attack from 0 to 180 °*, AEDC-TR-75-124, Vols. I and II, May 1976, Tullahoma, TN.

7. Allen, J. M.; Hemsch, M. J.; Burns, K. A.; and Oeters, K. J., *Parametric Fin-Body and Fin-Alone Database on a Series of 12 Missile Fins*, NASA LRC TM in publication, May 1996.

8. Washington, W. D. and Spring, D. J., "An Experimental Investigation of Wing-Tail Interference for a Typical Supersonic Missile," AIAA paper 82-1339, AIAA 9th Atmospheric Flight Mechanics Conference, 9-11 Aug 1982, San Diego, CA.

9. Wardlaw, A. B. and Davis, S., *A Second-Order-Gudonov Method for Supersonic Tactical Missiles*, NSWC TR 86-506, 1986.

10. Walters, R. W.; Slack, D. C.; Cimmella, P.; Applebaum, M. P.; and Frost, C., "A Users Guide to GASP," Virginia Polytechnic Institute and State University, Department of Aerospace and Ocean Engineering, Blacksburg, VA, Nov 1990.

REFERENCES (Continued)

11. Robinson, D. F., *ZEUS^{++} - A Graphical User Interface Flowfield Analysis Tool*, NSWCDD/TR-98/147, in publication.

12. Pitts, W. C.; Nielsen, J. N.; and Kaatari, G. E., *Lift and Center of Pressure of Wing-Body-Tail Combinations at Subsonic, Transonic, and Supersonic Speeds*, NACA TR 1307, 1957.

13. Moore, F. G.; McInville, R. M.; and Hymer, T., *The 1995 Version of the NSWC Aeroprediction Code: Part I – Summary of New Theoretical Methodology*, NSWCDD/TR-94/379, Feb 1995.

14. Nielsen, J. N,; Hemsch, M. J.; and Smith, C. A., *A Preliminary Method for Calculating the Aerodynamic Characteristics of Cruciform Missiles to High Angles of Attack Including Effects of Roll Angle and Control Deflections*, Report ONR-CR215-216,4F, Nov 1977, Office of Naval Research, 800 N. Quincy St., Arlington, VA 22217.

15. Moore, F. G. and McInville, R. M., *A New Method for Calculating Wing Alone Aerodynamics to Angle of Attack 180 °*, NSWCDD/TR-94/3, Mar 1994.

16. Moore, F. G. and McInville, R. M., *Extension of the NSWCDD Aeroprediction Code to the Roll Position of 45 Degrees*, NSWCDD/TR-95/160, Dec 1995.

17. Monta, W. J., *Supersonic Aerodynamic Characteristics of a Sparrow III Type Missile Model With Wing Controls and Comparison With Existing Tail-Control Results*, NASA TP 1078, Nov 1977.

18. Graves, E. B. and Fournier, R. H., *Stability and Control Characteristics at Mach Numbers From 0.20 to 4.63 of a Cruciform Air-to-Air Missile With Triangular Canard Controls and a Trapezoidal Wing*, NASA TMX-3070, May 1974.

19. Jorgensen, L. H., *Predictions of Static Aerodynamic Characteristics for Slender Bodies Alone and With Lifting Surfaces to Very High Angles of Attack*, NASA TR R-474, Sep 1977.

20. Blair, A. B., Jr.; Allen, J. M.; and Hernandez, G., *Effect of Tail-Fin Span on Stability and Control Characteristics of a Canard Controlled Missile at Supersonic Mach Numbers*, NASA TP 2157, Jun 1983.

21. Gudmundson, S. E. and Torngren, L., *Supersonic and Transonic Wind Tunnel Tests on Slender Ogive-Cylinder Body Single and in Combination With Cruciform Wings and Tails of Different Sizes*, Technical Note FFA AU-772, Apr 1972 (The Aeronautical Research Institute of Sweden, Aeronautics Department, Stockholm, Sweden).

REFERENCES (Continued)

22. Wardlaw, A. B., Jr.; Baltakis, F. P.; Martin, F. M.; and Priolo, F. J., "A Godunov Method for Supersonic Tactical Missiles," *Journal of Spacecraft and Rockets*, Vol. 24, No. 1, 1987, pp. 40-47.

23. Smith, E. H.; Salazar, M. E.; Hebbar, S. K.; and Platzer, M., "Aerodynamic Characteristics of the MMPT ATD Vehicle at High Angles of Attack," AIAA paper No. 93-3493, Aug 1993.

24. Howard, R. M. and Dunn, A., "Missile Loads at High Angles of Attack," Engineering Note in *Journal of Spacecraft and Rockets*, Vol. 28, No. 1, Jan-Feb 1991.

25. Dietz, W. E., Jr., and Altstatt, M. C., "Experimental Investigation of Support Interference on an Ogive Cylinder at High Incidence," *Journal of Spacecraft and Rockets*, Vol. 16, No. 2, Mar-Apr 1979.

26. Canning, T. N. and Nielsen, J. N., "Experimental Study of the Influence of Supports on the Aerodynamic Loads on an Ogive Cylinder at High Angles of Attack," AIAA paper 81-0007, 19th Aerospace Sciences Meeting, St. Louis, MO, 12-15 Jan 1981.

27. Smith, E. H.; Hebbar, S. K.; and Platzer, M., "Aerodynamic Characteristics of a Canard-Controlled Missile at High Angles of Attack," AIAA paper No. 93-0763, presented at 31st Aerospace Sciences Meeting, Reno, NV, 11-14 Jan 1993.

7.0 SYMBOLS AND DEFINITIONS

AOA	Angle of Attack
APC	Aeroprediction Code
AP02, AP98	2002 and 1998 versions of the APC respectively
AR	Aspect Ratio = b^2/A_W
LT	Linear Theory
NASA/LRC	National Aeronautics and Space Administration/Langley Research Center
NASA/MDAC	National Aeronautics and Space Administration/McDonnell Douglas Corporation
NSWCDD	Naval Surface Warfare Center, Dahlgren Division
SB, SBT	Slender Body, Slender-Body Theory
A_{REF}	Reference area (maximum cross-sectional area of body, if a body is present, or planform area of wing, if wing alone)(ft^2)
A_W	Planform area of wing in crossflow plane (ft^2)
b	Wing span (not including body)(ft)
C_A	Axial force coefficient
$C_{A_B}, C_{A_F}, C_{A_W}$	Base, skin-friction, and wave components, respectively, of axial force coefficient
C_{d_c}	Crossflow drag coefficient
C_D	Drag coefficient
C_L	Lift coefficient

C_M	Pitching moment coefficient (based on reference area and body diameter, if body present, or mean aerodynamic chord, if wing alone)
C_{M_L}	Linear component of pitching moment coefficient
$C_{M_{NL}}$	Nonlinear component of pitching moment coefficient
C_N	Normal force coefficient
C_{N_B}	Normal force coefficient of body alone
$C_{N_{B(V)}}$	Negative afterbody normal-force coefficient due to canard or wing-shed vortices
$C_{N_{B(W)}}, C_{N_{B(T)}}$	Normal-force coefficient on body in presence of wing or tail
C_{N_L}	Linear component of normal-force coefficient
$C_{N_{NL}}$	Nonlinear component of normal-force coefficient
$(C_{N_\alpha})_W, (C_{N_\alpha})_T$	Normal force coefficient slope of wing and tail respectively
$C_{N_{T(V)}}$	Negative normal-force coefficient component on tail due to wing or canard-shed vortex
C_{N_W}	Normal force coefficient of wing alone
$C_{N_{W(B)}}, C_{N_{F(B)}}$	Normal-force coefficient of wing or fin in presence of body
C_{N_α}	Normal-force coefficient derivative
c_r	Root chord (ft)
c_t	Tip chord (ft)
cal	Caliber(s) (one body diameter)
d_B	Body diameter (ft) at base
d_{ref}	Reference body diameter (ft)

$\frac{dK_{W(B)}}{d\alpha}, \frac{dK_{B(W)}}{d\alpha}$	Rate at which $K_{W(B)}$ or $K_{B(W)}$ decreases
deg	Degree(s)
$K_{B(W)}$, $K_{B(T)}$	Ratio of additional body normal-force coefficient in presence of wing, or tail-to-wing or tail-alone normal-force coefficient at $\delta = 0$ deg
$k_{B(W)}$, $k_{B(T)}$	Ratio of additional body normal-force coefficient due to presence of wing or tail at a control deflection to that of wing or tail alone at $\alpha = 0$ deg
$[K_{B(W)}]_{MIN}$	Minimum value of $K_{B(W)}$ as percent of slender-body theory value
$K_{W(B)}$, $K_{T(B)}$	Ratio of normal-force coefficient of wing or tail in presence of body to that of wing or tail alone at $\delta = 0$ deg
$k_{W(B)}$, $k_{T(B)}$	Ratio of wing or tail normal-force coefficient in presence of body due to a control deflection to that of wing or tail alone at $\alpha = 0$ deg
ΔK	Nonlinear component of wing-body or body-wing interference
$[\Delta K_{W(B)}]_{\alpha=0}$ and $[\Delta K_{B(W)}]_{\alpha=0}$	Amount that the experimental values of $K_{W(B)}$ and $K_{B(W)}$ exceed slender body theory at $\alpha = 0$ deg
ℓ, ℓ_n	Body length and nose length respectively
M_N	Mach number normal to body = $M_\infty \sin \alpha$
M_{N_c}	Normal Mach number where flow transitions from subcritical to supercritical conditions
M_∞	Freestream Mach number
N	Normal force
NF	Fin normal force
r	Local body radius (ft)
RBM	Root bending moment
R_{N_c}	Reynolds number where flow transitions from subcritical to supercritical conditions

r_W, r_T	Radius of body at wing or tail locations
s	Wing or tail semispan plus the body radius in wing-body lift methodology
X_{CP}	Center of pressure (in feet or calibers from some reference point that can be specified) in x direction
$(X_{CP})_L$, $(X_{CP})_{NL}$	Center of pressure of linear and nonlinear terms of normal force
x,y,z	Axis system fixed with x along centerline of body
α	Angle of attack (deg)
α_C	Angle of attack where wing-body interference factor starts decreasing (deg)
α_D	Angle of attack where the wing-body interference factor reaches a minimum (deg)
α_M	Angle of attack where $K_{W(B)}$ reaches a constant value
α_W, α_T	Local angle of attack of wing or tail ($\alpha_W + \delta$ or $\alpha_T + \delta$, respectively, in degrees)
α_1, α_2	Angles of attack used in nonlinear model for $K_{B(W)}$
δ	Control deflection (deg), positive leading edge up
δ_W, δ_T	Deflection of wing or tail surfaces (deg), positive leading edge up
η	Parameter used in viscous crossflow theory for nonlinear body normal force (in this context, it is the normal force of a circular cylinder of given length-to-diameter ratio to that of a cylinder of infinite length)
η_0	Value of η at $M_N = 0$
Φ	Roll position of missile fins ($\Phi = 0$ deg corresponds to fins in the plus (+) orientation; $\Phi = 45$ deg corresponds to fins rolled to the cross (×) orientation)
λ	Taper ratio of a lifting surface = c_t/c_r

Subscripts

c, t, w	Canard, tail, wing
CG	Center of gravity
∞	Freestream conditions

DISTRIBUTION

DOD ACTIVITIES (CONUS)

		Copies
ATTN	CODE 35 (ZIMET)	1
	CODE 351 (SIEGEL)	1
	CODE 351 (CHEW)	1
	CODE 332FD (LEKOUDIS)	1
CHIEF OF NAVAL RESEARCH		
BALLSTON CENTRE TOWER ONE		
800 NORTH QUINCY ST		
ARLINGTON VA 22217-5660		
ATTN	CODE 474T6OD (LOFTUS)	1
	CODE 4732HOD (SMITH)	1
	CODE 473COOD (PORTER)	1
	CODE 47311OD (HOUSH)	1
	CODE 47311OD (GLEASON)	1
	CODE 4722EOD (JETER)	1
	TECHNICAL LIBRARY	1
COMMANDER		
NAVAL AIR WARFARE CENTER		
WEAPONS DIVISION		
1 ADMINISTRATION CIRCLE		
CHINA LAKE CA 93555-6001		
ATTN	TECHNICAL LIBRARY	1
	G RUDACILLE PMS 38012 7	1
COMMANDER		
NAVAL SEA SYSTEMS COMMAND		
2531 JEFFERSON DAVIS HWY		
ARLINGTON VA 22242-5160		
ATTN	TECHNICAL LIBRARY	1
COMMANDER		
NAVAL AIR SYSTEMS COMMAND		
47122 LILJENCRANTZ ROAD UNIT 7		
PATUXENT RIVER MD 20670-5440		
ATTN	C KLEIN	1
	TECHNICAL LIBRARY	1
COMMANDER		
NAVAL AIR WARFARE CENTER		
WEAPONS DIVISION		
521 9TH ST		
POINT MUGU CA 93042-5001		
ATTN	T C TAI	1
	M J MALIA	1
	TECHNICAL LIBRARY	1
COMMANDER		
NSWC		
CARDEROCK DIVISION		
WASHINGTON DC 20034		
ATTN	R M HOWARD	1
	TECHNICAL LIBRARY	1
SUPERINTENDENT		
NAVAL POSTGRADUATE SCHOOL		
1 UNIVERSITY CIRCLE		
MONTEREY CA 93943-5001		
ATTN	HEAD WEAPONS DEPT	1
	HEAD SCIENCE DEPT	1
SUPERINTENDENT		
UNITED STATES NAVAL ACADEMY		
121 BLAKE RD		
ANNAPOLIS MD 21402-5000		
ATTN	DIAG DT 4T (PAUL MURAD)	2
DIRECTOR		
DEFENSE INTELLIGENCE AGENCY		
WASHINGTON DC 20301		
ATTN	BRENT WAGGONER	1
CODE 4072 BLDG 2540		
NAVAL WEAPONS SUPPORT CENTER		
CRANE IN 47522-5000		
ATTN	CODE 5252P (KRAUSE)	1
	TECHNICAL LIBRARY	1
COMMANDER		
INDIAN HEAD DIVISION		
NAVAL SURFACE WARFARE CENTER		
101 STRAUSS AVE		
INDIAN HEAD MD 20640-5035		

DISTRIBUTION (Continued)

	Copies
ATTN TECHNICAL LIBRARY COMMANDING GENERAL MARINE CORPS COMBAT DEVELOPMENT COMMAND 2048 SOUTH ST QUANTICO VA 22134-5129	1
ATTN E SEARS L E LIJEWSKI C COTTRELL TECHNICAL LIBRARY AFATL (ADLRA) (DLGC) EGLIN AFB FL 32542-5000	1 1 1 1 1
ATTN TECHNICAL LIBRARY USAF ACADEMY COLORADO SPRINGS CO 80912	1
ATTN TECHNICAL LIBRARY ADVANCED RESEARCH PROJECTS AGENCY DEPARTMENT OF DEFENSE WASHINGTON DC 20305	1
ATTN B BLAKE (BLD 146) J JENKINS (BLD 146) TECHNICAL LIBRARY COMMANDING OFFICER AFSC 2210 8TH STREET WRIGHT PATTERSON AFB OH 45433	1 1 1
ATTN EDWARD JENKINS NAIC TANW HQ NAIC TANW 4115 HEBBLE CREEK ROAD SUITE 28 WPAFB OH 45433-5623	1
ATTN J USSELTON W B BAKER JR TECHNICAL LIBRARY ARNOLD ENGINEERING DEVELOPMENT CENTER USAF TULLAHOMA TN 37389	1 1 1
ATTN H HUDGINS G FRIEDMAN TECHNICAL LIBRARY COMMANDING GENERAL ARRADCOM PICATINNY ARSENAL DOVER NJ 07801	1 1 1
ATTN R PUHALLA JR W STUREK C NIETUBICZ A MIKHAIL P PLOSTINS TECHNICAL LIBRARY COMMANDING GENERAL BALLISTIC RESEARCH LABORATORY ABERDEEN PROVING GROUND ABERDEEN MD 21005-5066	1 1 1 1 1 1
ATTN CODE TNC (BLACKLEDGE) RICH MATLOCK DIRECTOR INTERCEPTOR TECHNOLOGY BALLISTIC MISSILE DEFENSE OFFICE THE PENTAGON WASHINGTON DC 20350	1 1
ATTN SFAE SD ASP SFAE SD HED DEPUTY COMMANDER US ARMY STRATEGIC DEFENSE COMMAND P O BOX 1500 HUNTSVILLE AL 35807-3801	1 1
ATTN D WASHINGTON W WALKER R KRETZSCHMAR D FERGUSON JR COMMAND GENERAL US ARMY MISSILE COMMAND AMSMI RD SS AT REDSTONE ARSENAL AL 35898-5252	1 1 1 1
DEFENSE TECHNICAL INFORMATION CENTER 8725 JOHN J KINGMAN ROAD SUITE 0944 FORT BELVOIR VA 22060-6218	2

DISTRIBUTION (Continued)

	Copies
DIRECTOR DEFENSE PRINTING SERVICE BLDG 176 WASHINGTON NAVY YARD 901 M ST E WASHINGTON DC 20374-5087	1
ATTN CODE A76 TECHNICAL LIBRARY COMMANDING OFFICER CSSDD NSWC 6703 W HIGHWAY 98 PANAMA CITY FL 32407-7001	1
ATTN DR P WEINACHT AERODYNAMICS BRANCH PROPULSION AND FLIGHT DIV WTD AMSRL WT PB US ARMY RESEARCH LAB ABERDEEN PROVING GROUND MD 21005-5066	1
ATTN GREGG ABATE US AIR FORCE WRIGHT LABORATORY WL MNAA 101 W EGLIN BLVD STE 219 EGLIN AFB FL 32542-5000	1
ATTN JOHN GRAU US ARMY ARDEC COMMANDER US ARMY ARDEC AMSTA AR AET A BLDG 3342 PICATINNY ARSENAL NJ 07806-5000	1
ATTN FRANK MACDONALD NAWC CHINA LAKE COMMANDER CODE 473 20D NAVAIRWARCENNSDNDIV CHINA LAKE CA 93555	1
ATTN MARK LAMBERT NAWC CODE 4732HOD CHINA LAKE CA 93555	1
ATTN MICHAEL MUSACHIO DIRECTOR OFFICE OF NAVAL INTELLIGENCE 4251 SUITLAND ROAD (ONI 2321) WASHINGTON DC 20395	1
ATTN DR ALAN NICHOLSON MSC 5B DEFENSE INTELLIGENCE AGENCY MISSILE AND SPACE INTELLIGENCE CTR REDSTONE ARSENAL AL 35898-5500	1
ATTN EDWARD HERBERT US ARMY MISSILE COMMAND AMSMI RD MG GA BLDG 5400 ROOM 250 REDSTONE ARSENAL AL 35898	1
ATTN PAUL KOLODZIEJ NASA AMES RESEARCH CENTER MS 234 1 MOFFETT FIELD CA 94035	1
ATTN LCDR T HARTLINE USNR R NR ONI 2109 NAVAL RESERVE UNIT 112 CRESTVIEW CIRCLE MADISON AL 35758	1
ATTN CODE 4732HOD DAVID HALL PROPULSION PERFORMANCE OFFICE NAVAL AIR WARFARE CTR WEAPONS DIV 1 ADMINISTRATIVE CIR CHINA LAKE CA 93555-6001	1
ATTN DONALD SHEREDA WL FIMA BLDG 450 2645 FIFTH ST STE 30 WRIGHT PATTERSON AFB OH 45433-7936	1
ATTN ROBERT VAN DYKEN 473110D COMMANDER NAWC CHINA LAKE CA 93555	1
BMDO AQS 1725 JEFFERSON DAVIS HWY STE 809 ARLINGTON VA 22202	1

DISTRIBUTION (Continued)

	Copies
ATTN JEFFREY RANDORF US ARMY SPACE AND STRATEGIC DEFENSE COMMAND P O BOX 1500 CSSD-BC-SS 106 WYNN DRIVE HUNTSVILLE AL 35807-3801	1
NON-DOD ACTIVITIES (CONUS)	
NICHOLS RESEARCH CORPORATION MS 912 P O BOX 400002 4040 S MEMORIAL PKWY HUNTSVILLE AL 35815-1502	1
THE CNA CORPORATION P O BOX 16268 ALEXANDRIA VA 22302-0268	1
GIDEP OPERATIONS OFFICE CORONA CA 91720	1
ATTN TECHNICAL LIBRARY NASA AMES RESEARCH CENTER MOFFETT CA 94035-1099	1
ATTN C SCOTT D CURRY NASA JOHNSON SPACE CENTER HOUSTON TX 77058	1 1
ATTN TECHNICAL LIBRARY NASA WASHINGTON DC 20546	1
ATTN B HENDERSON D MILLER J ALLEN F WILCOX TECHNICAL LIBRARY NASA LANGLEY RESEARCH CENTER HAMPTON VA 23365	1 1 1 1 2
ATTN D G MILLER (L 219) TECHNICAL LIBRARY LAWRENCE LIVERMORE NATIONAL LABORATORY EARTH SCIENCES DIVISION UNIVERSITY OF CALIFORNIA P O BOX 808 LIVERMORE CA 94551	1 1
ATTN W RUTLEDGE (1635) R LAFARGE R EISLER TECHNICAL LIBRARY SANDIA NATIONAL LABORATORY P O BOX 5800 ALBUQUERQUE NM 87185-5800	1 1 1 1
ATTN WALT GUTIERREZ SANDIA NATIONAL LABORATORIES MAIL STOP 0825 P O BOX 5800 ALBUQUERQUE NM 87185-0825	1
ATTN ASSISTANT DEFENSE COOPERATION ATTACHE EMBASSY OF SPAIN WASHINGTON DC 20016	1
DE/AVT DEFENSE EQUIPMENT STAFF BRITISH EMBASSY 3100 MASSACHUSETTS AVE NW WASHINGTON DC 20008-3688	1
ATTN ASO LO IS ISRAEL AIR FORCE LIAISON OFFICER 700 ROBBINS AVE PHILADELPHIA PA 19111	1
ATTN GERMAN MILITARY REP US OA GMR TRAFFIC AND TRANSPORTATION DIVISION 10 SERVICES ROAD DULLES INTERNATIONAL AP WASHINGTON DC 20041	1

DISTRIBUTION (Continued)

	Copies
ATTN PROF F R DEJARNETTE NORTH CAROLINA STATE UNIVERSITY DEPT OF MECHANICAL AND AEROSPACE ENGINEERING BOX 7921 RALEIGH NC 27695	1
ATTN PROF J A SCHETZ VIRGINIA POLYTECHNIC AND STATE UNIVERSITY DEPT OF AEROSPACE ENGINEERING BLACKSBURG VA 24060	1
ATTN J M WU C BALASUBRAMAYAN TECHNICAL LIBRARY THE UNIVERSITY OF TENNESSEE SPACE INSTITUTE TULLAHOMA TN 37388	1 1 1
ATTN R NELSON TECHNICAL LIBRARY UNIVERSITY OF NOTRE DAME DEPT OF AEROSPACE AND MECHANICAL ENGINEERING BOX 537 NOTRE DAME IN 46556	1 1
ATTN PROF F NELSON DEPT OF MECH AND AERO ENG UNIVERSITY OF MISSOURI ROLLA ROLLA MO 65401	1
ATTN ROBERT ENGLAR GEORGIA TECH RESEARCH INSTITUTE AEROSPACE SCIENCE AND TECHNOLOGY LAB ATLANTA GA 30332	1
ATTN E LUCERO D FROSTBUTTER L PERINI TECHNICAL LIBRARY APPLIED PHYSICS LABORATORY JOHNS HOPKINS UNIVERSITY JOHNS HOPKINS ROAD LAUREL MD 20723-6099	1 1 1 1
ATTN B BROOKS R STANCIL R ELKINS LORAL VOUGHT SYSTEMS P O BOX 650003 M S EM 55 DALLAS TX 75265-0003	1 1 1
ATTN PROF J D ANDERSON DEPT OF AEROSPACE ENGINEERING UNIVERSITY OF MARYLAND COLLEGE PARK MD 20742	1
ATTN TECHNICAL LIBRARY HUGHES MISSILE SYSTEMS COMPANY P O BOX 11337 BLDG 802 MS A1 OLD NOGALES HWY TUCSON AZ 83734-1337	1
ATTN M DILLENIUS NIELSEN ENGINEERING AND RESEARCH INC 526 CLYDE AVE MOUNTAIN VIEW CA 95043	1
ATTN J XERIKOS N CAMPBELL TECHNICAL LIBRARY MCDONNEL DOUGLAS ASTRONAUTICS CO (WEST) 5301 BOLSA AVE HUNTINGTON BEACH CA 92647	1 1 1
ATTN J WILLIAMS S VUKELICH J FIVEL R GERBSCH (CODE 1111041) TECHNICAL LIBRARY MCDONNELL DOUGLAS ASTRONAUTICS CO (EAST) BOX 516 ST LOUIS MO 63166-0516	1 1 1 1 1
ATTN TECHNICAL LIBRARY UNITED TECHNOLOGIES NORDEN SYSTEMS NORWALK CT 06856	1

DISTRIBUTION (Continued)

	Copies
ATTN T LUNDY	1
D ANDREWS	1
TECHNICAL LIBRARY	1
LOCKHEED MISSILES AND SPACE CO INC	
P O BOX 1103	
HUNTSVILLE AL 35807	
ATTN W CHRISTENSON	1
D WARNER	1
ALLIANT TECHSYSTEMS INC	
600 SECOND ST NE	
HOPKINS MN 55343	
ATTN TECHNICAL LIBRARY	1
B SALEMI	1
J BOUDREAU	1
RAYTHEON COMPANY	
MISSILE SYSTEMS DIVISION	
P O BOX 1201	
TEWKSBURY MA 01876-0901	
ATTN LLOYD PRATT	1
AEROJET TACTICAL SYSTEMS CO	
P O BOX 13400	
SACRAMENTO CA 95813	
ATTN JOSEPH ANDRZEJEWSKI	1
MEVATEC CORP	
1525 PERIMETER PARKWAY	
SUITE 500	
HUNTSVILLE AL 35806	
ATTN DR G S SCHMIDT	1
LORAL DEFENSE SYSTEMS	
1210 MASSILLON ROAD	
AKRON OH 44315-0001	
ATTN W NORDGREN 721	1
GOULD INC OSD	
18901 EUCLID AVE	
CLEVELAND OH 44117	
ATTN TECH LIBRARY	1
AEROJET ELECTRONIC SYSTEMS	
P O BOX 296 III	
AZUSA CA 91702	

	Copies
ATTN P REDING	1
G CHRUSCIEL	1
TECHNICAL LIBRARY	1
LOCKHEED MISSILES AND SPACE CO INC	
P O BOX 3504	
SUNNYVALE CA 94088	
ATTN K C LEE	1
AEROTHERM CORP	
580 CLYDE AVE	
MOUNTAIN VIEW CA 94043	
ATTN TECH LIBRARY	1
FMC NAVAL SYSTEMS DIV	
4800 E RIVER ROAD	
MINNEAPOLIS MN 55421-1402	
ATTN JAMES SORENSON	1
VINCENT ALLEN	1
ORBITAL SCIENCES	
3380 SOUTH PRICE ROAD	
CHANDLER AZ 85248	
ATTN J FORKOIS	1
KAMAN SCIENCES CORP	
1500 GARDEN OF THE GODS ROAD	
P O BOX 7463	
COLORADO SPRINGS CO 80933	
ATTN RON EFROMSON	1
MIT LINCOLN LABORATORY	
244 WOOD STREET	
LEXINGTON MA 02173-0073	
ATTN D J GIESE	1
MAIL STOP 4C 61	
BOEING DEFENSE AND SPACE GROUP	
P O BOX 3999	
SEATTLE WA 98124-2499	
ATTN BRIAN WALKUP	1
ALLEGHENY BALLISTICS LAB	
210 STATE ROUTE 956 WV01-13	
ROCKET CENTER WV 26726-3548	
ATTN DR T LIN	1
TRW ELECTRONICS AND DEFENSE SECTOR	
BLDG 527/RM 706	
P O BOX 1310	
SAN BERNADINO CA 92402	

DISTRIBUTION (Continued)

	Copies
ATTN G VINCENT SPARTA INC 4901 CORPORATE DR HUNTSVILLE AL 35805	1
ATTN D P FORSMO TECHNICAL LIBRARY RAYTHEON COMPANY MISSILE SYSTEMS DIVISION HARTWELL RD BEDFORD MA 01730-2498	1 1
ATTN M S MILLER N R WALKER DYNETICS INC P O DRAWER B HUNTSVILLE AL 35814-5050	1 1
ATTN H A MCELROY GENERAL DEFENSE CORP P O BOX 127 RED LION PA 17356	1
ATTN ENGINEERING LIBRARY ARMAMENT SYSTEMS DEPT GENERAL ELECTRIC CO BURLINGTON VT 05401	1
ATTN TECHNICAL LIBRARY OAYNE AERONAUTICAL 2701 HARBOR DRIVE SAN DIEGO CA 92138	1
ATTN BRIAN EST BOEING ST LOUIS P O BOX 516 ST LOUIS MO 63166-0516	1
ATTN WILLIAM FACINELLI ALLIED SIGNAL P O BOX 22200 MS 1207 3B TEMPE AZ 85285	1
ATTN DR T P SHIVANANDA TRW BMD P O BOX 1310 SAN BERNADINO CA 92402-1313	1
ATTN T R PEPITONE AEROSPACE TECHNOLOGY INC P O BOX 1809 DAHLGREN VA 22448	1
ATTN ERIC MOORE MAIL STOP MER 24 1281 LOCKHEED SANDERS P O BOX 868 NASHUA NH 03061	1
ATTN DR BRIAN LANDRUM RI BLDG E33 PROPULSION RESEARCH CENTER UNIVERSITY OF ALABAMA HUNTSVILLE AL 35899	1
ATTN JIM ROBERTSON RESEARCH SOUTH INC 555 SPARKMAN DRIVE SUITE 818 HUNTSVILLE AL 35816-3423	1
ATTN BOB WHYTE ARROW TECH ASSOCIATES INC 1233 SHELBURNE ROAD D8 SO BURLINGTON VT 05403	1
ATTN JUAN AMENABAR SAIC 4001 NORTH FAIRFAX DRIVE STE 800 ARLINGTON VA 22209	1
ATTN TECHNICAL LIBRARY TELEDYNE RYAN AERONAUTICAL 2701 HARBOR DRIVE SAN DIEGO CA 92138	1
ATTN DR KIRIT PATEL SVERDRUP TECHNOLOGY INC TEAS GROUP BLDG 260 P O BOX 1935 EGLIN AFB FL 32542	1
ATTN FRANK LANGHAM MICRO CRAFT TECHNOLOGY 740 4TH ST MS 6001 ARNOLD AFB TN 37389	1

DISTRIBUTION (Continued)

	Copies
ATTN LAURA AYERS DELTA RESEARCH INC 315 WYNN DRIVE SUITE 1 HUNTSVILLE AL 35805	1
ATTN BRIAN BENNETT MCDONNELL DOUGLAS MC 064 2905 P O BOX 516 ST LOUIS MO 63166-0516	1
ATTN THOMAS FARISS LOCKHEED SANDERS P O BOX 868 MER24 1206 NASHUA NH 03061-0868	1
ATTN COREY FROST LOCKHEED MISSILES & SPACE CO INC P O BOX 070017 6767 OLD MADISON PIKE SUITE 220 HUNTSVILLE AL 35807	1
ATTN JEFFREY HUTH KAMAN SCIENCES CORPORATION 2560 HUNTINGTON AVE ALEXANDRIA VA 22303	1
ATTN WILLIAM JOLLY KAMAN SCIENCES 600 BLVD SOUTH SUITE 208 HUNTSVILLE AL 35802	1
ATTN STEPHEN MALLETTE KBM ENTERPRISES 15980 CHANEY THOMPSON RD HUNTSVILLE AL 35803	1
ATTN DONALD MOORE NICHOLS RESEARCH CORPORATION 4040 SOUTH MEMORIAL PARKWAY P O BOX 400002 MS 920C HUNTSVILLE AL 35815-1502	1
ATTN NANCY SWINFORD LOCKHEED MISSILES & SPACE CO P O BOX 3504 ORG E5-40 BLDG 1575E SUNNYVALE CA 94088-3504	1
ATTN DAVID RESSLER TRW BALLISTIC MISSILES DIV MS 953 2420 P O BOX 1310 SAN BERNARDINO CA 92402	1
ATTN MARK SWENSON ALLIANT TECHSYSTEMS MN11 262B 600 SECOND STREET NE HOPKINS MN 55343	1
ATTN LEROY M HAIR COLEMAN RESEARCH CORP 6820 MOQUIN DRIVE HUNTSVILLE AL 35806	1
ATTN SCOTT ALLEN ALLEN AERO RESEARCH 431 E SUNNY HILLS RD FULLERTON CA 92635	1
ATTN DARRYL HALL SAIC 997 OLD EAGLE SCHOOL RD SUITE 215 WAYNE PA 19087-1803	1
ATTN PETER ALEXANDER MCDONNELL DOUGLAS AEROSPACE 689 DISCOVERY DRIVE MS 11A1 HUNTSVILLE AL 35806	1
ATTN SAMUEL HICKS III TEXAS INSTRUMENTS 6600 CHASE OAKS BLVD MS 8490 PLANO TX 75086	1

DISTRIBUTION (Continued)

	Copies
ATTN BARRY LINDBLOM ALLIANT DEFENSE ELECTRONICS SYSTEMS INC P O BOX 4648 CLEARWATER FL 34618	1
ATTN DR SHIN CHEN THE AEROSPACE CORP M4 967 P O BOX 92957 LOS ANGELES CA 90009	1
ATTN ROBERT ACEBAL SAIC 1225 JOHNSON FERRY RD SUITE 100 MARIETTA GA 30068	1
ATTN EUGENE HART SYSTEM PLANNING CORP 1000 WILSON BLVD ARLINGTON VA 22209	1
ATTN ELAINE POLHEMUS ROCKWELL AUTONETICS & MISSILE SYSTEMS DIVISION D611 DL23 1800 SATELLITE BLVD DULUTH GA 30136	1
ATTN MICHAEL GLENN TASC 1992 LEWIS TURNER BLVD FT WALTON BEACH FL 32547	1
ADAPTIVE RESEARCH 4960 CORPORATE DRIVE SUITE 100 A HUNTSVILLE AL 35805-6229	1
ATTN STEVEN MARTIN SYSTEMS ENGINEERING GROUP INC 9841 BROKEN LAND PARKWAY SUITE 214 COLUMBIA MD 21046-1120	1

	Copies
ATTN C W GIBKE LOCKHEED MARTIN VOUGHT SYSTEMS MS SP 72 P O BOX 650003 DALLAS TX 75265-0003	1
ATTN CHRIS HUGHES EDO GOVERNMENT SYSTEMS DIV 1500 NEW HORIZONS BLVD AMITYVILLE NY 11701-1130	1
ATTN DANIEL LESIEUTRE NIELSEN ENGINEERING & RES INC 526 CLYDE AVENUE MOUNTAIN VIEW CA 94043-2212	1
ATTN CARL HILL FRANCIS PRIOLO STANDARD MISSILE COMPANY LLC 1505 FARM CREDIT DRIVE SUITE 600 MCLEAN VA 22102	1 1
ATTN THOMAS LOPEZ COLEMAN RESEARCH CORP 990 EXPLORER BLVD HUNTSVILLE AL 35806	1
ATTN JENNIE FOX LOCKHEED MARTIN VOUGHT SYSTEMS P O BOX 650003 MS EM 55 DALLAS TX 75265-0003	1
ATTN JOHN BURKHALTER AUBURN UNIVERSITY 211 AEROSPACE ENGR BLDG AUBURN UNIVERSITY AL 36849	1
ATTN DR MAX PLATZER NAVAL POSTGRADUATE SCHOOL DEPT OF AERONAUTICS & ASTRONAUTICS CODE AA PL MONTEREY CA 93943	1
ATTN MIKE DANGELO MIT LINCOLN LABORATORY 1745 JEFFERSON DAVIS HWY 1100 ARLINGTON VA 22202	1

DISTRIBUTION (Continued)

	Copies
ATTN RICHARD HAMMER JOHNS HOPKINS APPLIED PHYSICS LAB JOHNS HOPKINS ROAD LAUREL MD 20723-6099	1
ATTN MAURICE TUCKER BATTELLE HUNTSVILLE OPERATIONS 7501 S MEMORIAL PKWY STE 101 HUNTSVILLE AL 35802	1
ATTN STEVE MULLINS SIMULATION AND ENGINEERING CO INC 4935 CENTURY ST NW HUNTSVILLE AL 35816-1901	1
ATTN ROBERT BRAENDLEIU KAISER MARQUARDT 16555 SATICOY ST VAN NUYS CA 91406-1739	1
ATTN LAWRENCE FINK BOEING AIRCRAFT AND MISSILES P O BOX 3707 MC 4A 36 SEATTLE WA 98124-2207	1
ATTN ROY KLINE KLINE ENGINEERING CO INC 27 FREDON GREENDELL RD NEWTON NJ 07860-5213	1
ATTN THOMAS KLAUSE TRW P O BOX 80810 ALBUQUERQUE NM 87198	1
ATTN DAN PLATUS THE AEROSPACE CORPORATION P O BOX 92957 LOS ANGELES CA 90009	1
ATTN DR REX CHAMBERLAIN TETRA RESEARCH CORPORATION 2610 SPICEWOOD TR HUNTSVILLE AL 35811-2604	1
ATTN PERRY PETERSEN NORTHROP GRUMMAN CORP DEPT 9B51 MAIL ZONE XA 8900 EAST WASHINGTON BLVD PICO RIVERA CA 90660-3783	1
ATTN DR JAMES HAUSER AERO SPECTRA INC 2850 KENYON CIRCLE P O BOX 3006 BOULDER CO 80307	1
ATTN DARRELL AUSHERMAN TRW SPACE AND DEFENSE ONE SPACE PARK MAIL STATION R1-1062 REDONDO BEACH CA 90278-1071	1
ATTN JAY EBERSOHL ADVATECH PACIFIC INC 2015 PARK AVENUE SUITE 8 REDLANDS CA 92373	1
ATTN EDWARD RAWLINSON SY TECHNOLOGY INC 4900 UNIVERSITY SQUARE SUITE 8 HUNTSVILLE AL 35816	1
ATTN LAYNE COOK UNIVERSAL SPACE LINES 8620 WOLFF CT SUITE 110 WESTMINSTER CO 80030	1
ATTN PAUL WILDE ACTA INC 2790 SKYPARK DR SUITE 310 TORRANCE CA 90505-5345	1
ATTN DR MICHAEL HOLDEN CALSPAN UB RESEARCH CENTER P O BOX 400 BUFFALO NY 14225	1
ATTN RICHARD GRABOW SPACE VECTOR CORP 17330 BROOKHURST ST SUITE 150 FOUNTAIN VALLEY CA 92708	1
ATTN BRENT APPLEBY DRAPER LABORATORY 555 TECHNOLOGY SQ MS77 CAMBRIDGE MA 02139	1

DISTRIBUTION (Continued)

	Copies
ATTN JAMES JONES SPARTA INC 1901 N FORT MYER DR SUITE 600 ARLINGTON VA 22209	1
ATTN SCOTT HOUSER PHOENIX INTEGRATION 1872 PRATT DRIVE SUITE 1835 BLACKSBURG VA 24060	1
ATTN S ROM MURTY TELEDYNE BROWN ENGINEERING MS 200 300 SPARKMAN DRIVE HUNTSVILLE AL 35807	1
ATTN STUART COULTER SVERDRUP TECHNOLOGY 670 2ND ST MS4001 ARNOLD AIR FORCE BASE TULLAHOMA TN 37389-4001	1
ATTN DR RICHARD HOWARD NAVAL POSTGRADUATE SCHOOL DEPT OF AERONAUTICS AND ASTRONAUTICS CODE AA HO NPS MONTEREY CA 93943	1
ATTN J BRENT RUMINE MIT LINCOLN LABORATORY 244 WOOD STREET BUILDING S ROOM 52-327 LEXINGTON MA 02173-9185	1
NON-DOD ACTIVITIES (EX-CONUS)	
ATTN A BOOTH BRITISH AEROSPACE DEFENCE LTD MILITARY AIRCRAFT DIVISION WARTON AERODROME WARTON PRESTON LANCASHIRE PR4 1AX UNITED KINGDOM	1
ATTN R CAYZAC GIAT INDUSTRIES 7 ROUTE DE GUERCY 18023 BOURGES CEDEX FRANCE	1
ATTN MAJ F DE COCK ECOLE ROYALE MILITAIRE 30 AV DE LA RENAISSANCE 1040 BRUXELLES BELGIUM	1
ATTN J EKEROOT BOFORS MISSILES 691 80 KARLSKOGA SWEDEN	1
ATTN CH FRANSSON NATIONAL DEFENCE RESEARCH ESTABLISHMENT DEPT OF WEAPON SYSTEMS EFFECTS AND PROTECTION KARLAVAGEN 106B 172 90 SUNDBYBERG SWEDEN	1
ATTN M HARPER BOURNE DEFENCE RESEARCH AGENCY Q134 BUILDING RAE FARNBOROUGH HAMPSHIRE QU14 6TD UNITED KINGDOM	1
ATTN A H HASSELROT FFA P O BOX 11021 161 11 BROMMA SWEDEN	1
ATTN B JONSSON DEFENCE MATERIAL ADMINISTRATION MISSILE TECHNOLOGY DIVISION 115 88 STOCKHOLM SWEDEN	1
ATTN P LEZEAUD DASSAULT AVIATION 78 QUAI MARCEL DASSAULT 92214 SAINT CLOUD FRANCE	1
ATTN J LINDHOUT N L R ANTHONY FOKKERWEG 2 1059 CM AMSTERDAM THE NETHERLANDS	1

DISTRIBUTION (Continued)

	Copies
ATTN A MICKELLIDES GEC MARCONI DEFENCE SYSTEMS LTD THE GROVE WARREN LANE STANMORE MIDDLESEX UNITED KINGDOM	1
ATTN K MOELLER BODENSEEWERK GERAETETECHNIK GMBH POSTFACH 10 11 55 88641 UBERLINGEN GERMANY	1
ATTN RIBADEAU DUMAS MATRA DEFENSE 37 AV LOUIS BREGUET BP 1 78146 VELIZY VILLACOUBLAY CEDEX FRANCE	1
ATTN R ROGERS DEFENCE RESEARCH AGENCY BLDG 37 TUNNEL SITE CLAPHAM BEDS MK 41 6AE UNITED KINGDOM	1
ATTN S SMITH DEFENCE RESEARCH AGENCY Q134 BUILDING RAE FARNBOROUGH HAMPSHIRE QU14 6TD UNITED KINGDOM	1
ATTN J SOWA SAAB MISSILES AB 581 88 LINKOPING SWEDEN	1
ATTN D SPARROW HUNTING ENGINEERING LTD REDDINGS WOOD AMPTHILL BEDFORDSHIRE MK452HD UNITED KINGDOM	1
ATTN P STUDER DEFENCE TECHNOLOGY AND PROCUREMENT AGENCY SYSTEMS ANALYSIS AND INFORMATION SYSTEMS DIVISION PAPIERMUEHLESTRASSE 25 3003 BERNE SWITZERLAND	1
ATTN DR R G LACAU AEROSPATIALE MISSILE DEPT E/ECN CENTRE DES GATINES 91370 VERRIERE LE BUISSON FRANCE	1
ATTN J M CHARBONNIER VON KARMAN INSTITUTE 72 CHAUSSEE DE WATERLOO 1640 RHODE SAINT GENESE BELGIUM	1
ATTN P CHAMPIGNY DIRECTION DE L AERONAUTIQUE ONERA 29 AV DE LA DIVISION LECLERC 92320 CHATILLON SOUS BAGNEUX CEDEX FRANCE	1
ATTN DR P HENNIG DEUTSCHE AEROSPACE (DASA) VAS 414 ABWEHR AND SCHUTZ POSTFACH 801149 8000 MUENCHEN 80 GERMANY	1
ATTN DR S J YOON AGENCY FOR DEFENSE DEVELOPMENT AERODYNAMICS DIVISION (4-3-1) P O BOX 35-4 YUSEONG TAEJON KOREA	1
ATTN PETER CAAP HD FLIGHT SYS DEPT FAA AERONAUTICAL RESEARCH INST OF SWEDEN BOX 11021 BROMMA SWEDEN 16111	1

DISTRIBUTION (Continued)

	Copies
ATTN DAVE BROWN WEAPON SYSTEMS DIVISION AERONAUTICAL AND MARITIME RESEARCH LABORATORY P O BOX 1500 SALISBURY SOUTH AUSTRALIA 5108	1

INTERNAL

		Copies
B		1
B04		1
B04	(ZIEN)	1
B05	(GRAFF)	1
B05	(HORMAN)	1
B05	(STATON)	1
B10		1
B10	(HSIEH)	1
B51	(ARMISTEAD)	1
B60	(TECHNICAL LIBRARY)	3
C		1
D		1
G		1
G02		1
G04		5
G20		1
G205		1
G23		1
G23	(BIBEL)	1
G23	(CHADWICK)	1
G23	(COOK)	1
G23	(HANGER)	1
G23	(HARDY)	1
G23	(HYMER)	1
G23	(OHLMEYER)	1
G23	(ROWLES)	1
G23	(WEISEL)	1
G30		1
G305		1
G32	(DAY)	1
G33	(FRAYSSE)	1
G33	(MELTON)	1
G33	(RINALDI)	1
G50		1
G50	(SOLOMON)	1
G60		1
G70		1
G72		1
G72	(ALEXOPOULOS)	1
G72	(CHEPREN)	1
G72	(LEWIS)	1
G72	(MCINVILLE)	5
G72	(ROBINSON)	1
K		1
K40		1
K44	(ICHNIOWSKI)	1
N		1
T		1
T406		1